Institute of Thermoelectricity, Academy of Sciences and Ministry of Education and Science of Ukraine

Journal of THERMOELECTRICITY

International Research

Founded in December, 1993

published 6 times a year

No. 1 *2018*

Editorial Board

Editor-in-Chief LUKYAN I. ANATYCHUK

Petro I. Baransky
Lyudmyla N. Vikhor
Valentyn V. Lysko
Stepan V. Melnychuk
Bogdan I. Stadnyk
Oleg J. Luste
Elena I. Rogacheva
Andrey A. Snarskii

International Editorial Board

Lukyan I. Anatychuk, *Ukraine*
Steponas P. Ašmontas, *Lithuania*
Jean-Claude Tedenac, *France*
H.J. Goldsmid, *Australia*
L. Chen, *China*
T. Caillat, *USA*
Yuri Grin, *Germany*
A.I. Casian, *Moldova*
Takenobu Kajikawa, *Japan*
T. Tritt, *USA*
Sergiy O. Filin, *Poland*
D. Sharp, *USA*
Yuri Gurevich, *Mexico*

Founders – National Academy of Sciences, Ukraine
Institute of Thermoelectricity of National Academy of Sciences and Ministry of Education and Science of Ukraine

Certificate of state registration № КВ 15496-4068 ПР

Editors:

V. Kramar, P.V.Gorskiy, O. Luste, T. Podbegalina

Approved for printing by the Academic Council of Institute of Thermoelectricity of the National Academy of Sciences and Ministry of Education and Science, Ukraine

Address of editorial office:
Ukraine, 58002, Chernivtsi, General Post Office, P.O. Box 86.
Phone: +(380-372) 90 31 65.
Fax: +(380-3722) 4 19 17.
E-mail: jt@inst.cv.ua
http://www.jt.inst.cv.ua

Signed for publication 25.01.18. Format 70×108/16. Offset paper №1. Offset printing.
Printer's sheet 11.5. Publisher's signature 9.2. Circulation 400 copies. Order 5.

Printed from the layout original made by "Journal of Thermoelectricity" editorial board in the printing house of "Bukrek" publishers,
10, Radischev Str., Chernivtsi, 58000, Ukraine

Copyright © Institute of Thermoelectricity, Academy of Sciences and Ministry of Education and Science, Ukraine, 2016

CONTENTS

Zhengbing Hu[1],
Vitaly Deibuk[2], *Doctor Phys.-math. Science*


Zhengbing Hu

[1]School of Educational Information Technology Central China Normal University, Wuhan, China
[2]Institute of Thermoelectricity of the NAS and MES Ukraine, Nauky str., Chernivtsi, 58029, Ukraine;
e-mail: v.deibuk@chnu.edu.ua


Vitaly Deibuk

DESIGN OF TERNARY REVERSIBLE/QUANTUM SEQUENTIAL ELEMENTS

The extensive use of the principles of reversible computing makes it possible to minimize energy losses during the operation of computer devices. The design of reversible memory elements of the ternary logic is an actual task because they are necessary devices of modern electronics. In the paper, the main reversible sequential elements of the ternary logic were synthesized on the base of the permutative one-input and two-input gates proposed by Muthukrishnan and Stroud (MS-gates). Using the improved adaptive genetic algorithm, we proposed ternary reversible D-, T-, and JK-latches and flip-flops. To the best of our knowledge, ternary reversible T- and JK-flip-flops are synthesized for the first time on this basis. The proposed algorithm is also used for the synthesis of a reversible ternary Fredkin gate, resulting in the improvement of a quantum cost compared to the existing counterparts. The sequential elements synthesized in this work can be built by the liquid ion trap quantum technology thanks to the used MS-gates. Improvements with respect to the quantum cost, number of constant inputs, delay time, and number of garbage outputs are reported. This work is intended to attract the attention of specialists in thermoelectricity to the possibility of using reversible electronics to the design of thermoelectric devices. Bibl. 29, Fig. 8, Tabl. 2
Key words: flip-flops, latches, reversible computing, multiple-valued logic, genetic algorithms.

Introduction

Recently, the use of reversible logic for the transmission and processing of information is one of the promising areas of modern information technology [1-4]. This is due to the need to reduce energy losses in quantum computing, low-power CMOS technologies, bioinformatics, etc [5,6]. Rolf Landauer theoretically proved [5] that the erase of each bit of information is accompanied by the loss of $kT\ln 2$ Joules (T is absolute temperature and k – Boltzmann's constant), which has been experimentally confirmed recently [29]. Thus, the design of reversible electrical circuits consisting of reversible gates can lead to a reduction in energy losses. Heat dissipation is a significant problem in modern micro and nano-electronic microprocessor devices since thermal losses inevitably lead to the errors in the transmission and processing of information. Along with the traditional methods to prevent overheating, more and more scientist lately are addressed to advanced methods, such as thermoelectric coolers, reverse logic circuitry, etc. The combination of these two approaches, in our opinion, could make a significant breakthrough in the solving this problem.

The reversible gates are considered as the gates in which output states can uniquely restore input information. That is, in reversible gates, there is a bijective mapping of the set of input states onto a set of output states. The last condition means that in reversible logical gates the number of inputs is equal to the number of outputs [6,7]. Another consequence of the bijective conditions in reversible logical gates is the

forbiddance of a fan-out. In reversible circuits, in addition to informational inputs/outputs, there are also constant (ancillary) inputs and garbage outputs whose information should be recycled. An important characteristic of a reversible gate is its quantum cost, which is understood as the number of primitives from which the gate is built. The design of reversible circuits also requires the use of a universal (functionally complete) basis of reversible gates, by means of which it is possible to implement an arbitrary reversible logic circuit. The synthesis of optimal reversible logic device involves obtaining a device which is characterized by a minimum number of constant inputs and garbage outputs, a minimum quantum cost, and a minimum delay time.

The optimization problem has an analytical solution only in the case of designing reversible circuits of binary logic with a limited number of input signals [4]. At the same time, today analytical methods for the design of reversible devices of multi-valued logic are far from being completed [4,8]. The well-known advantages of multiple-valued logic devices make it possible to realize reversible computations in quantum computing algorithms in practice [9,10]. One of the promising ways to solve the above problem for the case of ternary logic is the use of artificial intelligence methods. In particular, evolutionary strategies, genetic programming and genetic algorithms have made it possible to find optimal solutions for many reversible combinational devices [11-14]. In [12-14] we used an adaptive genetic algorithm for the synthesis of some combination reversible devices of ternary logic. As basic gates, we used one- and two-qutrit Muthukrishnan-Stroud gates (MS-gates) [15], which can be considered as primitives with a quantum cost of one. The advantage of this basis is that it is universal, and its primitives can be physically realized by the liquid ion-trap quantum technology [9,10].

To create reversible computer devices of ternary logic, it is important to synthesize sequential reversible gates. In particular, the memory cell is a sequential circuit whose output state is determined by a combination of the input signals and the previous state of the device [7]. A distinctive feature of sequential circuits is the presence of the feedbacks. Different methods for synthesis of binary reversible latches and flip-flops are presented in [17-21]. At the same time, there are only a few studies of the design of reversible sequential ternary logic devices [22-26]. However, in many cases, the synthesis was carried out on the excess basis of the gates, which leads to an increase in the quantum cost of the obtained devices. In [26], we proposed optimal schemes of ternary reversible latches, where minimization was performed by the number of logical errors, the number of one- and two-qutrit MS-gates. In this paper, we present an extended optimization scheme that takes into account additional factors such as the number of ancillary (garbage) inputs (outputs), as well as the delay time of the sequential circuit. To test the proposed improved genetic algorithm for the synthesis of sequential circuits we have presented the design of a ternary reversible *D*-, *T*-, and *JK* - latches without ancillary inputs that are in good agreement with the previously known results [26]. On the basis of the improved genetic algorithm, *T*- and *JK*-flip-flops were synthesized for the first time. Obtained schemes of *D*-flip-flops based on master-slave architecture have a lower quantum cost compared to other works.

The rest of the paper is organized as follows. Section 2 defines the basic set of permutative reversible ternary gates and describes synthesis methodology. Section 3 presents the proposed design of ternary reversible latches. Section 4 shows the simulation results for the clocked reversible ternary flip-flops, and finally, the conclusion section closes the paper.

Synthesis metodology

Arbitrary manipulations with ternary quantum states can be described using their matrix representation [4,8]. Such 3x3 unitary matrices correspond to one-qutrit quantum gates, which are used in this work as primitives. Table 1 shows logical one-qutrit ternary permutative transforms corresponding to

the gates. The quantum cost of one-input gates can be taken equal to unity as follows from [11,12]. We used the ternary MS-gates for designing ternary quantum circuits. These two-qutrits gates have one control X_1 and one controlled X_2 input. The first output Y_1 repeats the control input $Y_1 = X_1$. If control signal $X_1 = 2$, the other output Y_2 is the transform of the controlled input X_2 (Table 1), otherwise $Y_2 = X_2$. Such a set of logic elements is functionally complete [16], which allows using it for the synthesis of various combinational and sequential reversible devices [12-14, 22-25]. Calculation of the complexity (quantum cost) of a ternary reversible circuit refers to the number of one- and two-inputs MS-gates used for the circuit synthesis.

Table 1

One-Qutrit Ternary Permutative Transforms

Input X	**Output**					
	Y(0) = X	**Y(+1) = X+1**	**Y(+2) =X+2**	**Y(01) =2X+1**	**Y(02) =2X+2**	**Y(12) =2X**
0	0	1	2	1	2	0
1	1	2	0	0	1	2
2	2	0	1	2	0	1

Earlier [26], we proposed an improved method of genetic synthesis of ternary reversible latches in the basis of one- and two-input MS-gates. However, this rather simple scheme of the genetic algorithm did not allow us to obtain more complex sequential devices with improved characteristics in comparison with those already known [22-25]. Therefore, in this paper, we propose somewhat complicated scheme of the algorithm. First of all, this concerns the change in the fitness function, which is known to be a key factor in the procedure of genetic optimization. The investigated scheme can be represented by a sequence of one- and two-input primitives, described above, arranged in parallel or in series. We place the control and controlled inputs in the upper part of the network. The auxiliary inputs are located at the bottom. The chromosome is a device diagram and is coded as ordered gene tuples. In this case, the corresponding column of the scheme (chromosome) we understand as a gene. [12]. For example, the coding of a chromosome corresponding to the scheme in Fig. 1, is represented as ((2,1,2), (0,2,5), (2,1,1), (1,2,2), (0,1,1), (1,2,1)). Here, each ordered triple corresponds to a gene (gate) and contains the following information: the number of the control line, the line number of a gate location, the type of gate. As the basis, six types of permutation gates were taken into account, as can be seen from Table 1. We take into account in the fitness functions F five terms that will control the process of selecting the optimal chromosomes:

$$F = k_1F_1 + k_2F_2 + k_3F_3 + k_4F_4 + k_5F_5, \quad (1)$$

where the first function F_1 corresponds to the condition of the minimum number of errors (*Error*) in the truth table of the synthesized logical reversible device:

$$F_1 = (Error + 1)^{-1}. \quad (2)$$

The condition for obtaining a circuit with the minimum number of non-zero gates dG in the chromosome of length dL is taken into account in the function F_2

$$F_2 = (dL - dG)/dL. \quad (3)$$

We will keep in mind that the length of the chromosome *dL* is the number of genes from which it is composed. The third term in (1) corresponds to the condition of the minimum number of controlled gates (d*GM*) in the chromosome:

$$F_3 = dGM / dG. \quad (4)$$

The last two functions in (1) are responsible for obtaining a chromosome with a minimum number g_i of ancillary inputs (garbage outputs) F_4 and also with a minimum delay time *s* of the signal transmission - F_5:

$$F_4 = (1 + g_i)^{-1}, \quad (5)$$

$$F_5 = \exp\left(-(1 - 1/s)^2\right). \quad (6)$$

Delay time of circuit (*s*) was estimated in relative units of a delay time of one logic element (t_0). k_i – weight coefficient of *i*-th fitness component (*i* = 1,…,5). The coefficients k_i were chosen dynamically according to

$$k_i(itr+1) = k_i(itr)\left(1 - \overline{F_i(itr)}\right), \quad (7)$$

where $k_i(itr)$ are the weight coefficients, $\overline{F_i(itr)}$ – fitness average in the *itr* generation (*i* = 2,…,5). Since the resultant circuit must not contain logical errors (*Error* = 0), the coefficient k_1 was assumed to be 1. To check the correctness of the obtained chromosomes (circuits), we compared their fitness- functions for ternary latch with our earlier work [26]. The above fitness function *F* contains two additional terms - F_4 and F_5 in comparison with [26]. This allowed to minimize the number of constant inputs (outputs) in the circuit and also to reduce to the minimum delay time. As was mentioned above, we estimate the quantum cost in this paper as the number of gates in the circuit. Thus, the obtained scheme will be considered as effective if the overall fitness function is the maximum. Detailed description of the other steps of the genetic algorithm is given in [14].

Quantum/reversible ternary latches

One of the important devices of an arbitrary computing system is a memory element. The simplest schemes that realize the possibility of information memorization are *D*-, *T*-, and *JK*-latches. The state of the output of such devices depends not only on the state of the input signals but also on the output states at the previous time. The need for further improvement of the ternary reversible latches is motivated by the requirement to reduce the energy consumption in modern computing devices. In the previous paper [26], we synthesized quantum/reversible ternary latches where MS-gates were used as the basis. This section presents the results of computer simulation of these latches using an improved fitness function (1). In our opinion, this procedure is necessary because it allows us to test the application of the modified model in comparison with the previous one. In this section, we also synthesized gates to duplicate the output signals (fan-out) that were necessary for the design of quantum/reversible latches.

Design of Ternary Reversible D-Latch

The characteristic equation describing the operation of the reversible ternary *D*-latches can be written as [27, 28]:

$$Q_{t+1} = D. \quad (8)$$

Here Q_{t+1} is the output state signal at time $t+1$. The characteristic equation of the clocked *D*-latch is:

$$Q_{t+1} = \begin{cases} Q_t, & Clk = 0 \\ *, & Clk = 1 \\ D, & Clk = 2 \end{cases} \tag{9}$$

The don't care state of the output is denoted by the symbol *. The proposed scheme of the clocked *D*-latch is shown in Fig. 1. The feedback is indicated by a dashed line. The obtained scheme coincided with that obtained earlier [26]; however, the expanded fitness function (1) allowed synthesizing this scheme 2 times faster.

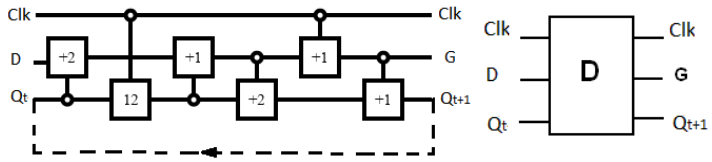

Fig. 1. Quantum/reversible ternary clocked D-latch and its block diagram

Figure 2 is a fan-out circuit. This circuit was also obtained using the improved genetic algorithm and is consistent with the results of Ref. 26.

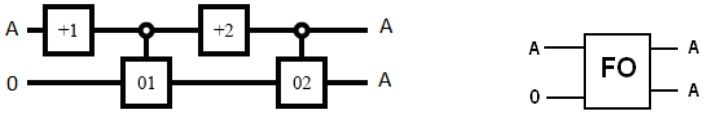

Fig. 2. Quantum/reversible ternary fan-out circuit and its block diagram

Design of Ternary Reversible T-Latch

The method described above has been used for the implementation of *T*-latches. The characteristic equation for asynchronous *T*-latch can be written as [28]

$$Q_{t+1} = T \oplus Q_t . \tag{10}$$

In the case of a clocked *T*-latch, the simulation can be performed on the basis of the following characteristic equation:

$$Q_{t+1} = \begin{cases} Q_t, & Clk = 0 \\ *, & Clk = 1 \\ T \oplus Q_t, & Clk = 2 \end{cases} \tag{11}$$

The simulated quantum/reversible ternary clocked *T*-latch circuit is shown in Fig. 3. *T*-latch remains in its previous state $Q_{t+1} = Q_t$ if $Clk = 0$. The device is in don't care condition if clocked signal is one. The input signal *T* is active if clocked signal is 2. Then the upper gate is active, and if $T = 1$, $Q_{t+1} = Q_t + 1$ and if $T = 2$, $Q_{t+1} = Q_t + 2$. The quantum cost (QC) of the circuit is 3, the circuit has one garbage output (*G*), and the delay time – $3t_0$.

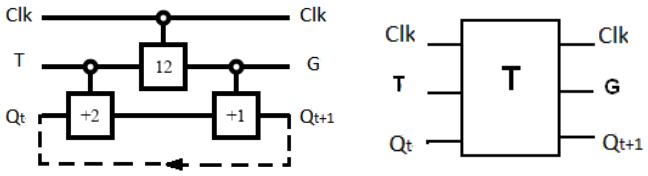

Fig. 3. Quantum/reversible ternary clocked T-latch and its block diagram

Design of Ternary Reversible JK-Latch

Fig. 4 shows the proposed quantum/ternary reversible *JK*-latch. The latch is synthesized according to the algorithm detailed in [23, 26] and has the following characteristics. The quantum cost – 8, the garbage outputs – 2(*G*1, *G*2), and the delay time – $6t_0$. The output signal $G2 = Q_t + 2$, where the sum is modulo three.

A ternary reversible *JK*-latch was synthesized in Ref. 23 on another basis. There were used two-input ternary gates with different levels of a controlled signal. Such a design, in our opinion, is associated with a more complicated physical implementation of the latches.

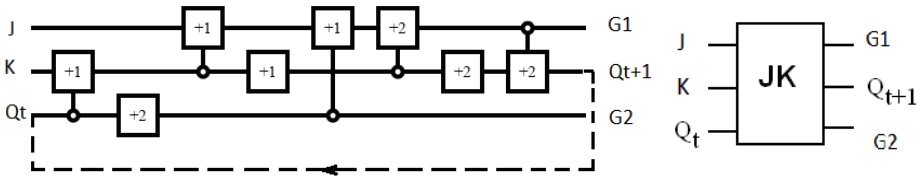

Fig. 4. Quantum/reversible ternary JK-latch and its block diagram

More flexible control of the operation of the reversible ternary *JK*-latch requires an appropriate clocked device. For its design, we take into account the fact that adding a one-input primitive (+1) to the third output of the non-clocked latch (Fig. 4) allows receiving an input signal Q_t.

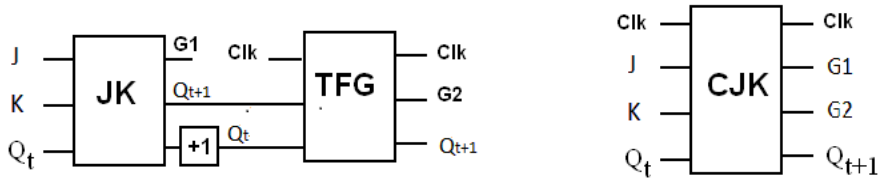

Fig. 5. Structure of ternary reversible clocked JK-latch and its block diagram

Using a control exchange gate (ternary Fredkin gate (TFG)) we can get a clocked *JK*-latch (CJK) whose structure and block diagram are shown in Fig. 5. In the same way, as in previous cases, the input state Q_t is repeated at its lower output in the case when the clock signal *Clk* = 0,1 and this output produces a Q_{t+1} signal when *Clk* = 2. Then a garbage output G2 will generate a signal, which can also be used, since

$$G2 = \begin{cases} Q_{t+1}, & Clk = 0,1 \\ Q_t, & Clk = 2 \end{cases} \tag{12}$$

The signal on the garbage output G1 must be recycled. The synthesized ternary reversible Fredkin gate in the one- and two-input permutative basis is presented in Fig. 6. So-defined reversible ternary Fredkin gate is an analog of the binary Fredkin gate and agrees with the definition given in [23, 25].

In addition, it is well known that this gate is conservative, that is, the number of digits 0, 1, 2, applied to the input is the same as on the outputs of the gate. The proposed implementation of the ternary Fredkin gate has a *QC* = 10, which is better than the results of the genetic synthesis of TFG presented in [23], where *QC* = 13.

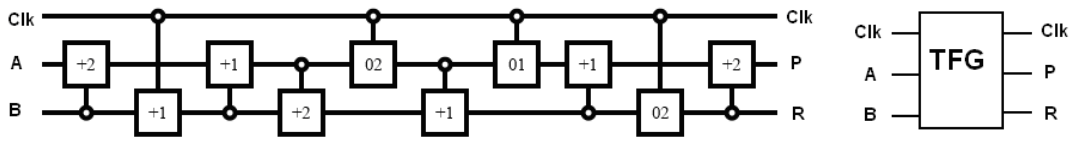

Fig. 6. Proposed design of ternary reversible Fredkin gate and its block diagram

Fig. 7 shows the implementation of a reversible ternary clocked *JK*-latch in the proposed basis. It is important to note that this realization does not have ancillary inputs, the number of garbage outputs is equal to 2, *QC* = 19 (*QC* = 22 [23]).
The obtained reversible ternary *D*-, *T*- and *JK*-latches coincide with those obtained in [26], but estimated time is lesser in 1.5 times on average.

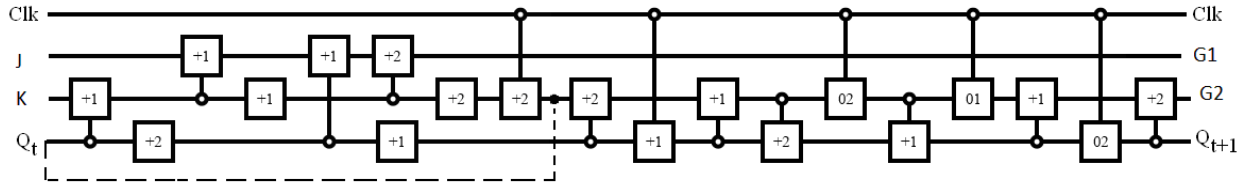

Fig. 7. Proposed design of ternary reversible clocked JK-latch

Design of clocked reversible ternary flip-flops

Unlike clocked latches which are controlled by the level of a clock pulse, flip-flops are sequential edge-triggered sensitive elements. Such elements have a high level of security and are widely used in computing devices. Traditionally, the master-slave architecture is used in digital electronics for the design of flip-flops, which means the use of two serially connected latches and one inverter. Since we have built the reversible clocked *D*-, *T*, and *JK*-latches, then the corresponding reversible flip-flops can be designed by replacing the corresponding elements with their reversible analogs. Fig. 8 shows the implementation of reversible *D*-, *T*-, and *JK*-flip-flops, where the *D*-latch selected as a slave gate, and the one-input element 02 is the inverter.

Before realization of the feedback in the *D*- and *T*-latches, the fan-out gate was used to copy the Q_{t+1} signal. Proposed reversible ternary *D*-, *T*-flip-flops have 2 auxiliary inputs and 2 garbage outputs, the quantum cost QC is 21 and 18, respectively. The edge-triggered *D*-flip-flop circuit, obtained in [24], has a QC = 25, that means a higher efficiency of the genetic synthesis method used by us. The parameters of the obtained *JK*-flip-flop are the following: one auxiliary input, three outputs, quantum cost QC = 30. Proposed ternary edge-triggered *D*-, *T*-, and *JK*-flip-flops were obtained for the first time in the above-described basis. Table 2 shows the parameters of the obtained circuits (in bold), in comparison with the results of other authors. It should be noted that all our synthesized circuits are obtained in one functionally complete basis of one- and two inputs MS-gates, whereas the results of work [23] are obtained in various redundant bases. In addition, the results were obtained using different thresholds of the input control signal, as well as three-input logic gates. In particular, the basis in the work [23] contains a ternary Fredkin gate, which is itself functionally complete. Synthesis of various reversible devices of ternary logic is not a self-aim, of course, but should be directed towards future physical implementation, the simplicity of which is one of the important goals. From these points, the minimality of the basis used in the sequential circuit design, in our opinion, will significantly simplify the physical implementation of the quantum/reversible sequential devices

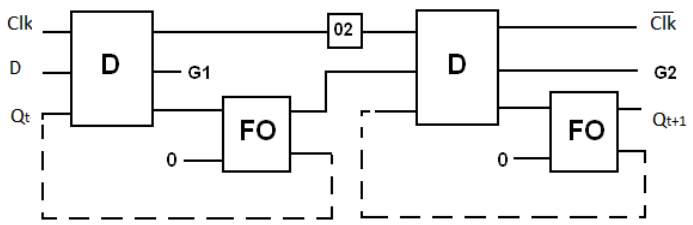

a)

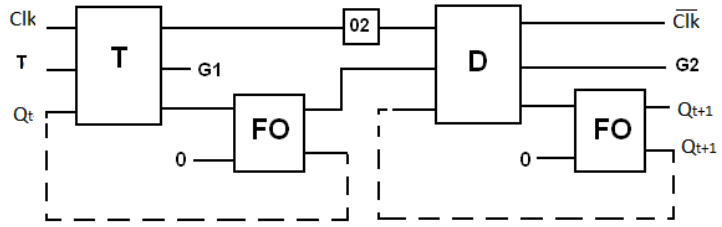

b)

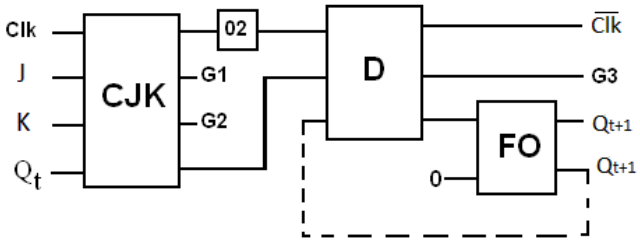

c)

Fig. 8. Design of ternary reversible edge-triggered Master-Slave flip-flops: D-FF(a), T-FF(b), JK-FF(c)

Table 2

Comparison of our new design (in bold) and previous works

Types	No. Gates	No. Ancilla Inputs	No. Garbage Outputs	QC
Edge-Trig. *D*-FF	**21** 13[24]	**2** 2 [24]	**2** 3 [24]	**21** 25[24]
Edge-Trig. *T*-FF	**18**	**2**	**2**	**18**
Edge-Trig. *JK*-FF	**30**	**1**	**3**	**30**
Ternary Fredkin gate	**10** 13 [23] 15 [25]	**0** 0 [23] 0 [25]	**0** 0 [23] 0 [25]	**10** 13 [23] 15 [25]

Conclusion

We present the new results of the design of basic reversible ternary sequential elements such as *D*-, *T*-, *JK*-flip-flops. The proposed circuits were synthesized and optimized on the basis of permutative one- and two-inputs MS-gates using the improved adaptive genetic algorithm. In comparison with other works, the proposed design is more effective in terms of quantum cost, the number of ancillary inputs and garbage outputs. We also developed the clocked *JK*-latch. Reversible ternary edge-triggered *D*-, *T*-, and *JK*-flip-flops are synthesized for the first time. The proposed algorithm was also used for the synthesis of combinational circuits; in particular, the synthesized ternary Fredkin gate has a quantum cost of ten, which improves the results obtained in [23]. The quantum/reversible sequential elements can be tested by the liquid ion trap quantum technology.

References

1. R.Drechsler, R.Wille, Reversible circuits: Recent accomplishments and future challenges for an emerging technology, in: *Progress in VLSI Design and Test*, Springer, Berlin-Heidelberg, 383–392 (2012).
2. M.Nielsen, I.Chuang, *Quantum Computation and Quantum Information* (Cambridge University Press, Cambridge, 2000), 700 p..
3. Z.Li, S.Chen, X.Song, et al., Quantum circuit synthesis using a new quantum logic gate library of NCV quantum gates, *Int. J. Theor. Phys.* **56**(4), 1023–1038 (2017).
4. D.M.Miller, M.A.Thornton, *Multiple-Valued Logic: Concepts and Representations* (Morgan & Claypool Publishers, 2008), 127 p..
5. R.Landauer, Irreversibility and heat generation in the computational process, *IBM J. Res. Develop*. **5**(1/2), 183–191 (1961).
6. C.H.Bennett, Logical reversibility of computation, *IBM J. Res. Develo*p. **17**(6), 525–532 (1973).
7. E.Fredkin and T.Toffoli, Conservative logic, *Int. J. Theor. Phys.* **21**(3/4), 219-253 (1982).
8. C.Moraga, On some basic aspects of ternary reversible and quantum computing," in *Proc. 44th IEEE Int. Symp. Multiple-Valued Logic*, Bremen, 178–183 (2014).
9. D.McHugh, J.Twamley, Trapped-ion qutrit spin molecule quantum computer, *New J. Physics.* **7**(1),.174/1–9 (2005).
10. B.Klimov, R.Guzman, J.C.Retamal, C.Saavedra, Qutrit quantum computer with trapped ions, *Phys. Rev*. **A67**(6), 062313/1-7 (2003).
11. M.Lukac M.Perkowski and M.Kameyama, Evolutionary quantum logic synthesis of Boolean reversible logic circuits embedded in ternary quantum space using structural restrictions, in *Proc. IEEE Congress on Evolutionary Comput.*, Barcelona, 1–8 (2010).
12. V.Deibuk, Reversible/Quantum Ternary Arithmetic Logic Unit Design, *Int. J. Innovative Comput. Inf. and Control.* **12**(5), 1523–1533 (2016).
13. V.G.Deibuk, A.V.Biloshytskyi, Design of a ternary reversible/ quantum adder using genetic algorithm, *Int. J. Inform. Technol. Comp. Sci*. **7**(9), 38–45 (2015).
14. V.Deibuk, A.Biloshytskyi, Genetic synthesis of new reversible/quantum ternary comparator, *Adv. Electrical Comp. Engineering.* **15**(3), 147-152 (2015).
15. A.Muthukrishnan, C.R.Stroud, Jr., Multivalued logic gates for quantum computation, *Phys. Rev.* **A62**(5), 052309/1–8 (2000).
16. P.Kerntopf, M.A.Perkowski and M.H.A.Khan, On universality of general reversible multiple-valued logic gates, in *Proc. 34th Int. Symp. on Multiple-Valued Logic*, Toronto, 68-73 (2004).
17. M.L.Chuang, C.Y.Wang, Synthesis of reversible sequential elements, *ACM J. Emerg. Technol. Comput. Syst.* **3**(1), 1-19 (2008).
18. P.L.Singh, A.Majumder, B.Chowdhuri, A.J.Mondal, T.S.Sheghawat, Reducing delay and quantum cost in the novel design of reversible memory elements, *Procedia Computer Science.* **37**, 189-198 (2015).
19. M.H.A.Khan, J.E.Rice, Improved synthesis of reversible secuential circuits, in *Proc. IEEE Int. Symposium on Circuits and Systems (ISCAS)*, Montreal, 2302-2305 (2016).
20. H.Thapliyal, N.Radganathan, Design of reversible sequential circuits optimizing quantum cost, delay, and garbage outputs, *ACM J. Emerg. Technol. Comput. Syst*. **6**(4), 1-31 (2010).
21. J.E. Rice, An introduction to reversible latches, *Computer J.* **51**(6), 700-709 (2008).
22. P.Houshmand, M.Haghparast, Design of a novel quantum reversible ternary up-counter, *Int. J. Quantum Information.* **13**(5), 1550038/13p (2015).

23. A.Niknafs, M.Mohammadi, Synthesis and optimization of multiple-valued combinational and sequential reversible circuits with don't cares, *Integration, the VLSI J*. **46**(1), 189-196 (2013).
24. M.Mohammadi, M.Eshghi, M.Haghparast, On design of Multiple-valued sequential reversible circuits for nanotechnology based systems, in *Proc. IEEE Region 10 Conference.* Hyderabad, 1-6 (2008).
25. M.H.A.Khan, Design of ternary reversible sequential circuits, in *Proc. 8th International Conference on Electrical and Computer Engineering*, Dhaka, 140-143 (2014).
26. Z.Hu, I.Yuriychuk, V.Deibuk, Ternary reversible/quantum latches, in *Proc. IEEE First Ukraine Conf. on Electrical and Computer Engineering (UKRCON)*, Kyiv, 904-907 (2017).
27. T.A.Irving, S.G.Shiva, H.T.Nagle, Flip-flops for multiple-valued logic, *IEEE Transactions on Computers.* **C-25**, 237-346 (1976).
28. C.Qixiang, Multi-valued full-function flip-flops, in *Proc. IEEE Int. Conf. on Circuits and Systems*, China, 928-931 (1991).
29. A.Berut, A.Arakelyan, A.Petrosian, S.Ciliberto, R.Dillenschneider, E.Lutz, Experimental verification of Landauer's principle linking information and thermodynamics, *Nature* **486**(7388), 187-189 (2012).

Submitted 06.02.2018

Женьбін Ху[1]
Дейбук В. Г.[2,3] *докт. фіз.-мат. Наук*

[1]Школа інформаційних технологій в освіті, Класичний університет
центрального Китаю, Ухань, Китай;
[2]Інститут термоелектрики НАН і МОН України,
вул. Науки, 1, Чернівці, 58029, Україна;
[3]Чернівецький національний університет
ім. Ю.Федьковича, вул. Коцюбинського, 2,
Чернівці, 58012, Україна, *e-mail: v.deibuk@chnu.edu.ua*

КОНСТРУЮВАННЯ ТРІЙКОВИХ ЗВОРОТНИХ/КВАНТОВИХ ПОСЛІДОВНІСНИХ ЕЛЕМЕНТІВ

Широке застосування принципів зворотних обчислень дає можливість мінімізувати втрати енергії при роботі комп'ютерних пристроїв. Конструювання зворотних елементів пам'яті трійкової логіки є актуальним завданням, оскільки це необхідні пристрої сучасної електроніки. У праці синтезовано основні зворотні послідовнісні елементи трійкової логіки у базисі перестановочних одно- та двовходових логічних елементів, запропонованих. Матакришна та Строудом (MS-вентилі). Використовуючи поліпшений адаптивний генетичний алгоритм, ми запропонували трійкові зворотні D-, T- та JK-тригери та тригерні системи на їх основі. Трійкові зворотні T- та JK-тригери в цьому базисі синтезовано нами вперше. Запропонований алгоритм також використано для синтезу зворотного трійкового вентиля Фредкіна, що привело до зменшення його квантової вартості в порівнянні з відомими аналогами. Послідовнісні елементи, синтезовані в даній роботі, можуть бути побудовані з використанням квантових технологій рідинних іонних пасток, де було реалізовано MS-вентилі. Поліпшення отримано також щодо квантової вартості, числа постійних входів, часу затримки й числа

надлишкових виходів. Дана робота покликана привернути увагу фахівців у галузі термоелектрики до можливості застосування зворотної електроніки при створенні термоелектричних пристроїв. Бібл. 29, рис. 8, табл. 2
Ключові слова: тригери, зворотні обчислення, багатозначна логіка, генетичні алгоритми.

ЖеньбинХу[1]
Дейбук В. Г[2,3] *докт. физ.-мат. Наук*

[1]Школа информационных технологий в образовании, Классический университет центрального Китая, Ухань, Китай;
[2]Институт термоэлектричества, ул. Науки, 1, Черновцы, 58029, Украина
[3]Черновицкий национальный университет им. Ю.Федьковича, ул. Коцюбинского, 2, Черновцы, 58000, Украина
e-mail: v.deibuk@chnu.edu.ua

КОНСТРУИРОВАНИЕ ТРОИЧНЫХ ОБРАТИМЫХ/КВАНТОВЫХ ПОСЛЕДОВАТЕЛЬНОСТНЫХ ЭЛЕМЕНТОВ

Широкое применение принципов обратимых вичислений дает возможность минимизировать потери энергии при работе компьютерных устройств. Конструирование обратимых элементов памяти троичной логики является актуальной задачей, поскольку это необходимые устройства современной электроники. В работе синтезированы основные обратимые последовательностные элементы троичной логики в базисе перестановочных одно- и двухвходовых логических элементов, предложенных. Матакришна и Строудом (MS-гейты). Используя улучшенный адаптивный генетический алгоритм, мы предложили троичные обратимые D-, T- и JK-триггеры и триггерные системы. Троичные обратимые T- и JK-триггеры синтезированы впервые в этом базисе. Предложенный алгоритм также использован для синтеза обратимого троичного вентиля Фредкина, что привело к улучшению его квантовой стоимости по сравнению с известными аналогами. Последовательностные элементы, синтезированные в данной работе, могут быть построены с использованием квантовых технологий жидкостных ионных ловушек. Улучшения получены также в отношении квантовой стоимости, числа постоянных входов, времени задержки и числа избыточных выходов. Данная работа призвана привлечь внимание специалистов в области термоэлектричества к возможности применения обратимой электроники при создании термоэлектрических устройств. Библ. 29, рис. 8, табл. 2
Ключевые слова: триггеры, обратимые вычисления, многозначная логика, генетические алгоритмы.

References

1. R.Drechsler, R.Wille, Reversible circuits: Recent accomplishments and future challenges for an emerging technology, in: *Progress in VLSI Design and Test*, Springer, Berlin-Heidelberg, 383–392 (2012).
2. M.Nielsen, I.Chuang, *Quantum Computation and Quantum Information* (Cambridge University Press, Cambridge, 2000), 700 p..
3. Z.Li, S.Chen, X.Song, et al., Quantum circuit synthesis using a new quantum logic gate library of

NCV quantum gates, *Int. J. Theor. Phys.* **56**(4), 1023–1038 (2017).
4. D.M.Miller, M.A.Thornton, *Multiple-Valued Logic: Concepts and Representations* (Morgan & Claypool Publishers, 2008), 127 p..
5. R.Landauer, Irreversibility and heat generation in the computational process, *IBM J. Res. Develop*. **5**(1/2), 183–191 (1961).
6. C.H.Bennett, Logical reversibility of computation, *IBM J. Res. Develo*p. **17**(6), 525–532 (1973).
7. E.Fredkin and T.Toffoli, Conservative logic, *Int. J. Theor. Phys.* **21**(3/4), 219-253 (1982).
8. C.Moraga, On some basic aspects of ternary reversible and quantum computing," in *Proc. 44th IEEE Int. Symp. Multiple-Valued Logic*, Bremen, 178–183 (2014).
9. D.McHugh, J.Twamley, Trapped-ion qutrit spin molecule quantum computer, *New J. Physics.* **7**(1),.174/1–9 (2005).
10. B.Klimov, R.Guzman, J.C.Retamal, C.Saavedra, Qutrit quantum computer with trapped ions, *Phys. Rev*. **A67**(6), 062313/1-7 (2003).
11. M.Lukac M.Perkowski and M.Kameyama, Evolutionary quantum logic synthesis of Boolean reversible logic circuits embedded in ternary quantum space using structural restrictions, in *Proc. IEEE Congress on Evolutionary Comput.*, Barcelona, 1–8 (2010).
12. V.Deibuk, Reversible/Quantum Ternary Arithmetic Logic Unit Design, *Int. J. Innovative Comput. Inf. and Control.* **12**(5), 1523–1533 (2016).
13. V.G.Deibuk, A.V.Biloshytskyi, Design of a ternary reversible/ quantum adder using genetic algorithm, *Int. J. Inform. Technol. Comp. Sci*. **7**(9), 38–45 (2015).
14. V.Deibuk, A.Biloshytskyi, Genetic synthesis of new reversible/quantum ternary comparator, *Adv. Electrical Comp. Engineering.* **15**(3), 147-152 (2015).
15. A.Muthukrishnan, C.R.Stroud, Jr., Multivalued logic gates for quantum computation, *Phys. Rev.* **A62**(5), 052309/1–8 (2000).
16. P.Kerntopf, M.A.Perkowski and M.H.A.Khan, On universality of general reversible multiple-valued logic gates, in *Proc. 34th Int. Symp. on Multiple-Valued Logic*, Toronto, 68-73 (2004).
17. M.L.Chuang, C.Y.Wang, Synthesis of reversible sequential elements, *ACM J. Emerg. Technol. Comput. Syst.* **3**(1), 1-19 (2008).
18. P.L.Singh, A.Majumder, B.Chowdhuri, A.J.Mondal, T.S.Sheghawat, Reducing delay and quantum cost in the novel design of reversible memory elements, *Procedia Computer Science.* **37**, 189-198 (2015).
19. M.H.A.Khan, J.E.Rice, Improved synthesis of reversible secuential circuits, in *Proc. IEEE Int. Symposium on Circuits and Systems (ISCAS)*, Montreal, 2302-2305 (2016).
20. H.Thapliyal, N.Radganathan, Design of reversible sequential circuits optimizing quantum cost, delay, and garbage outputs, *ACM J. Emerg. Technol. Comput. Syst*. **6**(4), 1-31 (2010).
21. J.E. Rice, An introduction to reversible latches, *Computer J.* **51**(6), 700-709 (2008).
22. P.Houshmand, M.Haghparast, Design of a novel quantum reversible ternary up-counter, *Int. J. Quantum Information.* **13**(5), 1550038/13p (2015).
23. A.Niknafs, M.Mohammadi, Synthesis and optimization of multiple-valued combinational and sequential reversible circuits with don't cares, *Integration, the VLSI J*. **46**(1), 189-196 (2013).
24. M.Mohammadi, M.Eshghi, M.Haghparast, On design of Multiple-valued sequential reversible circuits for nanotechnology based systems, in *Proc. IEEE Region 10 Conference.* Hyderabad, 1-6 (2008).
25. M.H.A.Khan, Design of ternary reversible sequential circuits, in *Proc. 8th International Conference on Electrical and Computer Engineering*, Dhaka, 140-143 (2014).

26. Z.Hu, I.Yuriychuk, V.Deibuk, Ternary reversible/quantum latches, in *Proc. IEEE First Ukraine Conf. on Electrical and Computer Engineering (UKRCON)*, Kyiv, 904-907 (2017).
27. T.A.Irving, S.G.Shiva, H.T.Nagle, Flip-flops for multiple-valued logic, *IEEE Transactions on Computers*. **C-25**, 237-346 (1976).
28. C.Qixiang, Multi-valued full-function flip-flops, in *Proc. IEEE Int. Conf. on Circuits and Systems*, China, 928-931 (1991).
29. A.Berut, A.Arakelyan, A.Petrosian, S.Ciliberto, R.Dillenschneider, E.Lutz, Experimental verification of Landauer's principle linking information and thermodynamics, *Nature* **486**(7388), 187-189 (2012).

Submitted 06.02.2018

P.V. Gorskiy

P.V. Gorskiy, *Doctor Phys.-math. science*

Institute of Thermoelectricity of the NAS and MES of Ukraine,
1, Nauky str, Chernivtsi, 58029, Ukraine;
e-mail: anatych@gmail.com

THE ROLE OF ELEMENTARY GROWTH PROCESSES IN THE FORMATION OF SINGLE CRYSTALS OF THERMOELECTRIC MATERIALS BASED ON BISMUTH TELLURIDE

In the article, by solving the diffusion equation in the space of dimensions for a supercooled melt, it is shown that the high growth rate of single crystals of thermoelectric materials based on bismuth telluride over hexagonal cleavage planes in comparison with the rate of their growth along the C axis is due to a sharp distinction in the diffusion coefficients and self-diffusion in these materials in hexagonal plane and perpendicular to it. It is also established that these materials are characterized by anisotropy of the surface tension coefficient at the solid-melt boundary, which is expressed in the fact that this coefficient in the hexagonal plane is substantially greater than in the direction perpendicular to it. This ratio of surface tension coefficients causes the so-called "noncompetitive" form of the solid phase nucleus, whereby only this nucleus is capable of absorbing material from the melt and further growth. Because of this, seeding during growth of such crystals in the slot containers is not needed, because such is the solidified volume formed at the initial stage of crystallization in the coldest part of the slot container. Regardless of whether growth is carried out by horizontal or vertical recrystallization, the hexagonal cleavage planes of the single crystal will be parallel to the wide faces of the slot container, and the axis perpendicular to them will be the C-axis of the single crystal. Bibl. 11, Fig. 1.

Key words: diffusion in the space of dimensions, diffusion coefficient, surface tension coefficient, critical size, noncompetitive nucleus, quasi-to-dimensional growth, slot container, cleavage planes, C-axis of single crystal.

Introduction

Thermoelectric material is the most expensive part of a thermoelectric energy converter (generator or cooler). As a rule, with traditional growth technologies, single-crystal ingots of the material are obtained, for example, in the form of long circular or, more precisely, elliptical cylinders [1]. However, thermoelectric legs forming part of generators or coolers usually have the shape of rectangular parallelepipeds of low height and relatively large cross-sectional area. Therefore, when cutting the ingot into legs, up to 30 % of the material goes to waste which significantly increases the cost of finished products. Thus, the problem of developing and realizing such growth technology is urgent, which would allow us to obtain oriented single-crystal plates instead of cylinders, whose thickness would be equal to the thickness of the leg, and the cross-sectional area would allow us to obtain a sufficiently large number of legs after cutting. But for this it is necessary to know how the objective elementary processes of crystal growth dictated by the physical nature of a particular material, can contribute to, or, on the contrary, hinder, the solution of this problem. The elucidation of these issues with reference to thermoelectric materials based on bismuth telluride is the purpose of this article.

Anisotropy of the growth rate of crystals of thermoelectric materials based on bismuth telluride and its role in the growth of single crystals

Let us examine in more detail the physical reasons causing the anisotropy of the growth rate of thermoelectric materials based on bismuth telluride and the consequences resulting from this anisotropy. It is known that, other things being equal, the crystal growth rate coinciding with the velocity of the "melt-crystal" boundary is mainly determined by the diffusion coefficients (self-diffusion) and thermal conductivity of the material in the solid and liquid phases under given growth conditions [2 – 4]. Moreover, it is determined by the coefficients of surface tension at the boundaries between the solid and liquid phases and the boundaries of the melt and the solid phase with the walls of the container.

To clarify the reasons for the anisotropy of the growth rate of crystals based on bismuth telluride, we take into account that this crystal has a symmetry group R3m and has two unit cells: rhombohedral and hexagonal [1]. In the solid phase, the diffusion and self-diffusion coefficients along the hexagonal planes are several orders of magnitude higher than the similar coefficients in the direction perpendicular to these layers, i.e., along the so-called C axis. Exactly for this reason the suppressive growth of the crystal will occur along the cleavage planes. To prove this statement, we give the equation that we obtained describing the growth of a crystal from a nucleus or an oriented seed of a so-called supercritical size. In its derivation, an approach was used which is described in [5] and based on the so-called diffusion equation in the space of dimensions. Although this approach was developed for the case of crystal growth from supersaturated solutions, it allows a simple generalization in the case of crystal growth from supercooled melts. The solution of the diffusion equation in the space of dimensions found by us for this case is as follows:

$$t=\frac{4\gamma_s^2 V_m}{Dc_\infty\lambda_m^2}\left\{\frac{\exp\left(x_f\right)}{2x_f\left[1+\kappa+\exp\left(x_f\right)\right]^2}-\frac{\exp\left(x_i\right)}{2x_i\left[1+\kappa+\exp\left(x_i\right)\right]^2}+\frac{1}{2x_f^2\left[1+\kappa+\exp\left(x_f\right)\right]}-\right.$$
$$\left.-\frac{1}{2x_i^2\left[1+\kappa+\exp\left(x_i\right)\right]}+\sum_{l=1}^{\infty}\frac{l^2}{(1+\kappa)^l}\left[\mathrm{Ei}\left(lx_i\right)-\mathrm{Ei}\left(lx_f\right)\right]\right\}, \quad (1)$$

where t – growth time, γ_s – coefficient of surface tension at “liquid-solid phase” boundary, V_m – molecule volume, D – diffusion coefficient, c_∞ – the ratio of the number of molecules in the active seeding volume to the volume of molten zone, λ_m – melting heat per molecule, $\kappa = \Delta T / T_m$, ΔT – supercooling, $x_i = 2\gamma_s V_m /(\lambda_m r_i)$, $x_f = 2\gamma_s V_m /(\lambda_m r_f)$, r_i, r_f – the initial and finite radii of solid phase volume, conventionally assumed to be spherical. Function Ei(z) is determined as follows:

$$\mathrm{Ei}(z)=\mathrm{P}\int_{-\infty}^{z}\frac{\exp(x)}{x}dx. \quad (2)$$

In this case, the critical radius of the solid phase nucleus is:

$$r_c=2\gamma_s V_m/\left[\lambda_m\ln\left(1+\Delta T/T_m\right)\right]. \quad (3)$$

The time dependence of the radius of the solidified volume, described by Eq.(1), is shown in Fig.1.

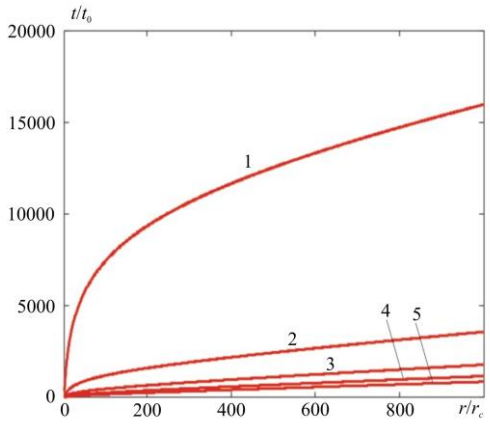

Fig.1. The time dependence of the radius of the solidified volume with different degrees of melt supercooling $\Delta T / T_m$: 1) 0.1; 2) 0.2; 3) 0.3; 4) 0.5.
The notation introduced in the figure is as follows: $t_0 = 4\gamma_s^2 V_m / D c_\infty \lambda_m^2$

It can be seen from the figure that the higher the degree of supercooling, the greater crystal growth rate. The estimation carried out according to Fig. 1 shows that this rate, if it is regulated by "diffusion in the space of dimensions" depends on the supercooling according to the law $v_g \infty (\Delta T)^{1.82}$. This estimate is close to those obtained in [6], although in it the deviation of the exponent from unity is associated with the presence of dislocation growth steps.

Eq. (1) admits a simple generalization for the case of anisotropic growth of a single crystal from a supercooled melt. For the case of crystals with hexagonal symmetry to which Bi_2Te_3 and alloys on its basis refer, two growth directions can be introduced: in the cleavage plane, in which the growth is isotropic and perpendicular to it. Then, instead of a single equation of the form (1), we must write two, which we represent in the form of one:

$$t_{\parallel,\perp} = \frac{4\gamma_{s\parallel,\perp}^2 V_m}{D_{\parallel,\perp} c_\infty (\lambda_m)^2} \left\{ \frac{\exp(x_{f\parallel,\perp})}{2x_{f\parallel,\perp}\left[1+\kappa+\exp(x_{f\parallel,\perp})\right]^2} - \frac{\exp(x_{i\parallel,\perp})}{2x_{i\parallel,\perp}\left[1+\kappa+\exp(x_{i\parallel,\perp})\right]^2} + \right.$$
$$+ \frac{1}{2x_{f\parallel,\perp}^2\left[1+\kappa+\exp(x_{f\parallel,\perp})\right]} - \qquad (4)$$
$$\left. - \frac{1}{2x_{i\parallel,\perp}^2\left[1+\kappa+\exp(x_{i\parallel,\perp})\right]} + \sum_{l=1}^{\infty} \frac{l^2}{(1+\kappa)^l}\left[\mathrm{Ei}(lx_{i\parallel,\perp}) - \mathrm{Ei}(lx_{f\parallel,\perp})\right] \right\}$$

Relation (3) with regard to growth anisotropy will be written as:

$$r_{c||,\perp} = 2\gamma_{s||,\perp} V_m / \left[\lambda_m \ln(1+\Delta T/T_m)\right]. \qquad (5)$$

It follows from Eq.(4) that if the coefficient of surface tension at the phase boundary is assumed to be isotropic, then along the cleavage planes the crystal must grow at least as many times faster than perpendicular to them, how many times the corresponding diffusion coefficients differ, i.e. based on the data of [1], it is approximately 3 – 5 orders of magnitude faster. If the real growth rates in the cleavage plane and perpendicular to it do not differ so much, this is most likely because the surface tension coefficient at the "liquid-solid phase" boundary is not completely isotropic, i.e. it is possible that not only $D_{||} > D_\perp$, but also $\gamma_{s||} > \gamma_{s\perp}$ and, consequently, as follows from the relation (5), $r_{c||} > r_{c\perp}$ Thus, for growth of single-crystal plates, the seed with the largest dimensions permissible by technological process in the

main growth directions and substantially smaller but exceeding the critical dimension in the direction perpendicular to them is preferred. However, if the relationship $r_{c||} >> r_{c\perp}$ holds, then seeding when growing a single crystal plate in the slot container is not needed, since the solidified volume formed at the initial stage in the coldest part of the melt-filled slot container is just such a seed, being the only and, therefore, noncompetitive supercritical nucleus. To it during further crystallization "adhere" oriented hexagonal columns, forming a plate.

Thus, single-crystal plates are obtained in the course of a noncompetitive quasi-two-dimensional growth. An additional factor providing such quasi-two-dimensionality is the anisotropy of the thermal conductivity of materials based on bismuth telluride, whose thermal conductivity in the hexagonal plane is greater than perpendicular to it [1].

The thermoelectric material thus obtained, other things being equal, would have a much higher degree of structural perfection and a higher degree of homogeneity of thermoelectric parameters along the length of the plate compared with materials obtained by other methods.

It is believed [1] that the high rate of diffusion of impurities in the direction of the cleavage planes is due to the weak coupling and large spacing between the layers Te (1) – *Te* (1). Diffusion of impurities perpendicular to the cleavage planes is difficult due to the presence of a tight packing of matrix atoms in this direction and a more complex coupling between them. However, the authors of [7] believe that a large difference between the diffusion coefficients in the hexagonal plane and perpendicular to it is due to a sharp difference in dislocation densities in these directions. On the other hand, from the evaluation formula given in [6] for the diffusion coefficient it follows that it is proportional to the vibration frequency of the molecules. And it should be greater in the hexagonal plane than in the direction perpendicular to it.

In view of the foregoing, it is clear that if a single crystal plate is produced by the horizontal recrystallization method, then the hexagonal planes of the single crystal will be parallel to those sides of the container in which the vectors of the temperature gradient and the acceleration of free fall lie simultaneously. And with vertical recrystallization, the predominant growth will occur along the wide sides of the container parallel to the temperature gradient, and the hexagonal planes will be parallel to them. And with vertical recrystallization, the predominant growth will occur along the wide sides of the container parallel to the temperature gradient, and the hexagonal planes will be parallel to them. The growth of the crystal along the narrow sides of the container parallel to the temperature gradient will be limited by the reaction forces exerted by the sides of the container, both on the melt and on the solid phase. Therefore, the axis perpendicular to the wide sides of the container parallel to the temperature gradient is, with an overwhelming probability, the *C*-axis of the single crystal.

The role of surface phenomena in the growth of single crystals of thermoelectric materials based on bismuth telluride

In [8 – 10], the influence of surface phenomena at the phase boundary on nucleation was considered with the growth of crystals from the melts. Let us apply the results of these studies to the analysis of the growth kinetics of crystals of thermoelectric materials from supercooled melts. In accordance with them, just as in accordance with relation (4), the rate of formation of nuclei of the solid phase decreases sharply with an increase in the surface tension coefficient at the wall-melt boundary, and, conversely, increases with decreasing this coefficient. Therefore, it makes sense to reduce the coefficient of surface tension at the "wide wall-melt" boundary and increase it at the "narrow wall-melt" boundary. This also follows from the equation of mechanical equilibrium of the solid phase nucleus on the container wall given in [10]. This can be achieved by placing, for example, along the narrow walls of the container the liners of other material

that has a greater surface tension coefficient at the boundary with the melt than that of the main container material. However, this need not be done if the ratio of the surface tension coefficients at the "container wall-melt" boundary and the reaction forces of the container walls are sufficient to suppress excessive growth in the direction of the *C*-axis.

Stabilization of the crystallization front

Taking into account the above, one can come to the conclusion that the most favorable for the growth of single-crystal plates is the crystallization front whose shape is closest to the flat. However, due to the concentration supercooling, a longitudinal inhomogeneity arises, which causes the stepped shape of the crystallization front [1]. The formation of concentration supercooling in the case when the equilibrium distribution coefficient of the impurity (for example, one of the components of the solid solution) is less than 1 can be explained as follows. The impurity accumulates at the crystallization front, and the liquidus temperature increases with increasing distance from the front. Therefore, with a small temperature gradient in the melt and a high growth rate, concentration supercooling occurs. According to the estimate carried out in [11], the critical value of the ratio of the temperature gradient *G* in the melt to the growth rate v is:

$$(G/v)_{cr} = \frac{mC_0(1-K_0)}{K_0 D_0}\ , \qquad (6)$$

where $m-$ the slope of the liquidus line, C_0 – the impurity concentration in the bulk of the melt, K_0 – coefficient of impurity distribution in the melt, D_0 – coefficient of impurity diffusion in the melt. If the ratio *G/v* is less than critical one determined by formula (6), then no concentration supercooling occurs. Thus, by relating the temperature gradient to the growth rate, it is possible to stabilize the crystallization front at the level of the minimum step height, and, therefore, the closest proximity of its shape to the flat one.

Conclusion

1. By solving the diffusion equation in the space of dimensions it is shown that the sharp anisotropy of the growth of bismuth telluride crystals from melts expressed in the predominant growth of these crystals along hexagonal cleavage planes is due to a sharp distinction in the diffusion coefficients in the hexagonal plane and perpendicular to it. It was found that the growth rate depends on the supercooling according to the law $v_g \propto (\Delta T)^{1.82}$.
2. Along with this, it was shown that bismuth telluride has a sharp anisotropy of the surface tension coefficient at the "melt-solid phase" boundary, expressed in the fact that in the hexagonal plane this coefficient is substantially greater than in the direction perpendicular to it.
3. The sharp anisotropy of surface tension coefficient causes specific, most preferable form of seed which must have the greatest dimensions in the hexagonal plane and a substantially smaller dimension, though exceeding the critical value, in the perpendicular direction. But then, when growing single-crystal plates of bismuth telluride in the slot container, seeding is not needed, since such is the solidified volume formed at the initial stage of crystallization in the coldest part of container. This volume, in fact, is the only noncompetitive nucleus to which during further crystallization “adhere” oriented hexagonal columns.
4. Thus, the hexagonal planes of a single crystal are parallel to the wide faces of the slot container, and the axis perpendicular to these faces is the C axis of the single crystal.

5. The above-mentioned features of the growth of bismuth telluride single crystals make it possible to effectively use the Bridgman method instead of the zone melting methods or the Czochralski method to obtain single-crystal plates, which greatly simplifies both the design and maintenance of equipment and the technological process.

The author considers it his pleasant duty to express his gratitude to academician L.I. Anatychuk for the proposed topic, the statement of the problem and the useful constructive discussion of the results obtained.

References

1. Goltsman B.M., Kudinov V.A., Smirnov I.A. (1972). *Poluprovodnikovyie termoelektricheskiye materialy na osnove Bi_2Te_3 [Semiconductor thermoelectric materials based on Bi_2Te_3]*. Moizhes B.Ya. (Ed.). M.: Nauka [in Russian].
2. Avdonin N.A. (1980). *Matematicheskoie opisaniie processov kristallizatsii [Mathematical description of crystallization processes]*. Riga: Zinatne [in Russian].
3. Strutynska L.T., Zhikharevich V.V. (2012). Simulation of Bi_2Te_3 thermoelectric material growth by vertical melting method. *J.Thermoelectricity*, 2, 79 – 87.
4. Anukhin A.I., Razinkov V.V. (2016). Crystallization of solid solutions of bismuth and antimony tellurides by zone melting and normal crystallization. *J.Thermoelectricity*, 1, 47 – 51.
5. Lifshits E.M., Pitaievskii L.P. (1979). *Fizicheskaia kinetika [Physical kinetics]*. M.:Nauka.
6. Hillig W., Turnbull D. (1956). Theory of crystal growth in undercooled pure liquids. *J. Chem. Phys.*, 24, 914.
7. Sagar A., Faust Jr. J.W. (1967). Dislocation studies in Bi_2Te_3 by etch-pit technique. *J. Appl. Phys.*, 38, 482-490.
8. Turnbull D., Fisher J.C. (1949). Rate of nucleation in condensed systems. *J. Chem. Phys.*, 17, 71 – 73.
9. Turnbull D. (1950). Formation of crystal nuclei in liquid metals. *J. Appl. Phys.*, 21, 1022 – 1028.
10. Turnbull D. (1950). Kinetics of heterogeneous nucleation. *J. Chem. Phys.*, 18, 198 – 203.
11. Tiller V. (1962). *V sbornike: Zhidkiie metally i zatverdevaniie [In: Liquid metals and solidification]*. M.: Metallurgizdat [in Russian].

Submitted 19.03.2018

Горський П.В. *докт. фіз.-мат. наук*

Інститут термоелектрики НАН і МОН України,
вул. Науки, 1,Чернівці, 58029, Україна,
e-mail: anatych@gmail.com

РОЛЬ ЕЛЕМЕНТАРНИХ ПРОЦЕСІВ РОСТУ У ФОРМУВАННІ МОНОКРИСТАЛІВ ТЕРМОЕЛЕКТРИЧНИХ МАТЕРІАЛІВ НА ОСНОВІ ТЕЛУРИДУ ВІСМУТУ

В статті шляхом розв'язання рівняння дифузії у просторі розмірів для переохолодженого розплаву показано, що велика швидкість росту монокристалів термоелектричних матеріалів на

основі телуриду вісмуту у гексагональних площинах спайності у порівнянні зі швидкістю їх росту вздовж С-вісі зумовлена різкою відмінністю коефіцієнтів дифузії та самодифузії у цих матеріалах у гексагональній площині та перпендикулярно до неї. Встановлено також, що цим матеріалам притаманна анізотропія коефіцієнта поверхневого натягу на межі «тверда фаза – розплав», яка полягає в тому, що цей коефіцієнт у гексагональній площині істотно більше, ніж у перпендикулярному до неї напрямку. Таке співвідношення коефіцієнтів поверхневого натягу зумовлює так звану «безконкурентну» форму зародка твердої фази, за якої лише він здатен до поглинання матеріалу з розплаву и подальшого росту. Внаслідок цього затравка при вирощуванні таких кристалів у щілинних контейнерах не потрібна, оскільки такою є затвердлий об'єм, утворений на початковій стадії кристалізації у найбільш холодній частині щілинного контейнера. Незалежно від того, здійснюється вирощування методом горизонтальної чи вертикальної перекристалізації, гексагональні площини спайності монокристалу будуть паралельні до широких граней щілинного контейнера, а вісь, перпендикулярна до них, буде С-віссю монокристалу. Бібл. 11, Рис. 1.

Ключові слова: дифузія у просторі розмірів, коефіцієнт дифузії, коефіцієнт поверхневого натягу, критичний розмір, безконкурентний зародок, квазідвовимірний ріст, щілинний контейнер, площини спайності, С-вісь монокристалу.

Горский П.В., *докт. физ.-мат. наук*

Институт термоэлектричества, ул. Науки, 1, Черновцы, 58029, Украина
e-mail: anatych@gmail.com

РОЛЬ ЭЛЕМЕНТАРНЫХ ПРОЦЕССОВ РОСТА В ФОРМИРОВАНИИ МОНОКРИСТАЛЛОВ ТЕРМОЭЛЕКТРИЧЕСКИХ МАТЕРИАЛОВ НА ОСНОВЕ ТЕЛЛУРИДА ВИСМУТА

В статье посредством решения уравнения диффузии в пространстве размеров для переохлажденного расплава показано, что большая скорость роста монокристаллов термоэлектрических материалов на основе теллурида висмута по гексагональным плоскостям спайности в сравнении со скоростью их роста вдоль С-оси обусловлена резким различием коэффициентов диффузии и самодиффузии в этих материалах в гексагональной плоскости и перпендикулярно к ней. Установлено также, что этим материалам присуща анизотропия коэффициента поверхностного натяжения на границе «твердая фаза – расплав», выражающаяся в том, что этот коэффициент в гексагональной плоскости существенно больше, чем в перпендикулярном к ней направлении. Такое соотношение коэффициентов поверхностного натяжения обуславливает так называемую «бесконкурентную» форму зародыша твердой фазы, при которой только он способен к поглощению материала из расплава и дальнейшему росту. Вследствие этого затравка при выращивании таких кристаллов в щелевых контейнерах не нужна, ибо таковой является отвердевший объем, образовавшийся на начальной стадии кристаллизации в наиболее холодной части щелевого контейнера. Независимо от того, осуществляется ли выращивание методом горизонтальной или вертикальной перекристаллизации, гексагональные плоскости спайности монокристалла будут параллельны широким граням щелевого контейнера, а ось, перпендикулярная к ним, будет С-осью монокристалла. Библ. 11, Рис. 1.

Ключевые слова: диффузия в пространстве размеров, коэффициент диффузии, коэффициент поверхностного натяжения, критический размер, бесконкурентный зародыш, квазидвумерный рост, щелевой контейнер, плоскости спайности, С-ось монокристалла.

References

1. Goltsman B.M., Kudinov V.A., Smirnov I.A. (1972). *Poluprovodnikovyie termoelektricheskiye materialy na osnove Bi_2Te_3 [Semiconductor thermoelectric materials based on Bi_2Te_3]*. Moizhes B.Ya. (Ed.). M.: Nauka [in Russian].
2. Avdonin N.A. (1980). *Matematicheskoie opisaniie processov kristallizatsii [Mathematical description of crystallization processes]*. Riga: Zinatne [in Russian].
3. Strutynska L.T., Zhikharevich V.V. (2012). Simulation of Bi_2Te_3 thermoelectric material growth by vertical melting method. *J.Thermoelectricity*, 2, 79 – 87.
4. Anukhin A.I., Razinkov V.V. (2016). Crystallization of solid solutions of bismuth and antimony tellurides by zone melting and normal crystallization. *J.Thermoelectricity*, 1, 47 – 51.
5. Lifshits E.M., Pitaievskii L.P. (1979). *Fizicheskaia kinetika [Physical kinetics]*. M.:Nauka.
6. Hillig W., Turnbull D. (1956). Theory of crystal growth in undercooled pure liquids. *J. Chem. Phys.*, 24, 914.
7. Sagar A., Faust Jr. J.W. (1967). Dislocation studies in Bi_2Te_3 by etch-pit technique. *J. Appl. Phys.*, 38, 482-490.
8. Turnbull D., Fisher J.C. (1949). Rate of nucleation in condensed systems. *J. Chem. Phys.*, 17, 71 – 73.
9. Turnbull D. (1950). Formation of crystal nuclei in liquid metals. *J. Appl. Phys.*, 21, 1022 – 1028.
10. Turnbull D. (1950). Kinetics of heterogeneous nucleation. *J. Chem. Phys.*, 18, 198 – 203.
11. Tiller V. (1962). *V sbornike: Zhidkiie metally i zatverdevaniie [In: Liquid metals and solidification]*. M.: Metallurgizdat [in Russian].

Submitted 19.03.2018

S. Bhattacharya

S. Bhattacharya[1], *doctor, assistant research professor*
H. J. Goldsmid[2], *doctor*

[1]Department of Physics and Astronomy, Clemson Nanomaterials Institute, Clemson University, Clemson, SC, USA; *e-mail: bbhatta@g.clemson.edu*

H. J. Goldsmid

[2]School of Physics, University of New South Wales, Sydney, Australia *e-mail: hjgoldsmid@bigpond.com*

DETERMINATION OF THE THERMOELECTRIC FIGURE OF MERIT THROUGH THE MAXIMUM TEMPERATURE DEPRESSION USING THE PELTIER COOLING EFFECT

It is well known that the maximum temperature depression that can be obtained by means of the Peltier effect is simply related to the figure of merit, Z, of a thermocouple. However, for good thermoelectric materials, with ZT of the order of unity or greater, this temperature depression, T, can be very large and it is difficult to assign the measurement to a particular temperature. This is less of a problem if the thermocouple consists of a semiconductor and a metal since ZT and T_{max} are then much smaller. We show that the measurement of T_{max} for a semiconductor-metal couple can yield a value for the dimensionless figure of merit, T, of the semiconductor. We also show that there are attractive features in the measurement of T_{max} for a couple, in which the ratio of the form factors for the two branches is very far from optimised. Bibl. 5, Fig. 2.
Key words: thermoelectricity; Peltier cooling; figure of merit; measurement.

Introduction

It has long been realised that the figure of merit, Z, of a thermocouple is simply related to the maximum temperature depression, $\Delta T_{\max}$, which can be achieved using the Peltier effect [1]. The relationship is

$$\Delta T_{\max} = \frac{1}{2} Z T_c^2 , \tag{1}$$

where T_c is the cold junction temperature. However, when ZT is of the order of unity or greater, $\Delta T_{\max}$ may be more than 100 K and it is difficult to assign the value of Z to any particular temperature. Furthermore, the figure of merit in this equation is that for a thermocouple, whereas we are usually more interested in the figure of merit, z, for a single material. Here we shall consider the situation in which the thermocouple consists of a semiconductor, with a high positive or negative Seebeck coefficient, joined to a metal that has a Seebeck coefficient close to zero.

Principle of the Method

One of our present aims is to show that the need for a second branch is actually an advantage in the determination of z for a single material. It will be assumed that the second branch is a metal, for which the transport properties are well established. The figure of merit of a couple, with optimised length to width ratios for the branches, is given by

$$z = \frac{\left(\alpha_S - \alpha_M\right)^2}{\left\{\left(\lambda_S / \sigma_S\right)^{1/2} + \left(\lambda_M / \sigma_M\right)^{1/2}\right\}^2}. \tag{2}$$

Here α, σ and λ are the Seebeck coefficient, electrical conductivity and thermal conductivity respectively and the subscripts S and M refer to the semiconducting and metallic branches of the couple. For the metallic branch, the Seebeck coefficient, α_M, will usually be close to zero and λ_M/σ_M will have the value, given by the Wiedemann-Franz-Lorenz law, $(\pi^2/3)(k/e)^2T$. For most thermoelectric materials λ_S/σ_S will not be very much greater than the WFL value and Z will be of the order of $z_S/4$ where

$$z_S = \frac{\alpha_S^2 \sigma_S}{\lambda_S}, \tag{3}$$

z_S being the single-material figure of merit. This means that, if $z_S T$ is close to unity, ΔT_{max} for the semiconductor – metal couple will probably be less than about 30 K. Thus, the value of Z given by the measurement will be representative of a fairly narrow temperature range. The range can be further narrowed if the form factor for the metal branch departs from its optimum value. Generally,

$$z = \frac{\left(\alpha_S - \alpha_M\right)^2}{KR}, \tag{4}$$

where $K = (\lambda_S A_S/L_S + \lambda_M A_M/L_M)$ and $R = (\rho_S L_S/A_S + \rho_M L_M/A_M)$. L represents length, A is cross-section area and ρ is electrical resistivity.

It is realised that the determination of ZT does not immediately give a value for z_S. Even so, one obvious benefit of the ΔT_{max} method is a definite confirmation of any high zT value as indicated by other measurements. There is no way that ΔT_{max} can be large unless the figure of merit is large. On the other hand, alternative methods of finding the thermoelectric properties often lead to an over-optimistic value of the figure of merit.

For example, suppose that the Harman method [2] is being used. In this technique the electrical resistance is determined under adiabatic and isothermal conditions. The ratio of these resistances should be equal to $(zT + 1)$. This is certainly true if the material is homogeneous but it can be erroneous if an inhomogeneous sample is being tested [3]. In an extreme case, suppose that the sample consists of more-or-less equal parts of p-type and n-type material, so that the overall Seebeck coefficient is zero. The true figure of merit must then, of course, also be zero even though the finite difference between the isothermal and adiabatic resistances would suggest otherwise.

Using the ΔT_{max} method, the figure of merit, z_S, and the ratio σ_S/λ_S for the semiconductor can be determined from ZT if the Seebeck coefficient, α_S, is known. It is noted that the Seebeck coefficient is probably the easiest of the three thermoelectric parameters to determine since it does not depend on the dimensions of the sample [4].

The product KR is given by

$$KR = \left(\lambda_S \frac{A_S}{L_S} + \lambda_M \frac{A_M}{L_M}\right)\left(\frac{L_S}{\sigma_S A_S} + \frac{L_M}{\sigma_M A_M}\right), \tag{5}$$

which may be rewritten as

$$KR = \frac{\lambda_S}{\sigma_S} + \frac{\lambda_M}{\sigma_M} + \frac{\lambda_S}{\sigma_M} F + \frac{\lambda_M}{\sigma_S}\frac{1}{F} \tag{6}$$

where $F = A_S L_M / A_M L_S$. It can be assumed that λ_M and σ_M are both known and σ_S is determined separately so equation (6) allows us to relate λ_S to KR.

As an example, let us consider a couple consisting of an n-type bismuth telluride alloy and pure nickel. We use data for the bismuth telluride alloy (exf8h-SPS) based on those given in the paper by Puneet et al. [5]. The selected parameters are:

$(\alpha_S - \alpha_M)$ = -123 μV/K, σ_S = 0.16 x 10^6 S/m, λ_S = 1.6 W/m K, σ_M = 14.6 x 10^6 S/m and λ_M = 94.1 W/m K.

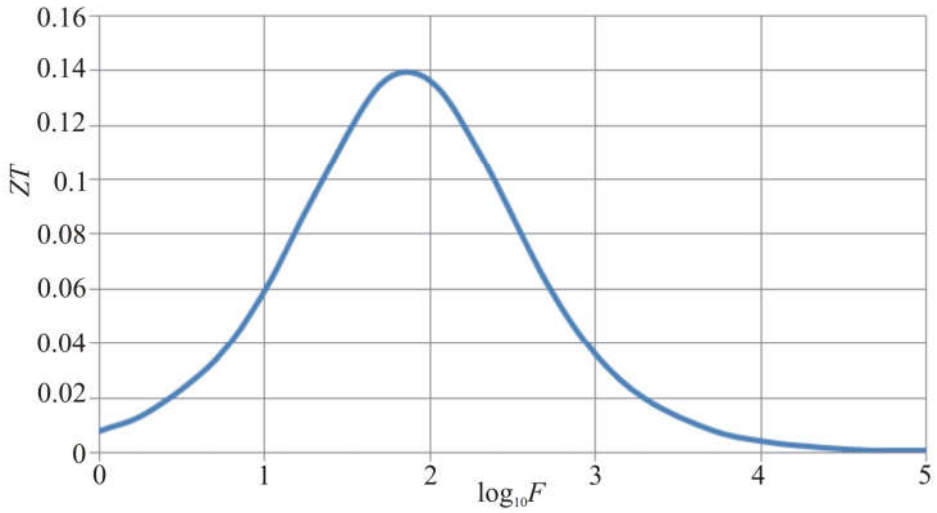

Fig. 1. Plot of ZT against $\log_{10} F$ where F, the form factor ratio, is equal to $A_S L_M / A_M L_S$. The semiconducting branch is an n-type bismuth telluride alloy with properties close to those reported by Puneet et al. [5]. The metallic branch is made from nickel.

Fig. 1 shows the variation of ZT with F over 5 decades of the form factor ratio. The maximum ZT of about 0.14 occurs when F is about 70. At this value of ZT, ΔT_{max} at room temperature is equal to about 21 K. This still implies some uncertainty as to the temperature for which the results apply. By changing F by an order of magnitude lower or higher than its optimum value, ZT is reduced to about 0.04 and ΔT_{max} becomes about 6º. This is large enough to measure accurately yet small enough for the temperature of measurement to be well defined.

As observed from Figure 1, the thermocouple will have its highest figure of merit when KR has its minimum value and this will occur when $F^2 = \lambda_M \sigma_M / \lambda_S \sigma_S$. At this value of F,

$$(KR)_{\min} = \left(\frac{\lambda_S^{1/2}}{\sigma_S^{1/2}} + \frac{\lambda_M^{1/2}}{\sigma_M^{1/2}} \right)^2 , \qquad (7)$$

It is noted that the optimum value of F can be calculated if ΔT_{max} is determined using at least three different form factor ratios.

Non-Optimised Form Factor Ratio

We now examine in more detail the situation when the metal branch is not optimised and, in particular, we look at the effect of making this branch either very short or very long. This has the advantage of reducing ΔT_{max} still further and, therefore, the data can be assigned to an even narrower temperature range.

Let us first suppose that the ratio of length to cross-section area for the metal branch is much less than its optimum value. Then, $K_M >> K_S$ and $R_S >> R_M$. Applying this condition, we find that $KR \approx K_M R_S$ and the approximate value for ZT is $\alpha^2 T/K_M R_S$. This enables us to estimate R_S and, thus, the electrical conductivity of the semiconductor. However, it is probably easier to determine σ_S more directly. In this context we must remind ourselves that the potential drop across a sample includes a Seebeck contribution as well as one due to electrical resistance. The Seebeck contribution is sometimes eliminated by using an alternating current but we suggest that a better method may be to increase the direct current until the Peltier cooling and Joule heating just balance one another and ΔT becomes zero. Surprisingly, this approach does not seem to have been widely used.

If the ratio of length to cross-section area for the metal branch is much greater than the optimum value, ZT becomes approximately equal to $\alpha^2 T/K_S R_M$, allowing us to estimate K_S and, thence, the thermal conductivity of the semiconductor.

It is of interest to consider the expression for KR, equation (6) when F is very much larger than its optimum value. We adopt two different approximations. In approximation #1 we ignore all but the largest term in the expression for KR so that $KR \approx \lambda_S A_S L_M/L_S \sigma_M A_M$, allowing λ_S to be estimated. However, as shown in Figure 2 (upper curve), the resulting value of ZT is not particularly close to the true value unless F is at least 2 orders of magnitude greater than its optimum. When F is this large, ZT is too small to be determined accurately.

In approximation #2 we include the first two terms on the right-hand side of equation (6) but we replace $(\lambda_S/\sigma_S + \lambda_M/\sigma_M)$ by $2\,\lambda_M/\sigma_M$ so that

$$KR = 2\frac{\lambda_M}{\sigma_M} + \frac{\lambda_S}{\sigma_M} F \tag{8}$$

Our justification for doing this is that, for a good thermoelectric material, the ratio of thermal to electrical conductivity is unlikely to be very much greater than the Wiedemann-Franz value. Also, the first two terms on the right-hand side of equation (6) are small compared with the third term. The lower curve in Figure 2 shows the ratio of ZT from this approximation to its true value. This approximate value of ZT, denoted by $Z_{\text{approx}}T$, differs by no more than about 3% from the true value when F is an order of magnitude greater than its optimum. Thus, equation (8) enables us to make a rapid determination of the thermal conductivity of the semiconductor.

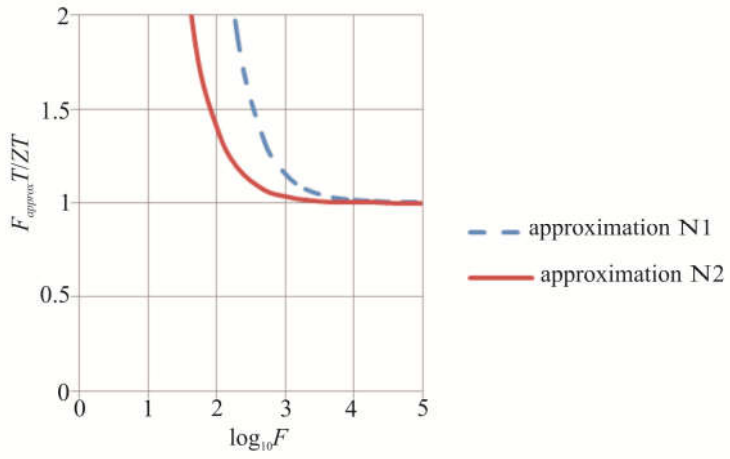

Fig. 2. Plot of $Z_{approx}T/ZT$ against $\log_{10}F$. In approximation #1, $Z_{approx}T \approx \alpha^2 T/K_M R_S$ and in approximation #2, $Z_{approx}T \approx \alpha^2 T/K_M R_S + 2\,\lambda_M/\sigma_M$.

Finally, we must point out that no account has been taken of transfer of heat by radiation or by conduction along the electrical leads. As in other thermal conductivity measurements, the loss terms can be determined if measurements are made on samples with different lengths and cross-sections.

Conclusion

To summarise, it is emphasised that the measurement of the maximum temperature depression, ΔT_{max}, is an indisputable way of validating any claim of a high figure of merit for a new thermoelectric material. The value of ΔT_{max} for a couple between this material and a metal is substantially less than it would be if both the negative and positive branches were good thermoelectric materials. The resulting figure of merit can, therefore, be assigned to a fairly narrow range of temperature. It has been shown that by selecting three different form factors for the metallic branch the optimum dimensions can be deduced, allowing the ratio of electrical to thermal conductivity in the semiconductor to be found. The Seebeck coefficient of the semiconductor is easily determined since it does not depend on the dimensions of the sample. Thus, the single-material figure of merit is obtained.

We have shown that it is advantageous to measure the maximum temperature depression, ΔT_{max}, when the ratio of length to cross-section area for the metal branch is much greater than the optimum value. ΔT_{max} can then be reduced to no more than a few degrees, so that $z_S T$ can be assigned to a particular temperature.

The calculation of $z_S T$ requires the knowledge of the electrical conductivity of the semiconductor. In principle, this can be found from a measurement of ΔT_{max} when the ratio of length to cross-section area for the metal branch is much less than the optimum value. However, it is probably more convenient to determine the electrical resistance of the semiconductor directly using a current that is large enough to make ΔT equal to zero.

References

1. Ioffe, A. F., *Semiconductor Thermoelements and Thermoelectric Refrigeration*, London, Infosearch, (1956), p. 99.
2. Harman, T.C., "Special techniques for measurement of thermoelectric properties", J. Appl. Phys., **29**, 1373 (1958).
3. Goldsmid, H. J., J. Thermoelectricity, "Experiments on the direct measurement of the thermoelectric figure of merit", No. 1, 5 (2006).
4. Goldsmid, H. J., *Introduction to Thermoelectricity*, Second Edition, Heidelberg, Springer, (2016), p. 131.
5. Puneet, P., Podila, R., Karakaya, M., Zhu, S., He, J., Tritt, T. M., Dresselhaus, M. S., and Rao, A. M., "Preferential scattering by interfacial charged defects for enhanced thermoelectric performance in few-layered n-type Bi_2Te_3". P. Sci. Reports, **3**, 3212 (2013).

Submitted 15.02.2018

Бхаттачарія С.,[1] *доктор, асистент-професор*,
Голдсмід Х. Дж.,[2] *доктор наук*

[1]Факультет фізики та астрономії, Інститут наноматеріалів Клемсону,
Університет Клемсону, шт. Південна Кароліна, США
e-mail: arao@g.clemson.edu;

[2]Школа фізики, Університет Нового Південного Уельсу, Сідней, Австралія
e-mail: hjgoldsmid@bigpond.com

ВИЗНАЧЕННЯ ТЕРМОЕЛЕКТРИЧНОЇ ДОБРОТНОСТІ ЧЕРЕЗ МАКСИМАЛЬНЕ ЗНИЖЕННЯ ТЕМПЕРАТУРИ ПРИ ВИКОРИСТАННІ ЕФЕКТУ ОХОЛОДЖЕННЯ ПЕЛЬТЬЄ

Добре відомо, що максимальне зниження температури, яке можна отримати з допомогою ефекту Пельтьє, пов'язане простим співвідношенням з добротністю, Z термопари. Однак для добрих термоелектричних матеріалів, у яких ZT порядку одиниці або вище, таке зниження температури ΔT може бути дуже великим, і важко віднести вимірюване значення до конкретної температури. Це не проблема, якщо термопара складається з напівпровідника й металу, оскільки ZT та ΔT_{max} в цьому випадку істотно менше. Ми покажемо, що вимірювання ΔT_{max} для пари напівпровідник-метал може дати значення безрозмірної добротності ZT напівпровідника. Ми також покажемо, що існують особливості у вимірюванні ΔT_{max} для пари, у якій співвідношення форм-факторів для двох гілок дуже далеке від оптимізованого. Бібл. 5, Рис. 2.

Ключові слова: термоелектрика, охолодження Пельтье, добротність, вимірювання.

Бхаттачария С.,[1] *доктор, асистент-професор*,
Голдсмид Х. Дж.,[2] *доктор наук*

[1]Факультет физики и астрономии, Институт наноматериалов Клемсона,
Университет Клемсона, шт.Южная Каролина, США;
e-mail: arao@g.clemson.edu;
[2]Школа физики, Университет Нового Южного Уэльса,
Сидней, Австралия; *e-mail: e-mail: hjgoldsmid@bigpond.com*

МАКСИМАЛЬНОЕ СНИЖЕНИЕ ТЕМПЕРАТУРЫ ПРИ ИСПОЛЬЗОВАНИИ ЭФФЕКТА ОХЛАЖДЕНИЯ ПЕЛЬТЬЕ

Хорошо известно, что максимальное снижение температуры, которое может быть получено с помощью эффекта Пельтье, связано простым соотношением с добротностью Z термопары. Однако для хороших термоэлектрических материалов, у которых ZT порядка единицы или выше, такое снижение температуры ΔT может быть очень большим, и трудно отнести измеренное значение к конкретной температуре. Это не проблема, если термопара состоит из полупроводника и металла, поскольку ZT и ΔT_{max} в этом случае намного меньше. Мы покажем, что измерение ΔT_{max} для пары полупроводник-металл может дать значение безразмерной добротности zT полупроводника. Мы также покажем, что существуют особенности в измерении ΔT_{max} для пары, в которой соотношение форм-факторов для двух ветвей очень далеко от оптимизированного. Библ. 5, Рис. 2.

Ключевые слова: термоэлектричество, охлаждение Пельтье, добротность, измерение.

References

1. Ioffe, A. F., *Semiconductor Thermoelements and Thermoelectric Refrigeration*, London, Infosearch, (1956), p. 99.
2. Harman, T.C., "Special techniques for measurement of thermoelectric properties", J. Appl. Phys., **29**, 1373 (1958).
3. Goldsmid, H. J., J. Thermoelectricity, "Experiments on the direct measurement of the thermoelectric figure of merit", No. 1, 5 (2006).
4. Goldsmid, H. J., *Introduction to Thermoelectricity*, Second Edition, Heidelberg, Springer, (2016), p. 131.
5. Puneet, P., Podila, R., Karakaya, M., Zhu, S., He, J., Tritt, T. M., Dresselhaus, M. S., and Rao, A. M., "Preferential scattering by interfacial charged defects for enhanced thermoelectric performance in few-layered n-type Bi_2Te_3". P. Sci. Reports, **3**, 3212 (2013).

Submitted 15.02.2018

L. I. Anatychuk

L.I. Anatychuk[1,2] *acad. National Academy of Sciences of Ukraine,*
A.V. Prybyla[1,2] *Candidate Phys.-math. Sciences*

[1]Institute of Thermoelectricity of the NAS and MES of Ukraine, 1, Nauky str, Chernivtsi, 58029, Ukraine;
[2]Yu.Fedkovych Chernivtsi National University, 2, Kotsiubynskyi str., Chernivtsi, 58000, Ukraine
e-mail: anatych@gmail.com

A. V. Prybyla

OPTIMIZATION OF HEAT EXCHANGE SYSTEM OF THERMOELECTRIC LIQUID-LIQUID HEAT PUMP

This paper presents the results of optimization of heat exchange system of thermoelectric liquid-liquid heat pump and determines conditions fort its efficiency increase, in particular, for its use as a high-performance heater for space –purpose water regeneration device. Bibl. 3, Fig. 5.
Key words: thermoelectric heat pump, efficiency, distillation unit, heat exchanger.

Introduction

General characterization of the problem. Efficiency improvement of thermoelectric heat pumps (THP) that have found application in various-purpose cooling and heating systems [1 - 5] is an important and complicated task that can be solved with the use of modern computer design methods [6, 7]. Also, an important fact is that the achieved values of THP efficiency are close to the limit, which requires their research taking into account the most accurate and complete physical models.

In papers [7, 8], a study was conducted to determine the influence of the quality of heat exchange system on the efficiency of liquid-liquid thermoelectric heat pump, in particular the effect of energy consumption on heat carrier pumping. It was established that optimization of heat exchange system of THP is an important factor of increasing overall THP efficiency.

The purpose of the work is optimization of heat exchange system of thermoelectric liquid-liquid thermal pump in order to improve its overall efficiency.

Physical model

The investigations were carried out using a physical model of THP liquid heat exchanger which is represented in Fig.1. Heat carrier *3* with flow rate *G* circulates in heat exchanger channels *2*. Heat flux Q_1 through the heat exchanger base *1* is transferred to heat carrier as a result of which its temperature varies from T_1 to T_2. For the intensification of heat exchange, the rod of variable diameter (Fig.2), located inside the heat exchanger channel, is used.

On the whole, a physical model of THP comprises a system of identical heat exchangers *1* in Fig.3 assuring passage of heat flux Q_h through the hot side of thermoelectric modules, thermoelectric modules *3* in Fig.3, heat exchangers *2* in Fig.3 assuring passage of heat flux Q_X through the cold side of thermoelectric modules and a system of hydraulically bound channels *4* in Fig.3 providing for circulation of liquid in the thermoelectric heat pump.

The model takes into account temperature difference loss in heat exchangers, as well as energy

consumption on pumping of heat carrier through heat exchange system.

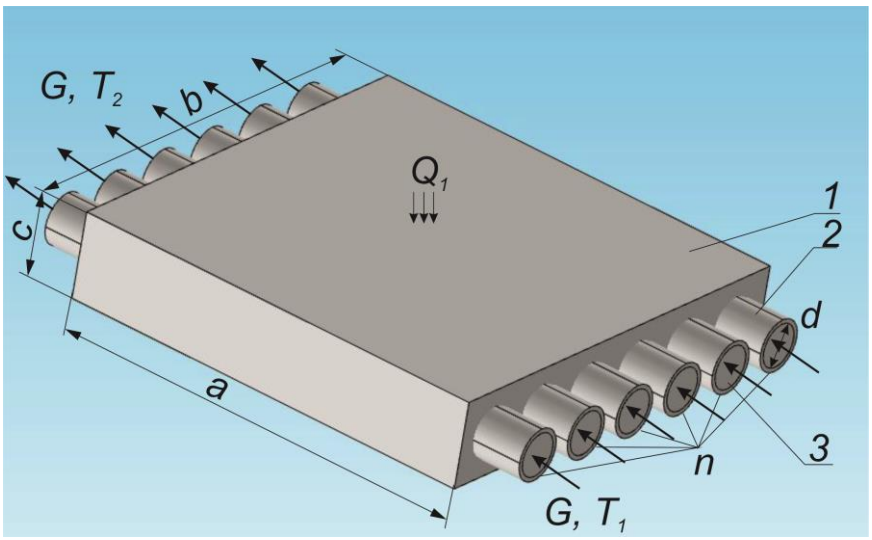

Fig. 1. Physical model of liquid heat exchanger of thermoelectric heat pump:
1 – heat exchanger base, 2 – heat exchanger channels, 3 –heat carrier

To assure optimal operation of thermoelectric modules, each of them has individual power supply.

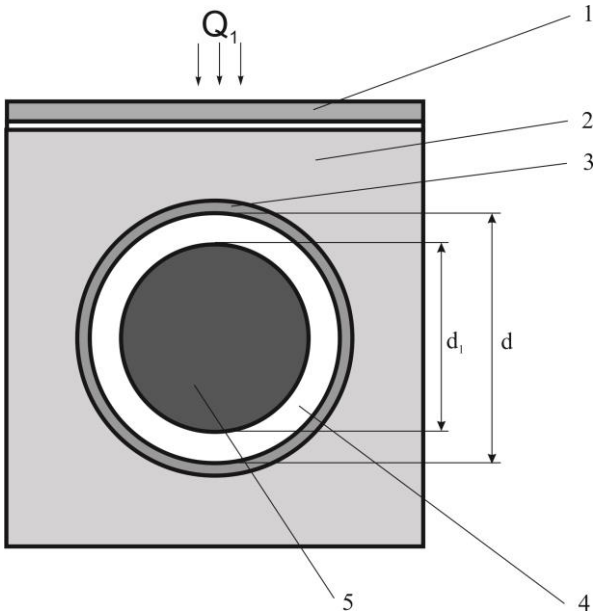

Fig. 2. Fragment of liquid heat exchanger of thermoelectric heat pump in section:
1 – thermoelectric module location, 2 – heat exchanger base, 3 – heat exchanger channel,
4 – heat carrier, 5 –heat exchange intensifier.

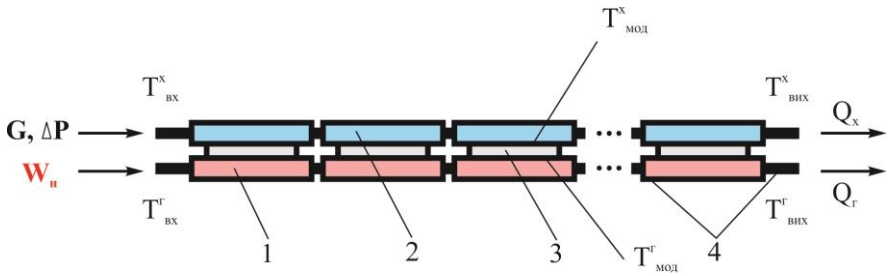

Fig. 3. Physical model of thermoelectric heat pump.

Mathematical and computer description of the model

To describe heat and electric current fluxes, we will use the laws of conservation of energy

$$div\vec{E} = 0 \tag{1}$$

and electric charge

$$div\vec{j} = 0, \tag{2}$$

where

$$\vec{E} = \vec{q} + U\vec{j}, \tag{3}$$

$$\vec{q} = \kappa\nabla T + \alpha T\vec{j}, \tag{4}$$

$$\vec{j} = -\sigma\nabla U - \sigma\alpha\nabla T. \tag{5}$$

Here, $\vec{E}$ is energy flux density, $\vec{q}$ is thermal flux density, $\vec{j}$ is electric current density, U is electric potential, T is temperature, α, σ, κ are the Seebeck coefficient, electric conductivity and thermal conductivity.

With regard to (3) – (5), one can obtain

$$\vec{E} = -(\kappa + \alpha^2\sigma T + \alpha U\sigma)\nabla T - (\alpha\sigma T + U\sigma)\nabla U. \tag{6}$$

Then the laws of conservation (1), (2) will acquire the form:

$$-\nabla\left[(\kappa + \alpha^2\sigma T + \alpha U\sigma)\nabla T\right] - \nabla\left[(\alpha\sigma T + U\sigma)\nabla U\right] = 0, \tag{7}$$

$$-\nabla(\sigma\alpha\nabla T) - \nabla(\sigma\nabla U) = 0. \tag{8}$$

These nonlinear differential equations of second order in partial derivatives (7) and (8) determine the distribution of temperature T and potential U in thermoelements.

An equation describing the process of heat transport in the walls of heat exchangers in the steady-state case is written as follows:

$$\nabla(-k_1 \cdot \nabla T_1) = Q_1. \tag{9}$$

where k_1 is thermal conductivity of heat exchanger walls, ∇T_1 is temperature gradient, Q_1 is heat flux.

The processes of heat-and-mass transfer of heat carriers in heat exchanger channels in the steady-state case are described by equations [9]

$$-\Delta p - f_D \frac{\rho}{2d_h} v|\vec{v}| + \vec{F} = 0, \tag{10}$$

$$\nabla(A\rho\vec{v}) = 0, \tag{11}$$

$$\rho AC_p\vec{v} \cdot \nabla T_2 = \nabla \cdot Ak_2\nabla T_2 + f_D \frac{\rho A}{d_h}|\vec{v}|^3 + Q_2 + Q_{wall}, \tag{12}$$

where p is pressure, ρ is heat carrier density, A is cross-section of the tube, $\vec{F}$ is the sum of all forces, C_p is heat carrier heat capacity, T_2 is temperature, $\vec{v}$ is velocity vector, k_2 is heat carrier thermal

conductivity, f_D is the Darcy coefficient, $d = \frac{4A}{Z}$ is effective diameter, Z is perimeter of tube wall, Q_2 is heat which is released due to viscous friction [W/m] per unit length of heat exchanger, Q_{wall} is heat flux coming from the heat carrier to the tube walls [W/m]

$$Q_{wall} = h \cdot Z \cdot (T_1 - T_2), \tag{13}$$

where h is heat exchange coefficient which is found from equation

$$h = \frac{Nu \cdot k_2}{d}. \tag{14}$$

The Nusselt number is found with the use of the Gnielinski equation ($3000 < Re < 6 \cdot 10^6$, $0.5 < Pr < 2000$)

$$Nu = \frac{\left(\frac{f_d}{8}\right)(Re - 1000)\,Pr}{1 + 12.7\left(\frac{f_d}{8}\right)^{\frac{1}{2}}\left(Pr^{\frac{2}{3}} - 1\right)}, \tag{15}$$

where $Pr = \frac{C_p \mu}{k_2}$ is the Prandtl number, μ is dynamic viscosity, $Re = \frac{\rho v d}{\mu}$ is the Reynolds number.

The Darcy coefficient f_D is found with the use of the Churchill equation for the entire spectrum of the Reynolds number and all the values of e / d (e is roughness of wall surface)

$$f_D = 8\left[\left(\frac{8}{Re}\right)^{12} + (A + B)^{-1.5}\right]^{1/12}, \tag{16}$$

where $A = \left[-2.457 \cdot \ln\left(\left(\frac{7}{Re}\right)^{0.9} + 0.27(e/d)\right)\right]^{16}$, $B = \left(\frac{37530}{Re}\right)^{16}$.

Solving Eqs. (7) – (12), we obtain the distributions of temperatures, electric potential (for thermoelements), velocities and pressure (for heat carrier).

The above differential equations with the respective boundary conditions were solved using Comsol Multiphysics package of applied programs.

Computer simulation results

Below are given the results of calculations of the parameters of thermoelectric pump according to physical models shown in Figs.1-3. The influence of dimensions (d_1 in Fig.2) of heat exchange intensifier on the loss of temperature difference between the heat carrier and the external surface of heat exchanger (accommodating the thermoelectric module) was investigated. Also, the influence of this loss on the general efficiency of thermoelectric heat pump was analyzed with regard to energy consumption W_{pump} on heat carrier pumping through heat exchange system. For these parameters, the optimal number of thermoelectric modules N was determined to assure the required cooling capacity Q_0, as well as the optimal supply current I_{opt} of each module to assure the highest integral coefficient of performance ε^{int}.

The initial data for calculations:

cooling capacity – 600 W;

heat carrier temperature at inlet to hot heat transfer loop – 36 ºC;

heat carrier temperature at inlet to cold heat transfer loop – 31 ºC;

heat carrier flow rate in each loop – 22 ml/s.

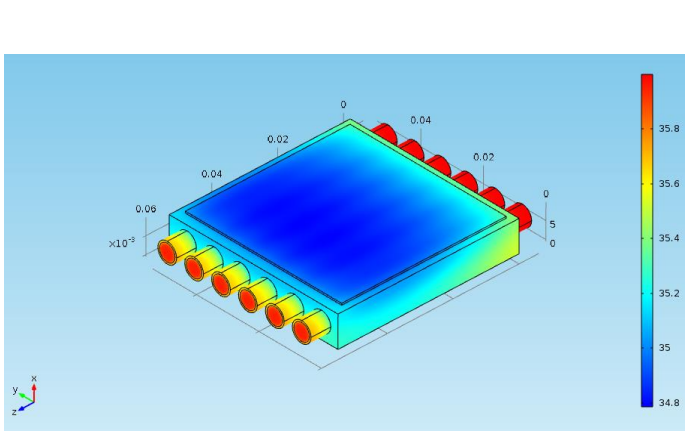

Fig. 4. Typical temperature distribution in liquid heat exchanger

Typical temperature distribution in THP liquid heat exchanger is shown in Fig.4. The analysis of this temperature distribution for cases of different ratios between the diameters of heat exchanger intensifier and the diameter of heat exchanger channel enabled us to determine its influence on the overall efficiency of thermoelectric heat pump. Fig.5 shows a dependence of the integral coefficient of performance of thermoelectric heat pump (with regard to energy consumption on pumping $\varepsilon_{втр}$ and without regard to it ε) on the size of a gap formed by heat exchanger channel and heat exchange intensifier, whereby the gap size l=6 mm corresponds to no heat exchange intensifier option.

Thus, the results of computer optimization of THP heat exchange system made it possible to determine the conditions for heat exchange intensification in liquid heat exchanger leading to improvement of THP integral efficiency. It was established that with the size of the gap l=0.25 mm formed by heat exchanger channel and heat exchange intensifier, the coefficient of performance of THP with regard to energy consumption on heat carrier pumping reaches 2.1 (which corresponds to the loss in heat exchange system ΔT=1 K). Thus, the efficiency of THP has been increased by 24% as compared to THP option without heat exchange intensifiers in heat exchanger channels.

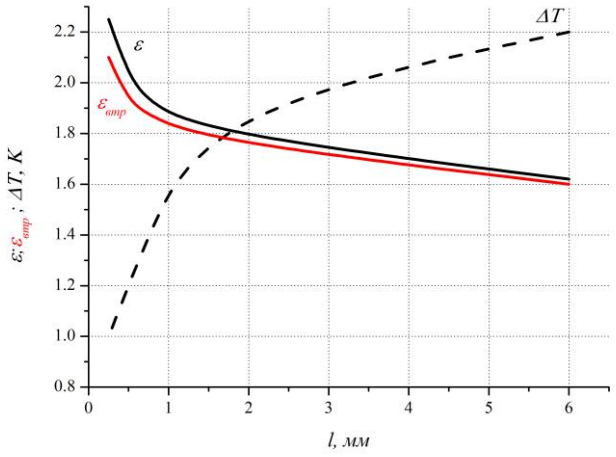

Fig. 5 Dependence of integral coefficient of performance of thermoelectric heat pump (with regard to energy consumption on heat carrier pumping ε_{cons} and without regard to it ε) and loss of temperature difference in heat exchanger ΔT on the size of the gap l formed by heat exchanger channel and heat exchange intensifier (l=6 mm corresponds to no pin option)

Conclusion

1. At similar dimensions of the heater and thermocouple, heat loss due to thermal conductivity of the thermocouple and heat exchange with the environment can lead to a decrease of maximum temperature in the heater center by a factor of 1.5, which significantly affects the parameters of the thermal converter and can be largely compensated by evacuation or filling the work space of the thermal converter with the low thermal conductivity inert gas.
2. It is relevant to study the opportunity of using in the design of thermal converter of heaters with a variable section or made of different materials.

References

1. Tashchuk D.D. (2012). Optimization of temperature distribution in thermoelectric measuring transducer. *J.Thermoelectricity*, 4, 95 – 98.
2. Mykytiuk P.D. (2017). Factors of influence on the accuracy of thermal converters. *J.Thermoelectricity*, 5, 76 – 83.
3. Anatychuk L.I., Kuz R.V., Tashchuk D.D. (2015). Differential thermoelectric AC converter in the non-simultaneous comparison mode. *J.Thermoelectricity*, 4, 77 – 82.

Submitted 07.02.2018

Анатичук Л.І. *ак. НАН України,*[1,2]
Прибила А.В. *кандидат фіз.-мат. наук*[1,2]

[1]Інститут термоелектрики, вул. Науки, 1;Чернівці, 58029, Україна;
[2]Чернівецький національний університет імені Юрія Федьковича,
вул. Коцюбинського 2, Чернівці, 58012, Україна;
[3]Вищий державний навчальний заклад України «Буковинський державний
медичний університет», Театральна площа, 2, Чернівці, 58002, Україна

ПРО ВПЛИВ ТЕРМОПАРИ НА РОЗПОДІЛ ТЕМПЕРАТУРИ В НАГРІВНИКУ ВИМІРЮВАЛЬНОГО ТЕРМОПЕРЕТВОРЮВАЧА

Досліджено вплив термопари на розподіл температури в нагрівнику термоперетворювача для випадку подібності геометричних розмірів термопари і нагрівника.
Встановлено, що втрати тепла за рахунок теплопровідності термопари та її теплообміну з оточуючим середовищем зменшують температуру в центрі нагрівника майже в 1,5 рази. Запропоновано варіанти підвищення ефективності використання тепла в термоперетворювачі. Бібл. 3, Рис. 5.
Ключові слова: термоперетворювач, термопара, нагрівник, розподіл температури.

Анатычук Л.И.[1,2] *ак. НАН Украины,*
Прибыла А.В.[1,2] *канд.физ.-мат. наук*

[1]Институт термоэлектричества, ул. Науки, 1;Черновцы, 58029, Украина;
[2]Черновицкий национальный университет имени Юрия Федьковича,
ул. Коцюбинского 2, Черновцы, 58012, Украина;
[3]Высшее государственное учебное заведение Украины «Буковинский государственный

медицинский университет», Театральная площадь, 2, Черновцы, 58002, Украина

О ВЛИЯНИИ ТЕРМОПАРЫ НА РАСПРЕДЕЛЕНИЕ ТЕМПЕРАТУРЫ В НАГРЕВАТЕЛЕ ИЗМЕРИТЕЛЬНОГО ТЕРМОПРЕОБРАЗОВАТЕЛЯ

Исследовано влияние термопары на распределение температуры в нагревателе термопреобразователя для случая подобия геометрических размеров термопары и нагревателя.

Установлено, что потери тепла за счет теплопроводности термопары и ее теплообмена с окружающей средой уменьшают температуру в центре нагревателя почти в 1, 5 раза. Предложены варианты повышения эффективности использования тепла в термопреобразователе. Библ.3, Рис.5.

Ключевые слова: термопреобразователь, термопара, нагреватель, распределение температуры.

References

1. Tashchuk D.D. (2012). Optimization of temperature distribution in thermoelectric measuring transducer. *J.Thermoelectricity,* 4, 95 – 98.
2. Mykytiuk P.D. (2017). Factors of influence on the accuracy of thermal converters. *J.Thermoelectricity*, 5, 76 – 83.
3. Anatychuk L.I., Kuz R.V., Tashchuk D.D. (2015). Differential thermoelectric AC converter in the non-simultaneous comparison mode. *J.Thermoelectricity*, 4, 77 – 82.

Submitted 07.02.2018


Y. I. Bokhan

Y. I.Bokhan, *Cand. physical sciences*
A. A.Varnava

Vitebsk branch of Educational Establishment
"The Belarusian State Academy of Communications",
Belarus, Vitebsk, 210604, 45, Ilinsky str.
yuibokhan@gmail.com


A. A. Varnava

THERMOELECTRIC CERAMIC ELEMENT WITH A NEGATIVE TEMPERATURE FACTOR OF RESISTANCE

A model of a thermoelement with the legs made of materials possessing a negative temperature factor of resistance is proposed. A system of equations describing the process of heat and charge transfer is obtained by the methods of the expanded irreversible thermodynamics. The results of calculations of the character of heat and charge transfer for various ratios of relaxation time are presented. Bibl. 10, Fig. 2.
Key words: thermoelement, thermistor, nanoceramics.

Introduction

The promising direction in the field of developing effective thermoelectric materials is creation of various nanostructures, such as quantum dots, nano whiskers, superlattices, bulk nanocomposites [1]. The quantity of works, both theoretical, and experimental, devoted to research on thermoelectric nanomaterials, has been steadily growing recently, and the results are rather optimistic, at least, from the standpoint of fundamental science.

Increase of thermoelectric figure of merit in nanomaterials is connected with two physical phenomena [2]:

- decrease of lattice thermal conductivity is caused by occurrence of numerous boundaries that are effective scattering centers for phonons, but have little impact on electronic transport;
- increase of forbidden bandwidth with a simultaneous increase of the density of states near the Fermi level; although in this case the electrical conductivity decreases, but the thermal e.m.f. increases, and under certain conditions it can lead to increase of the power factor.

However, for creation of semiconductor properties in nanocrystalline ceramic materials we can use the method of roasting in the recovery atmosphere [3 – 5]. Such method, together with usage of materials with NTRC allows raising the efficiency of the thermoelements, especially in the high-temperature field where ceramic materials are the steadiest. It is possible to create both *n*- and *p*-type conductivity by selecting the composition of gas atmosphere.

An elementary thermoelement is the basis for any thermoelectric cooling device. It represents two semiconductor legs connected in series, one leg possessing electronic conductivity (*n*), and the other - hole (*p*) conductivity. At the set current the value of temperature decrease depends on thermal load [2]. For increasing the figure of merit of a thermal element, the materials based on bismuth telluride are considered to be more promising [3]. However, they have a narrow temperature gradient range and are difficult to manufacture. Therefore, it is interesting to develop materials of conductive semiconductor ceramics based on interjacent metal oxides or composite materials [4]. That is why ceramic materials with a negative temperature coefficient of resistance (NTCR) (thermistors) [5 – 6] are of particular interest. Such materials can change conductivity value in wide ranges, and it offers good prospects for their usage as materials of legs.

Research method

Increase of thermoelectric figure of merit in nanomaterials is associated with two physical phenomena [2]:

- decrease of the lattice thermal conductivity occurring in nanomaterials with numerous boundaries that are effective scattering centers for phonons, but have little impact on electronic transport;
- increase of forbidden bandwidth in nanomaterials, with the simultaneous increase of the density of states near the Fermi level; although in this case the electrical conductivity decreases, but the thermal EMF increases, and under certain conditions it can lead to increase of the power factor. It is possible to create both n- and p-type conductivity by selecting the composition of gas atmosphere.

With the help of the valence-controlled process, oxide ceramic materials can be transferred to the semiconductor state. For this purpose, different methods are used. For example, the recovery method: firing of ceramics in reducing ambient of non-isovalent substitution. In this case, it is possible to obtain acceptable conductivity, while maintaining low thermal conductivity. In ceramic materials, one can enhance the scattering mechanism at low thermal conductivity, which leads to increase of the figure of merit [2].

$$z = \left[\frac{(\alpha_1 - \alpha_2)}{\sqrt{\chi_1 \rho_2} + \sqrt{\chi_2 \rho_1}} \right]^2 \quad (1)$$

where α_1 and α_2 are thermoelectric coefficients, χ_1, χ_2 are thermal conductivity coefficients, ρ_1, ρ_2 are resistivities of thermoelement legs.

In thermoelectric nanocomposites, the grain size does not exceed several tens of nanometers. To increase the thermoelectric efficiency, it is necessary to fulfill the following condition: the grain size should be smaller than the phonon path length, but larger than the mean free path of charge carriers (electrons or holes).

In nanocomposites it is obvious that when the grain size decreases, the fraction of the grain boundaries will increase, and it will lead to a gradual decrease of the thermal conductivity of material. Naturally, the scattering of electrons at the grain boundaries will take place, and their mobility will be decreased. However, the decrease of thermal conductivity in the bulk nanocomposites may be more significant than the decrease of electrical conductivity. Thus, the bulk nanocomposites that consist of nanoscale grains of the thermoelectric material separated by typical grain boundaries can potentially have a high thermoelectric figure of merit, as they will have both high electrical conductivity and low thermal conductivity at the same time. Therefore, the usage of the materials with NTCR as the nanocomposite legs makes it possible to create thermoelements with essentially nonlinear properties [6].

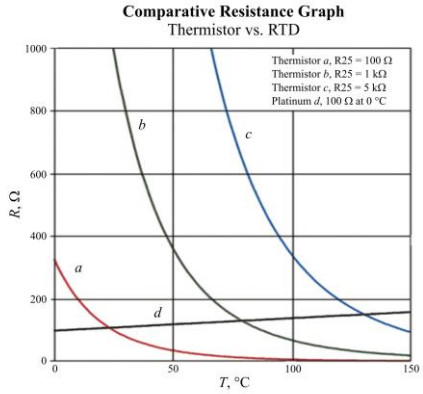

Fig. 1. Typical temperature dependence of resistance for a thermistor with NTCR

For example, in the case of isomorphous substitution, the number of spinels goes into the state of semiconductor conductivity with NTCR. Lithium doping of nickel oxide in the spinel leads to sharp increase of conductivity due to the replacement by lithium ions of nickel ions in the octahedral positions. The formation of the solid solution with the uncompensated charge allows the variation of the lithium concentration to create a different type of conductivity [6].

$$\frac{x}{2}Li_2O+(1-x)NiO+\frac{x}{4}O_2\rightarrow\left(Ni_{1-2x}^{2-}Li_x^{+}Ni_x^{3+}\right)O \tag{2}$$

Let us observe reaction of partial recovery of nickel from oxide for replacement of lithium oxide in octahedral positions. For this purpose, we calculate change of Gibbs' potential and, on its basis, the required concentration of *CO*. Such reaction it is represented in the form:

$$2NiO+CO\rightarrow Ni_2O+CO_2 \tag{3}$$

In this case Ni^+ substitutes Li^+ and introduces additional distortion in a lattice because of the difference in ionic radiuses (Li^+ ~ 0,68 Å; Ni^+ ~ 0,70 Å) [6]. The calculation of conditions for proceeding of reaction (2) shows that over the temperature range 700 – 900 K the reaction is allowed thermodynamically, and from temperature 800 K also kinetically [7]. It is consistent with the experimental results known from the literature on nickel recovery by various gases.

The predominant model of the conductivity of thermistors with NTCR is a model of hopping conductivity in the approximation of the "nonadiabatic" polaron of a small radius leading to the temperature dependence of conductivity [6]:

$$\sigma=\pi^{\frac{3}{2}}\frac{e^2l^2J^2E^{-\frac{1}{2}}}{h(kT)^2}\exp\left(-\frac{E}{kT}\right) \tag{4}$$

where: l is effective hopping length, J is parameter of scattering, E is energy of hop activation, T is temperature. Such nonlinear temperature dependence of electrical conductivity leads to a substantial non-equilibrium process of the heat and charge transfer in thermoelement legs. It should be noted that in the case of a thermoelectric effect the process has a nonlocal character both in the coordinate and time.

An extended irreversible thermodynamics is one of the most consistent and detailed thermodynamic theories [8] which is not based on the principle of local equilibrium and takes into account spatial nonlocality of transport processes. In addition to the classical independent variables used by the local equilibrium thermodynamics of irreversible processes, extended irreversible thermodynamics uses independent variables of dissipative flows, in our case it is a heat flux q and a charge flux *I*, to describe the state of the system far from the local equilibrium.

Thus, in the locally non-equilibrium system, entropy S is a function of both classical variables and dissipative flows:

$$S=S\{U(x,t),v(x,t),C(x,t),q(x,t),I(x,t)\}. \tag{5}$$

It should be noted that from the physical point of view the new variables significantly differ from the classical ones. Classical variables obey the laws of conservation and change relatively slowly during the evolution of the system, whereas the flows do not obey the laws and are relatively "fast" variables, whose rate of change can be high when the system is relaxed to local equilibrium. The introduction of the flows as independent variables is completely justified from the physical point of view. Indeed, if there is any flow in the system, this means a directed movement of the heat carriers or charges, i.e. such system is more ordered compared to a system where there are no such flows. Consequently, the entropy which is

known to be a measure of "disorder", must be less than the entropy in the system without the flows. Using the extended set of independent variables in the definition of locally non-equilibrium entropy (5) and the classical formulation of the second law of thermodynamics with allowance for new locally non-equilibrium terms in the expressions for the production of entropy and its flow, extended irreversible thermodynamics leads to differential equations for dissipative flows of evolutionary (relaxation) type:

$$q + \tau_T \frac{\partial q}{\partial t} = -\lambda \nabla T - l^2 \nabla^2 q\,, \tag{6}$$

$$\tau_e \frac{\partial i}{\partial t} = -\left(i - \sigma_e E'\right), \tag{7}$$

where $E' = E - T\nabla(T^{-1}\mu_e)$, τ_T, τ_e is relaxation time of heat and charge, l is reference length of nonlocality, σ_e is conductivity, μ_e is chemical potential, λ is thermal conductivity coefficient, E is electric field strength, T is temperature.

Thus, the inclusion of dissipative flows in the series of independent variables leads to the fact that these flows are no longer determined by the gradient of the corresponding transfer potential, as in the classical local-equilibrium case, but they are solutions of the evolution equations (6 – 7). These equations describe the process of relaxation of dissipative flows to their local equilibrium values.

While analyzing the system of equations (6 – 7), we use the following approximations. We assume that the coefficient of thermal conductivity and the relaxation time of the heat are constant and temperature independent. Such assumption is correct in connection with the fact that the calculation of the heat relaxation time must be carried out with regard to the propagation of heat in the system. In other words, in the case of the propagation of heat, the problem is self-consistent. Taking into account that the distribution of the heat and charge front may be considered in a single grain, we can assume that the spread of non-locality is rather weak, and the process describes the approach of the permanent τ_T and τ_e.

The τ_e is an expression for the relaxation time of conduction electrons of a nondegenerate atomic semiconductor $\tau_e \sim \varepsilon^{-1/2}\,T^{-1}$ [9], where ε is the energy of the order of semiconductor forbidden bandwidth. Such an expression for the charge relaxation time is an approximation that has temperature dependence. It is necessary to solve the kinetic equation for the charge propagation taking into account the dispersion law in the conduction mechanism [9]. However, in our case, such task is complicated by the fact that it is necessary to consider the flow of the charge along the grain surface. It complicates the solution of the kinetic equation, which must be solved taking into consideration the percolation flow model.

It is usually assumed that the chemical potential does not depend on temperature and is approximately equal to the Fermi energy. However, for a nondegenerate semiconductor with the essentially nonlinear temperature dependence of conductivity (2), it is necessary to take into account the temperature dependence of the chemical potential [10], which has a logarithmic temperature dependence:

$$\mu_e = kT \ln\left[\frac{4}{3\sqrt{\pi}}\left(\frac{\varepsilon}{kT}\right)^{\frac{3}{2}}\right] < 0 \tag{8}$$

where k is the Boltzmann constant.

Thus, the problem of calculating the heat transfer in this system is nonstationary. To solve it, we assume the model to be one-dimensional, and omit the second-order terms in the temperature gradients. The initial and boundary conditions are assumed to be standard [7]. Such assumptions allow us to make a qualitative analysis of the nature of heat and charge propagation in the system. We examine the model at the distances of the grain size order. The generalization of the sample dimensions requires the

establishment of an averaging procedure, which differs from the standard method, i.e. the introduction of certain average or effective parameters requires additional considerations and cannot be carried out by simple averaging.

Results and discussion

The results of numerical simulation are shown in Fig. 3. The system analysis (6 – 7) was carried out for various τ_T/τ_e ratios, and the dimensionless time t/τ_T was used.

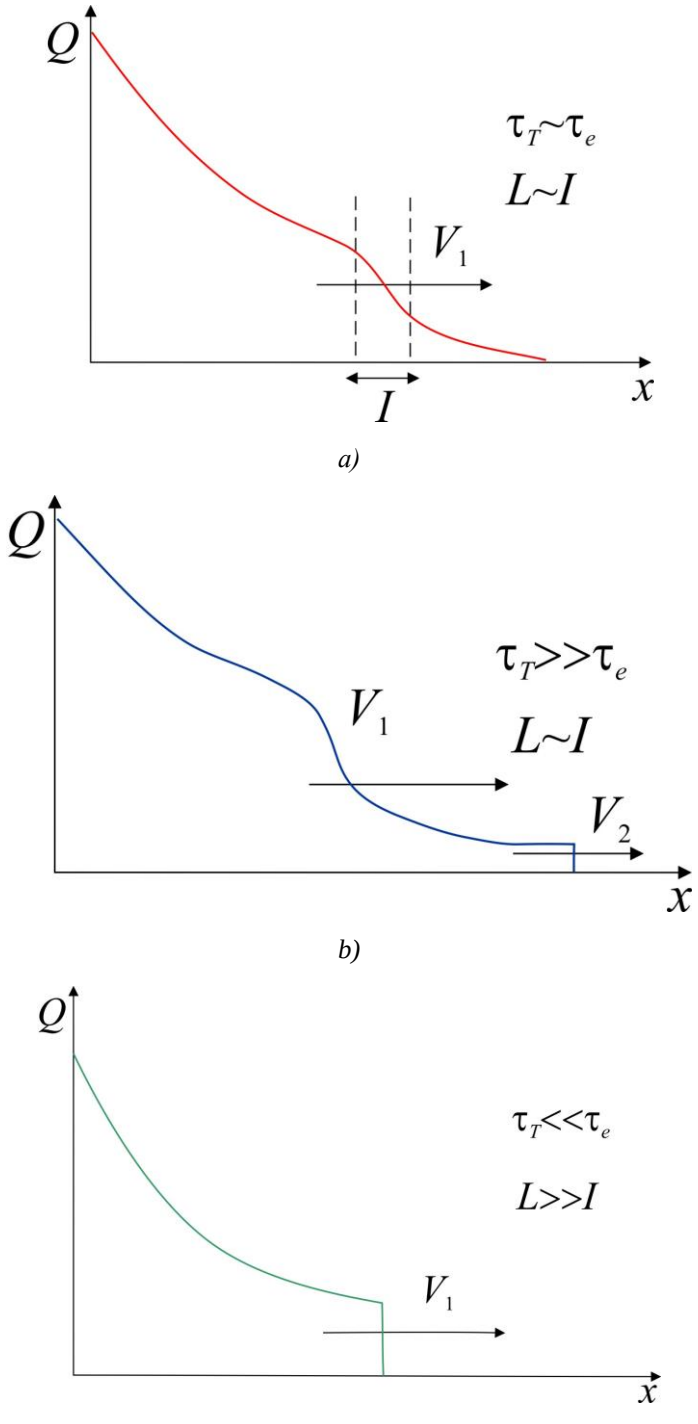

Fig.2. Propagation of heat in a thermoelement for various ratios τ_T, τ_e, L,

The result of the simulation is presented in Fig. 3a, provided that the times of relaxation of heat and charge are close. In this case, the propagation of heat occurs almost simultaneously with the charge density. It has a character close to a solitary wave. Such a result is quite obvious, since in this case the Joule heat is released simultaneously with heat transfer, and the increase of the charge current occurs with the velocity that is close to the velocity of propagation of heat V_1. The characteristic feature of such propagation is formation of the wave along the length of the conductivity hop.

In the case when there is $\tau_T >> \tau_e$ (Fig. 3,*b*), the break of propagation front occurs and the Joule heat wave V_2 outpaces the actual heat transfer wave due to the temperature gradient. Thus, in this case two waves are formed, which are spatially separated. At the same time, the relaxation of the heat does not occur during the hopping of the charge, and the system is in a locally non-equilibrium state. In other words, charge transfer generates a locally non-equilibrium state in which the charge flow is a fast variable.

In the case when there is $\tau_T << \tau_e$ (Fig. 3,*c*), the heat relaxation occurs faster than the charge transfer, and heat propagation front coinciding with the charge transfer is formed. It should be noted here that the steepness of the front is determined by the mechanism of hopping conductivity and the approximations in the calculation. When there is more correct calculation, there will be no gaps on the front.

The mode of heat transfer will be especially manifested in functionally graded materials [3], especially along the grain boundaries. By creating a regular structure with the required relaxation time ratios, it is possible to achieve the wave character of the heat transfer and charge transfer. It will allow creating devices that simultaneously measure and regulate the temperature.

Investigating movement of a charging and temperature wave, it is possible to estimate the ratio of relaxation times. It will allow at qualitative level to draw certain conclusions about the transfer mechanism. Such a possibility is very relevant for ceramic materials.

Conclusion

The local non-equilibrium process of heat and charge transfer in this paper can be realized in the legs of semiconductors the materials of which possess a negative coefficient of resistance. First of all, this is due to the essentially nonlinear temperature dependence of conductivity. The determination of the quality factor of such a structure is a separate task, since it is necessary to calculate the thermoelectromotive force within the assumptions made. In contrast to conventional semiconductors, one should take into consideration the kinetics of charge and heat transfer. In this case, it is necessary to take into account the structure of the leg material and the mechanism of heat dissipation.

References

1. Gogotsi Yury. (2006). (Ed.) *Nanomaterials handbook*. CRC press, Taylor & Francis group.
2. Rowe D.M. (2006). (Ed.) *Thermoelectrics handbook: macro to nano*. CRC Press. Taylor & Francis group.
3. Anatychuk L.I. (2007). Current status and some prospects of thermoelectricity. *J. Thermoelectricity*, 2, 7-20.
4. Clarke D.R. (2014). Oxide thermoelectric devices: a major opportunity for the global ceramics community. *Proc. of 5th International Congress on Ceramics* (China, Beijing, August 2014).
5. Terasaki I. (2011). High-temperature oxide thermoelectrics. *J.Appl. Phys.*, 110, 053705.
6. Feteira A. (2009). Negative temperature coefficient resistance (NTSR) of ceramic thermistors: an industrial perspective. *J. Am. Ceram. Soc*., 92 (5), 967-983.

7. Bokhan Y. I., Varnava A. A. (2018). Roasting of ceramic materials with the negative temperature resistance coefficient of recovery atmosphere. *J. Materials Sciences and Applications*, 4(3), 47-50.
8. Lebon G., Jou D., Casas-Vázquez J. (2008). *Understanding non-equilibrium thermodynamics*. Springer.
9. Kviany M. (2008). *Heat transfer physics*. Oxford: University Press.
10. Girifalco L.A. (2000). *Statistical mechanics of solids*. Oxford: University Press.

Submitted 13.03.2018

Бохан Ю.І., *канд. фіз.-мат наук*
Варнава А.А.

Вітебська філія установи освіти
«Білоруська державна академія зв'язку»,
вул. Ільїнського, 45, Білорусь, 210604, Вітебськ
e-mail: yuibokhan@gmail.com

ТЕРМОЕЛЕКТРИЧНИЙ КЕРАМІЧНИЙ ЕЛЕМЕНТ З НЕГАТИВНИМ ТЕМПЕРАТУРНИМ КОЕФІЦІЄНТОМ ОПОРУ

Запропоновано модель термоелемента з гілками з матеріалів, що володіють негативним температурним коефіцієнтом опору. Систему рівнянь, які описують процеси переносу тепла та заряду, отримано методами розширеної нерівноважної термодинаміки. Наведено результати розрахунків характеру переносу тепла й заряду для різних співвідношень між часами релаксації. Бібл. 10, Рис. 2..
Ключові слова: *термоелемент, термістор, нанокераміка*.

Бохан Ю.И., *канд. физ.-мат наук*
Варнава А.А.

Витебский филиал учреждения образования
«Белорусская государственная академия связи»,
ул. Ильинского, 45, Беларусь, 210604, Витебск
e-mail: yuibokhan@gmail.com

ТЕРМОЭЛЕКТРИЧЕСКИЙ КЕРАМИЧЕСКИЙ ЭЛЕМЕНТ С ОТРИЦАТЕЛЬНЫМ ТЕМПЕРАТУРНЫМ КОЭФФИЦИЕНТОМ СОПРОТИВЛЕНИЯ

Предложена модель термоэлемента с ветвями из материалов, обладающих отрицательным температурным коэффициентом сопротивления. Система уравнений, описывающих процесс переноса тепла и заряда, получена методами расширенной необратимой термодинамики. Представлены результаты расчетов характера переноса тепла и заряда для различных соотношений времени релаксации. Библ. 10, Рис. 3.

Ключевые слова: термоэлемент, термистор, нанокерамика.

References

1. Gogotsi Yury. (2006). (Ed.) *Nanomaterials handbook*. CRC press, Taylor & Francis group.
2. Rowe D.M. (2006). (Ed.) *Thermoelectrics handbook: macro to nano*. CRC Press. Taylor & Francis group.
3. Anatychuk L.I. (2007). Current status and some prospects of thermoelectricity. *J. Thermoelectricity*, 2, 7-20.
4. Clarke D.R. (2014). Oxide thermoelectric devices: a major opportunity for the global ceramics community. *Proc. of 5th International Congress on Ceramics* (China, Beijing, August 2014).
5. Terasaki I. (2011). High-temperature oxide thermoelectrics. *J.Appl. Phys.*, 110, 053705.
6. Feteira A. (2009). Negative temperature coefficient resistance (NTSR) of ceramic thermistors: an industrial perspective. *J. Am. Ceram. Soc*., 92 (5), 967-983.
7. Bokhan Y. I., Varnava A. A. (2018). Roasting of ceramic materials with the negative temperature resistance coefficient of recovery atmosphere. *J. Materials Sciences and Applications*, 4(3), 47-50.
8. Lebon G., Jou D., Casas-Vázquez J. (2008). *Understanding non-equilibrium thermodynamics*. Springer.
9. Kviany M. (2008). *Heat transfer physics*. Oxford: University Press.
10. Girifalco L.A. (2000). *Statistical mechanics of solids*. Oxford: University Press.

Submitted 13.03.2018

M.V.Maksimuk

M.V.Maksimuk

Institute of Thermoelectricity of the NAS and MES of Ukraine,
1, Nauky str, Chernivtsi, 58029, Ukraine;
e-mail: anatych@gmail.com

BENCH TESTS OF THERMOELECTRIC STARTING PRE-HEATER FOR CARS

The results of bench tests of the energy characteristics of thermoelectric heat source for start heating of vehicle engines at low ambient temperatures are presented.
It is shown that the use of a thermoelectric converter as a source of electric power provides the autonomous operation of the pre-heater components and allows solving the problem of vehicle battery discharge during the operation of the start equipment. Bibl. 17, Fig. 10.
Key words: starting pre-heater, thermoelectric generator.

Introduction

Today the problem of internal combustion engines start-up under low ambient temperatures is solved through use of starting pre-heaters commercially produced by a number of companies – Eberspecher, Webasto, Truma (Germany), Ateso (Czeck Republic), Teplostar (Russia), Mikuni (Japan). Such heaters run on different fuels and are used in the cars, trucks, buses, yachts and boats.

Many years' experience of vehicles operation shows that start heating not only assures reliable engine start, but also allows increasing its service life by a factor of 1.5 – 2 during a year [1] and reducing toxic discharge by a factor of 5 [2], while saving up to 300 l of fuel during one winter season [3]. Moreover, comfortable conditions provided by start heating eliminate completely the possibility of accident due to cold impact on the driver.

However, despite ample opportunities, starting pre-heaters have not found mass application yet. The main reason that cancels out the advantages of start heating is the need for electric energy for power supply to heater components, which is taken from the batteries leading to their discharge and creating essential difficulties during engine startup. To avoid battery discharge during start heating, it is reasonable to use thermoelectric generator as a source of electricity for such heaters [4].

A 70 – 90 W thermoelectric generator that operates from the heat of starting pre-heater and assures power supply to its components has been created at the Institute of Thermoelectricity [5 – 7]. Moreover, the excess electric energy of thermal generator can be used for recharging the battery.

Experimental tests of the thermoelectric heater under bench conditions proved the efficiency of the design and confirmed the results of computer calculations carried out in [8]. However, the study of the sample under low temperatures showed that the thermal power of the heater is not enough to heat the engine to an optimum start temperature – 70 ° C [9].

To increase the amount of heat used to heat the internal combustion engine coolant, in the heater design it is reasonable to apply the modified version of the thermoelectric modules "Altec-1061" developed in [10]. The idea of such a modification is to reduce the height of thermoelement legs, thus reducing the thermal resistance of modules and increasing the total thermal flow through the thermopile.

Due to the use of thermoelectric converter optimized for a new level of thermal power, computer design methods were used to find the main structural and energy characteristics of a new version of thermoelectric starting pre-heater on diesel fuel for pre-heating of cars with engine displacement up to 4 l. Calculations showed that in the case of using a new modification of modules the thermal power of the heater can be expected to increase by a factor of 1.5 – 2, for the level of 2.5 – 3 kW, with electric power 85 – 110 W. Such values of thermal and electric power will assure engine temperature optimal for start-up, the autonomous operation of functional components of the heater, as well as battery recharge during start heating [11].

The purpose of this work is to study the thermal and electrical parameters of the developed heater under bench conditions for confirmation of conformity to design characteristics.

Structure and operating principle of thermoelectric starting pre-heater

The schematic and appearance of thermoelectric starting pre-heater are shown in Fig.1.

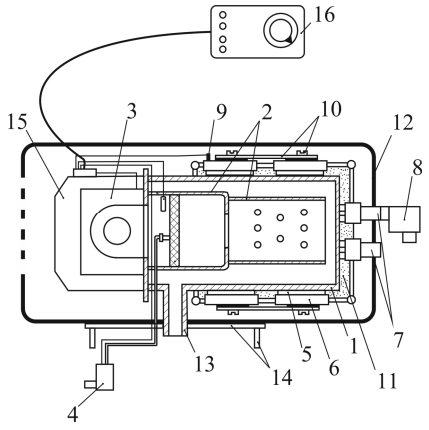

a)

b)

Fig.1. Schematic (a)and appearance (b) of thermoelectric starting pre-heater:
1 – hot heat exchanger; 2 – heat source; 3 – fan; 4 – fuel pump;
5 – thermopile; 6 – cold heat exchanger; 7 – input and output connecting pipes;
8 – circulating pump; 9 – overheat sensor; 10 – clamping mechanism;
11 – thermal insulation; 12 – case; 13 – exhaust pipe; 14 – fastening system;
15 – electronic unit; 16 – control panel.

This thermoelectric heater is composed of a hot side heat exchanger **1**, which holds the source of heat **2** in its interior space. Fuel and air delivery to the source of heat is carried out by a fan **3** and a fuel pump **4**. A thermopile **5** is located on the exterior surface of the hot heat exchanger the heat from which is removed by heat exchangers **6**.

Cold heat exchangers are combined into a single hydraulic circuit with the engine cooling system by connecting pipes **7**. The circulation of the liquid coolant in the "heater-engine" circuit is carried out by pump **8**. To control the temperature of the coolant, one of the cold heat exchangers has an overheating sensor **9**. The thermal contact between the thermopile and heat exchangers is provided with a clamping device **10**. The free space between the hot and cold heat exchangers is filled with thermal insulation **11**. An automobile heater with a fan, electronic unit, heat exchangers, thermopile and clamping device is placed into case **12**. Fuel combustion products are removed to environment by an exhaust pipe **13**. By means of fastening system **14** the heater is placed on the frame of the car. Start-up and control of all heater devices is done by electronic unit **15** from control panel **16.**

A thermopile is composed of 12 generator modules Altec-1061 optimized for use in starting pre-heaters and electrically connected parallel-in-series. Modules connection was adjusted so that the output voltage of the heater matched the voltage of the car storage battery.

A diesel burner *Ersatzbrenner D TT-C MB* was used as a source of heat in the structure of the heater, pulse pump *BTL.DP30.02.12V DAEMPFLER E-TEIL* and liquid pump 12V U4847 TT C/E of the starting pre-heater "ThermoTopEvo 4» (Webasto) [8]" were used as fuel and circulating pumps, and air fan "Delta" was used as a fan [13].

The heater works as follows. Thermal energy from fuel combustion heats up the hot heat exchanger, passes through thermoelectric modules and is removed by the liquid heat carrier circulating in the heat exchangers of the heater and engine cooling system. Therefore, thermal energy removed from the thermopile is used for the engine warm-up, while electric power is used to power heater components and recharge the automobile storage battery, if necessary.

Results of test bench research

Research on the energy characteristics of the developed thermoelectric diesel heater was carried out on the experimental test bench shown in Fig. 2.

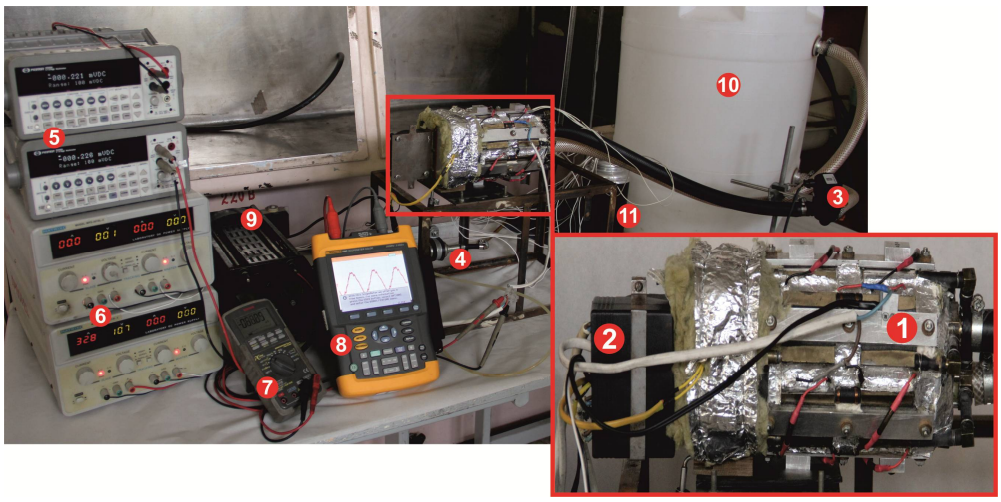

Fig.2. Schematic of experimental test bench for studying the energy characteristics of thermoelectric starting pre-heater: 1 – thermoelectric heater without outside case; 2 – electronic unit; 3 – circulation pump; 4 – fuel pump;5 – voltmeter; 6 – supply unit; 7 – digital ammeter; 8 – oscilloscope; 9 – rheostat; 10 – thermostat; 11 – Dewar with ice and thermocouples [9].

The research was conducted in two stages:

- at the first stage, the heater operating modes, as well as algorithms for its start-up and achieving the maximum power mode were developed;

- at the second stage, the energy characteristics of the heater were compared with the car battery. In this case, the work of the components was controlled by the electronic unit.

Results of studying characteristics of thermoelectric automobile starting pre-heater are given in Fig.3 and in Table1.

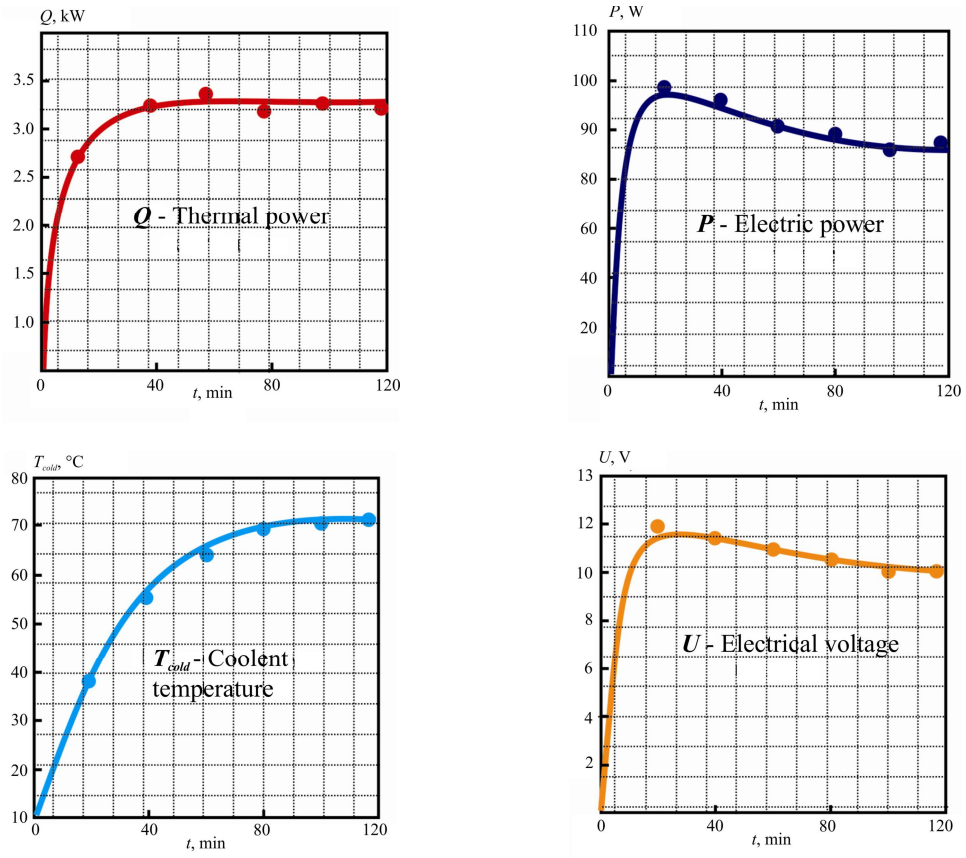

Fig.3. Dependence of the energy characteristics of thermoelectric automobile starting pre-heater on operation time t.

Table 1

Operating modes of thermoelectric starting pre-heater

Operating mode	Time after startup, min.	Thermal power of heat source, *W*	Fuel consumption, *g/h*	Air consumption, m^3/h	Heat carrier consumption, m^3/h
I	1	950	80	4.20	0.3
II	2	1250	105	4.80	
III	3	1540	130	5.50	
IV	4	2310	195	7.49	
V	5	2965	250	7.99	
VI	6	3560	300	8.19	

From the given data it is seen that the maximum thermal power of the heater reaches the level of 3 kW, which ensures coolant warm-up in the 80-th minute from the moment of its startup, while the first version of starting pre-heater provided a similar thermal mode during two hours of operation [9]. Thus, the use in the design of the heater of modified thermoelectric modules "Altec-1061" gives an opportunity to

increase the heat output of the heater by a factor of ~ 1.5 to 2 and to shorten the time of engine coolant warmup.

The steady-state operating mode of the heater is set in the 30-th minute of operation at the hot exchanger temperature 280 °C and output gas temperature ~300°C. In so doing, the electric power of the heater is equal on the average to 90 W, the voltage is within 10 – 12 V.

The steady-state operating mode of the heater (mode VI) is provided at heat source thermal power 3.6 kW and cold heat carrier flow rate 0.3 m^3/h. However, for a reliable start-up and stable operation of the heater the scheme of smoothly achieving the mode is implemented, whereby thermal power of the heater and fuel-air mixture consumption increase gradually (Table1).

Fig.4 shows dependences of maximum electric power P and heater efficiency η on the temperature of cold heat carrier T_{cold}.

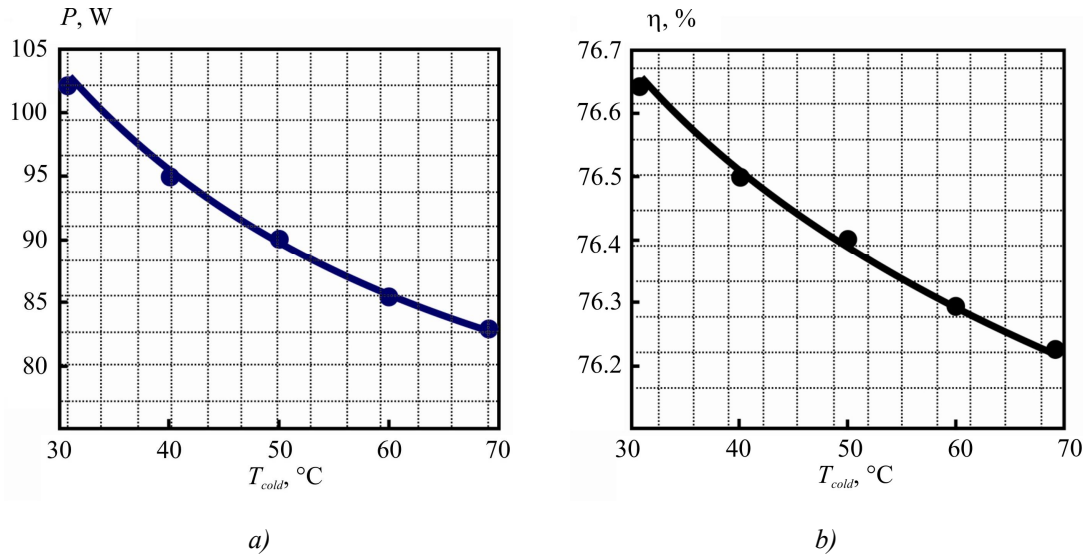

a) *b)*

Fig.4. Dependence of maximum electric power P (a) and efficiency η (b) on the temperature of cold heat carrier.

It is worth noting that the efficiency of the heater in this case is determined by both thermal and thermoelectric efficiency, since along with the electrical energy, it is important to provide the required level of thermal power used for engine heating.

The distribution of electric power by the heater components is shown in Fig.5.

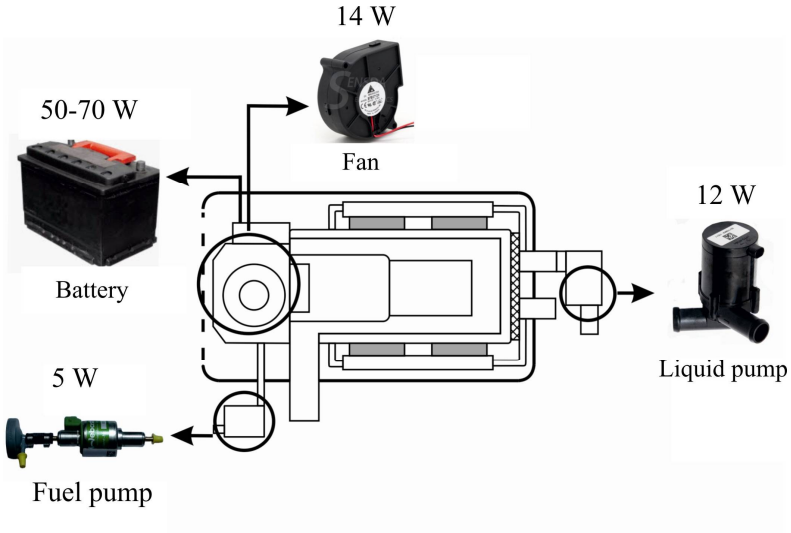

Fig.5. Electric power distribution by the heater components [14]

Consequently, taking into account that the total electric power consumption of the heater components is ~ 30 W (fuel pump 5 W, fan 14 W, liquid pump 12 W), 50 – 70 W of thermal generator electricity can be used for recharging the battery

The results of research on the work of the thermoelectric starting pre-heater in conjunction with the car battery are shown in Figs. 6 – 10. The structure and programmed algorithms of the electronic unit that controls the heater operating modes are similar to those of its first version [15]. The only difference is the presence of two additional modes of operation (V and VI, Table 1), which are realized by a gradual decrease in the fuel supply period by a fuel pump [16].

From the above data it follows that the behavior of both temperature and electrical dependences is practically identical. After switching on the device and until the desired heat carrier temperature is reached, the electronic unit gradually increases the thermal power of the heat source to the maximum. At the same time, there is an increase in the temperature characteristics of the T_{cold}, T_{hot}, T_{gaz} and the transition from the battery power mode of components to thermal generator power mode. As the output power of the generator increases, the electronic unit sends the excess electric energy for recharging the battery.

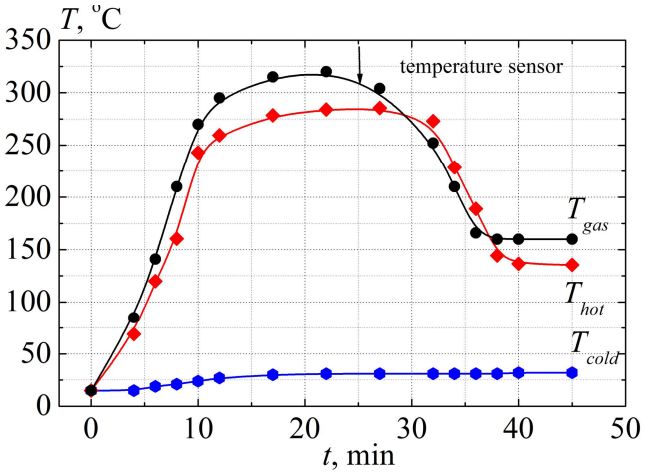

a)

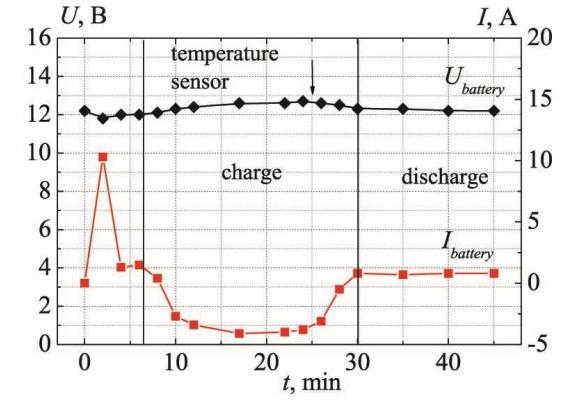

b)

Fig.6. Results of research on the work of thermoelectric automobile heater with electronic control unit: T_{gas} – exhaust gas temperature; T_{hot} – temperature of the hot heat exchanger; T_{cold} – temperature of the cold heat exchanger; U_{bat} – battery voltage; I_{bat} – current in "heater"-"battery" circuit. The set heat carrier temperature is 30°C.

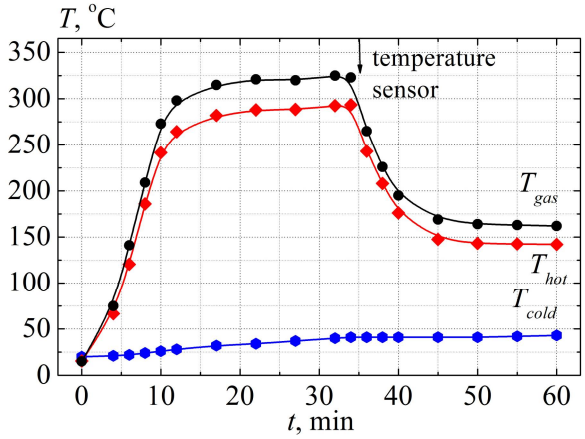

a)

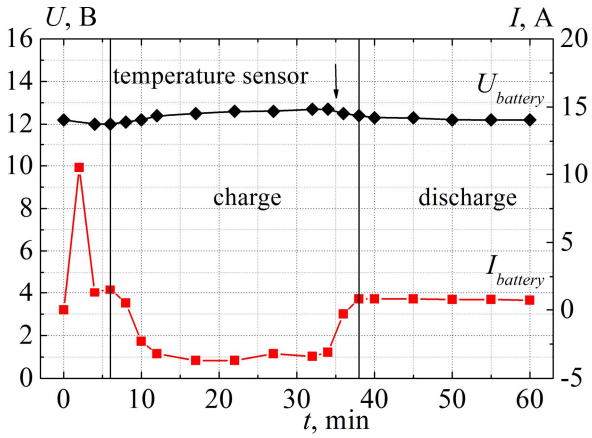

b)

Fig.7. Results of research on the work of thermoelectric automobile heater with electronic control unit. The set heat carrier temperature is 40°C. The designations are similar to Fig.6.

On reaching the set temperature of the heat carrier, the electronic unit in accordance with the output signal of the digital thermal sensor increases the period of fuel supply to the burner – the heater begins to operate in the mode of maintaining the set temperature. At the same time, the temperature of the hot heat exchanger and the temperature of the gases fall, and the temperature on the cold heat exchangers is stabilized. It should be noted that in this operating mode, the power generated by thermoelectric modules is not enough to recharge the battery, so the electronic unit, by reversing the current in the "heater" – "battery" circuit, switches power supply to components from the modules back to the battery. In this case, the discharge current of the battery is only ~ 0.5 A, which is unquestionably very small in comparison with its capacity (for example, the discharge current at the work of the Webasto Thermo Top Evo 4 liquid starting pre-heater is an order of magnitude greater, namely 3 – 5 A) . Therefore, it can be argued that in the mode of maintaining the temperature of the heat carrier the heater actually works without the use of battery power.

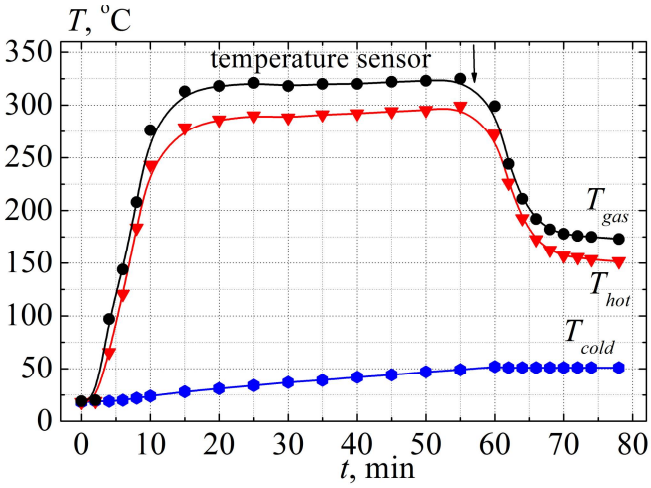

a)

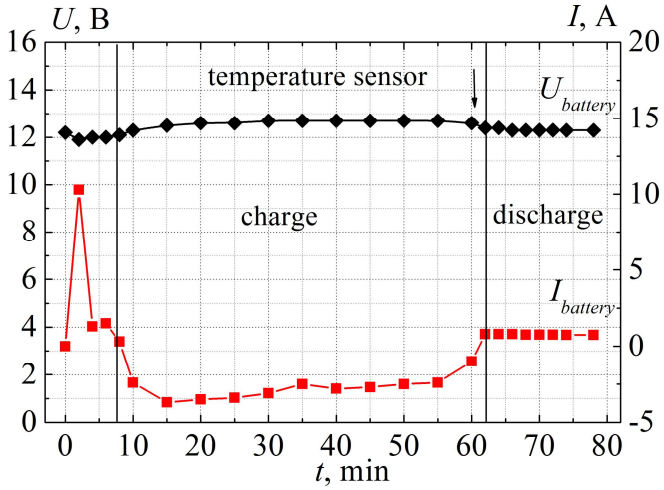

b)

Fig.8. Results of research on the work of thermoelectric automobile heater with electronic control unit. The set heat carrier temperature is 50°C. The designations are similar to Fig.6

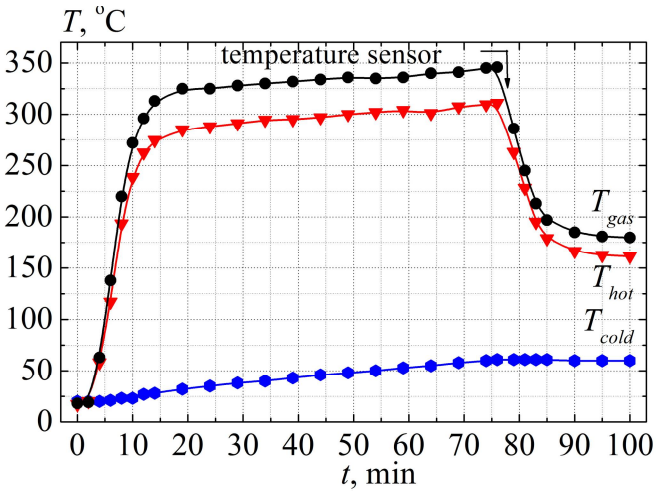

a)

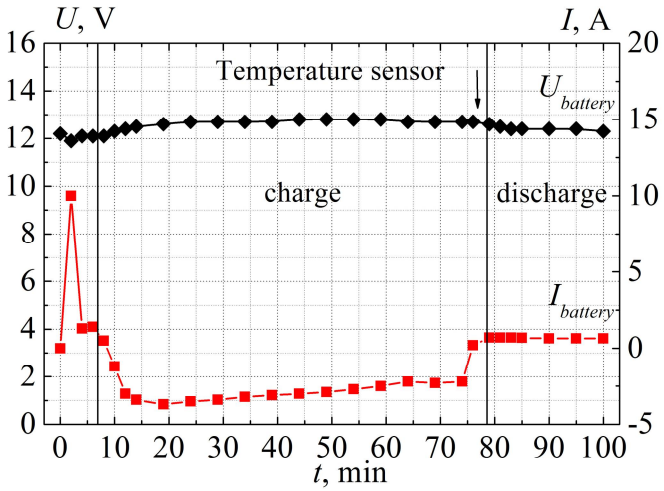

b)

Fig.9. Results of research on the work of thermoelectric automobile heater with electronic control unit. The set heat carrier temperature is 60°C. The designations are similar to Fig.6.

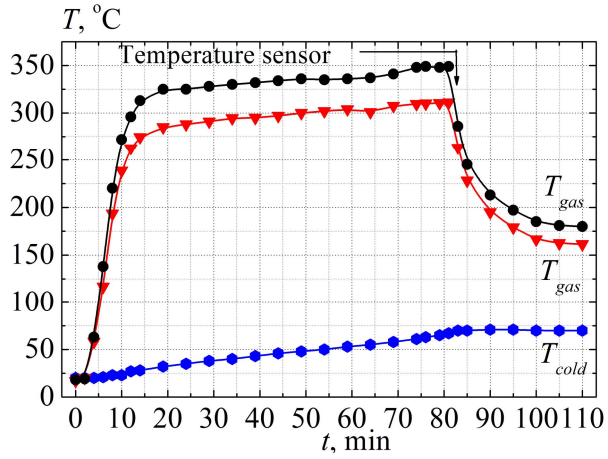

a)

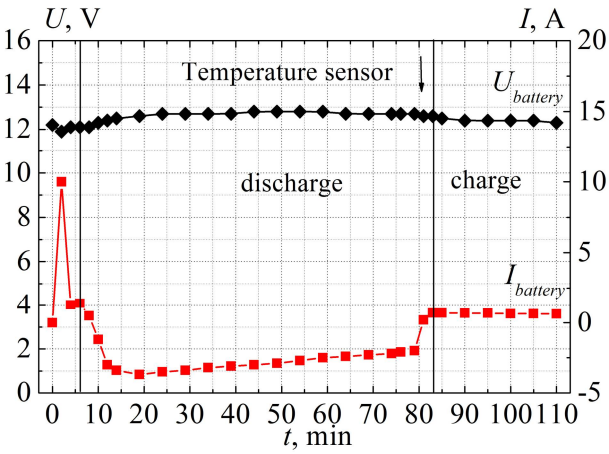

b)

Fig.10. The results of research on the work of thermoelectric automobile heater with electronic control unit. The set heat carrier temperature is 70°C. The designations are similar to Fig.6.

Thus, during operation of the heater, the excess electric energy of the generator used to charge the battery is 30 – 40 Watts. Thus, about 20-30 watts of electric power are left in the reserve, which can additionally be used to power other automotive equipment during start heating. However, this value will be variable and will be determined by the state of charge of the vehicle battery [17].

It should also be noted that in the course of research an emergency situation was artificially created during the work of the heater, by successive disconnection from power supply of a fuel pump, a fan, a circulating pump. The results confirm the rationality of the chosen algorithm to protect the system from overheating and other hazardous situations: the electronic unit initializes an error in the work of the heater (the disappearance of the flame in the combustion chamber, the overheating of the cold side of the modules, etc.) and stops its operation - the heater switches to the "purge" mode. In this case, the control panel displays a signal about the corresponding type of the error.

Conclusion

1. The conformity of thermal and electric parameters of thermoelectric starting pre-heater to its design characteristics is confirmed.
2. It is established that the use of modified thermoelectric modules "Altec-1061" allows increasing thermal productivity of thermoelectric starting pre-heater by a factor of 1.5 – 2, to the level of 3 kW, as compared to its first version.
3. It is shown that the electric power output of the developed thermoelectric starting pre-heater is within 80-100 W at a temperature of the hot heat exchanger 280 °C and the cold heat exchanger temperatures 30 – 70 °C. Maximum heater efficiency is 76.6 %.
4. It is determined that the mode of maximum heater power is achieved at the heat source thermal power 3.6 kW, fuel consumption 300 g/h and air consumption 8.19 m^3/h. In so doing, the cold heat carrier consumption is 0.3m^3/h.
5. The algorithm of operation of electronic control unit of thermoelectric heater components is shown. When the heater enters the autonomous operating mode, the electronic unit disconnects power supply of components from the battery and, as the electric power output of the generator increases, it directs the excess electric energy for recharging the battery.
6. It is established that the excess electric energy that can be used for recharging the battery is 50-70 W. However, the real value of charging current will be determined by the state of battery charge.
7. It is shown that control of heater work operation is done by intelligent algorithm of flame, air and fuel delivery and battery charge control, which assures stable operation of device and creates a reliable protection system in case of emergency.

References

1. Korchuganova M.A., Syrbakov A.P. (2013). Predpuskovoi zhidkostnyi podogrevatel diselnykh dvigatelei na baze puskovogo dvigatelia PD-10U [Starting liquid pre-heater of diesel engines based on starting engine PD-10U]. *Sovremennyie problemy nauki i obrazonaviia – Modern Problems of Science and Education,* 1 [in Russian].
2. Naiman V.S. (2007). *Vse o predpuskovykh obogrevateliakh i otopiteliakh [All about starting pre-heaters]*. Moscow: ACT [in Russian].
3. Retrieved from http://www.webasto-surgut.ru
4. Mykhailovsky V.Ya., Maksimuk M.V. (2014). Automobile operating conditions at low temperatures. The necessity of applying heaters and the rationality of using thermal generators for their work.

J.Thermoelectricity, 3, 20-31.
5. *Patent of Ukraine № 102303* (2013). Anatychuk L.I., Mykhailovsky V.Ya. Thermoelectric power supply for automobile. [in Ukrainian].
6. *Patent of Ukraine № 72304* (2012). Anatychuk L.I., Mykhailovsky V.Ya Automobile heater with thermoelectric power supply [in Ukrainian].
7. *Patent of Ukraine №124999* (2018). Maksimuk M.V. Automobile heater with thermoelectric power supply [in Ukrainian].
8. Mykhailovsky V.Ya., Maksimuk M.V. (2016). Computer design of thermoelectric automobile starting pre-heater operated with diesel fuel. *J. of Thermoelectricity,* 1, 52–65.
9. Anatychuk L.I., Mykhailovsky V.Ya., Maksimuk M.V., Andrusiak I.S. (2016). Experimental research on thermoelectric automobile starting pre-heater operated with diesel fuel. *J. of Thermoelectricity,* 4, 84–94.
10. Maksimuk M.V. (2017). On the optimization of thermoelectric modules of automobile starting pre-heater. *J.Thermoelectricity*, 1, 57–67.
11. Maksimuk M.V. (2017). Design of automobile starting pre-heater with a thermoelectric generator. Diesel version. *J.Thermoelectricity*, 2, 32-43.
12. Webasto. UK Product Catalogue.
13. Retrieved from http://www.deltaww.com
14. Mykhailovsky V.Ya., Maksimuk M.V. (2015). Rational powers of thermal generators for starting pre-heaters of vehicles. *J. of Thermoelectricity,* 4, 65–74.
15. Maksimuk M.V., Andrusiak I.S. (2016). Electronic control unit for thermoelectric automobile starting pre-heater. *J. of Thermoelectricity,* 5, 44–51.
16. *Patent of Ukraine № 90764* (2014). Mykhailovsky V.Ya., Zvozdetskyi P.V., Maksimuk M.V. Control system of starting liquid pre-heater for internal combustion engines [in Ukrainian].
17. Bubnov Yu.I., Orlov S.B. (2005). *Germetichnyie khimicheskiie istochniki toka: elementy i akkumuliatory. Oborudovaniie dlia ispytanii i ekspluatatsii. – Spravochnik [Sealed chemical current sources: elements and batteries. Testing and operating equipment*. - *Handbook*]. Saint-Petersburg: Khimizdat [in Russian].

Submitted 29.02.2018

Максимук М.В.

Інститут термоелектрики НАН і МОН України, вул. Науки, 1,
Чернівці, 58029, Україна*, e-mail: anatych@gmail.com*

СТЕНДОВІ ДОСЛІДЖЕННЯ ТЕРМОЕЛЕКТРИЧНОГО ПЕРЕДПУСКОВОГО ДЖЕРЕЛА ТЕПЛА ДЛЯ АВТОМОБІЛІВ

Наведено результати стендових досліджень енергетичних характеристик термоелектричного джерела тепла для передпускового підігріву двигунів автотранспортних засобів в умовах понижених температур навколишнього середовища. Показано, що використання термоелектричного перетворювача в якості джерела електричної енергії забезпечує автономну роботу компонент передпускових нагрівників та дозволяє вирішити проблему розрядки акумуляторної батареї автомобіля під час експлуатації передпускового обладнання. Бібл. 17, Рис. 10.

Ключові слова: передпусковий нагрівник, термоелектричний генератор.

Максимук Н.В.

Институт термоэлектричества, ул. Науки, 1, Черновцы, 58029, Украина
e-mail: anatych@gmail.com

СТЕНДОВЫЕ ИССЛЕДОВАНИЯ ТЕРМОЭЛЕКТРИЧЕСКОГО ПРЕДПУСКОВОГО ИСТОЧНИКА ТЕПЛА ДЛЯ АВТОМОБИЛЕЙ

Приведены результаты стендовых исследований энергетических характеристик термоэлектрического источника тепла для предпускового подогрева двигателей автотранспортных средств в условиях сниженных температур окружающей среды. Показано, что использование термоэлектрического преобразователя в качестве источника электрической энергии обеспечивает автономную работу компонентов предпусковых нагревателей и позволяет решить проблему разрядки аккумуляторной батареи автомобиля во время эксплуатации предпускового оборудования. Библ. 17, Рис. 10.
Ключевые слова: предпусковой нагреватель, термоэлектрический генератор.

References

1. Korchuganova M.A., Syrbakov A.P. (2013). Predpuskovoi zhidkostnyi podogrevatel diselnykh dvigatelei na baze puskovogo dvigatelia PD-10U [Starting liquid pre-heater of diesel engines based on starting engine PD-10U]. *Sovremennyie problemy nauki i obrazonaviia – Modern Problems of Science and Education,* 1 [in Russian].
2. Naiman V.S. (2007). *Vse o predpuskovykh obogrevateliakh i otopiteliakh [All about starting pre-heaters]*. Moscow: ACT [in Russian].
3. Retrieved from http://www.webasto-surgut.ru
4. Mykhailovsky V.Ya., Maksimuk M.V. (2014). Automobile operating conditions at low temperatures. The necessity of applying heaters and the rationality of using thermal generators for their work. *J.Thermoelectricity*, 3, 20-31.
5. *Patent of Ukraine № 102303* (2013). Anatychuk L.I., Mykhailovsky V.Ya. Thermoelectric power supply for automobile. [in Ukrainian].
6. *Patent of Ukraine № 72304* (2012). Anatychuk L.I., Mykhailovsky V.Ya Automobile heater with thermoelectric power supply [in Ukrainian].
7. *Patent of Ukraine №124999* (2018). Maksimuk M.V. Automobile heater with thermoelectric power supply [in Ukrainian].
8. Mykhailovsky V.Ya., Maksimuk M.V. (2016). Computer design of thermoelectric automobile starting pre-heater operated with diesel fuel. *J. of Thermoelectricity,* 1, 52–65.
9. Anatychuk L.I., Mykhailovsky V.Ya., Maksimuk M.V., Andrusiak I.S. (2016). Experimental research on thermoelectric automobile starting pre-heater operated with diesel fuel. *J. of Thermoelectricity,* 4, 84–94.
10. Maksimuk M.V. (2017). On the optimization of thermoelectric modules of automobile starting pre-heater. *J.Thermoelectricity*, 1, 57–67.
11. Maksimuk M.V. (2017). Design of automobile starting pre-heater with a thermoelectric generator. Diesel version. *J.Thermoelectricity*, 2, 32-43.

12. Webasto. UK Product Catalogue.
13. Retrieved from http://www.deltaww.com
14. Mykhailovsky V.Ya., Maksimuk M.V. (2015). Rational powers of thermal generators for starting pre-heaters of vehicles. *J. of Thermoelectricity,* 4, 65–74.
15. Maksimuk M.V., Andrusiak I.S. (2016). Electronic control unit for thermoelectric automobile starting pre-heater. *J. of Thermoelectricity,* 5, 44–51.
16. *Patent of Ukraine № 90764* (2014). Mykhailovsky V.Ya., Zvozdetskyi P.V., Maksimuk M.V. Control system of starting liquid pre-heater for internal combustion engines [in Ukrainian].
17. Bubnov Yu.I., Orlov S.B. (2005). *Germetichnyie khimicheskiie istochniki toka: elementy i akkumuliatory. Oborudovaniie dlia ispytanii i ekspluatatsii. – Spravochnik [Sealed chemical current sources: elements and batteries. Testing and operating equipment*. - *Handbook*]. Saint-Petersburg: Khimizdat [in Russian].

Submitted 29.02.2018

P. D. Mykytiuk

P.D.Mykytiuk[1, 2], *Candidate Phys.-math. Sciences*
O.Yu.Mykytiuk[3] *Candidate Phys.-math. Sciences, docent*

[1]Institute of Thermoelectricity of the NAS and MES of Ukraine, 1, Nauky str, Chernivtsi, 58029, Ukraine;
[2]Yu.Fedkovych Chernivtsi National University, 2, Kotsiubynskyi str., Chernivtsi, 58000, Ukraine
e-mail: anatych@gmail.com
[3]Higher State Educational Institution of Ukraine "Bukovinian State Medical University", 2, Theatre Square, Chernivtsi, 58002, Ukraine

O. Yu. Mykytiuk

IMPACT OF THERMOCOUPLE ON TEMPERATURE DISTRIBUTION IN THE HEATER OF MEASURING THERMAL CONVERTER

The impact of thermocouple on temperature distribution in the heater of thermal converter for the case of similar thermocouple and heater geometry is investigated. It is established that heat loss due to thermal conductivity of the thermocouple and its heat exchange with the environment reduce the temperature in the heater center by a factor of almost 1.5. Variants of increasing the efficiency of using heat in thermal converter are proposed. Bibl. 9, Fig. 2.

Key words: thermal converter, thermocouple, heater, temperature distribution.

Introduction

In [1 – 3], temperature distribution in structural members of thermoelectric measuring converter is studied, with regard to heat exchange with the environment. However, these works do not study in full measure the character of impact of thermal processes occurring in thermocouple on temperature distribution in the heater for the case when geometric dimensions of the heater and thermocouple are similar. Taking into account such impact will significantly improve the parameters and characteristics of the thermal converters in the process of their design.

The purpose of this work is to study the impact of thermocouple on temperature distribution in the heater of thermal converter.

Model of thermal converter for calculation of temperature distribution in its structural members

To take into account the impact of thermocouple on temperature distribution in the heater, we will make calculations for "heater-thermocouple" system, Fig. 1.

Let us write thermal balance conditions taking into account the Joule effect, thermal conductivity, heat exchange with the environment for the heater:

$$\frac{\kappa_h \cdot S_h d^2 T(x_h)}{dx_h^2} - C_{0h}(T(x_h) - T_0)\pi d_h + \frac{I_h^2 \cdot \rho_h}{S_h} = 0 \qquad (1)$$

and the thermocouple:

$$\frac{\kappa_t \cdot S_t d^2 T(x_t)}{dx_t^2} - C_{0h}(T(x_t) - T_0)\pi d_t = 0, \tag{2}$$

where d_t is diameter of the cylinder thermocouple base (for thermocouple in the form of a regular prism which is considered the reduced diameter d_t is given by the condition of equality of the areas of cylinder and prism base, that is $d_t = 2\sqrt{\frac{S_t}{\pi}}$).

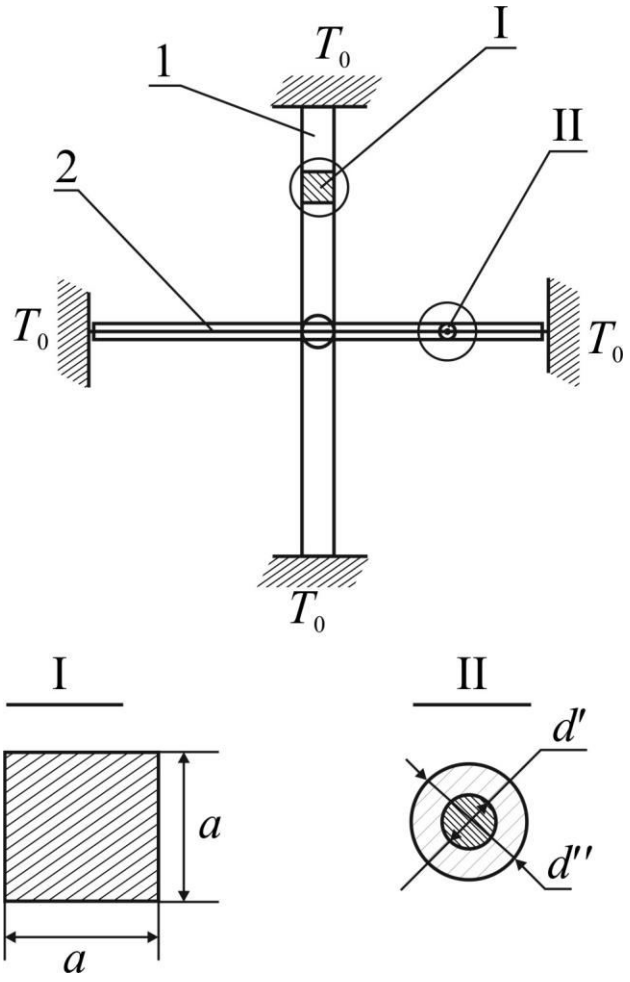

Fig.1. Model of thermal converter for calculation of temperature distribution in its structural members: 1 – heater; 2 – thermocouple; d' – diameter of microwire without glass insulation; d'' –diameter of microwire in glass insulation

Denoting:

$$\theta_h = T(x_h) - T_0,\ \theta_t = T(x_t) - T_0; \tag{3}$$

$$a_h = \frac{\pi d_h}{\kappa_h S_h} \tag{4}$$

$$b_h = \frac{\rho_h \cdot I_h^2}{\kappa_h \cdot S_h^2} \tag{5}$$

$$a_t = \frac{\pi d_t C_{0t}}{\kappa_t S_t} \tag{6}$$

we get:

$$\frac{d^2\theta_h(x_h)}{dx_h^2} - a_h\theta_h(x_h) + b_h = 0 \tag{7}$$

$$\frac{d^2\theta_t(x_t)}{dx_t^2} - a_t\theta_t(x_t) = 0 \tag{8}$$

The boundary conditions in this case:

$$\theta_h(0)=\theta_t(0)$$

$$\kappa_h S_h \frac{\partial\theta_h(x_h)}{\partial x_h}\Big|_{x_h=0} = -\kappa_t S_t' \frac{\partial\theta_t(x_t)}{\partial x_t}\Big|_{x_t=0} \tag{9}$$

Considering jointly the solutions of equations (7) and (8), with regard to the boundary conditions (9) after a series of cumbersome transformations, which are omitted in this paper, we obtain an expression for the distribution of temperature in the heater, taking into account the impact of the thermocouple on it:

$$\theta_h(x_h) = \frac{\rho_h I_h^2}{C_{0h} S_h P_h} chN_h(x_h - 1)\left[\frac{1 + k\dfrac{\text{th}N_h x_h}{\text{th}N_t x_t}}{1 + k\dfrac{\text{th}l_h}{\text{th}l_t N_t}} \cdot \frac{ch(N_h x_h)}{ch(N_h l_h)} - \frac{ch(N_h x_h) - 1}{ch(N_h l_h) - 1}\right], \tag{10}$$

where $l_н$, $l_т$ is half the length of the heater and thermocouple, respectively;

$$N_t = \sqrt{\frac{C_{0t} \cdot \rho_t}{\kappa_t S_t}};$$

$$N_h = \sqrt{\frac{C_{0h} \cdot \rho_h}{\kappa_h S_h}}$$

$$k = \frac{\kappa_t S_t N_t}{\kappa_h S_h N_h};$$

$P_н$ is perimeter of cross-section with the area $S_н$.

To estimate the share of different heat exchange mechanisms in this model, we will write an expression for maximum temperature drop with regard to individual mechanisms of heat losses.

With losses only due to thermal conductivity of thermocouple and heater materials, ΔT_{max} is described by the expression:

$$\Delta T_{max} = \frac{U_h^2}{8\kappa_h\rho_h} \cdot \left(\frac{1}{1 + \dfrac{R_h}{R_t}\dfrac{\kappa_t\rho_t}{\kappa_h\rho_h}}\right) \tag{11}$$

Account of convective heat exchange yields the expression:

$$\Delta T_{max} = \frac{b_h}{a_h} \cdot \left(\frac{1 - Schx_h}{1 + k\dfrac{\text{th}x_h}{\text{th}x_t}}\right), \tag{12}$$

where $x_h = \sqrt{a_h} l_h$, $x_t = \sqrt{a_t} l_t$.

Calculations show that when taking into account heat losses due to thermal conductivity of the thermocouple, the maximum temperature in the heater center is decreased approximately by a factor of 1.5. At the same time, the main part of the heat loss is due to the heat exchange of the thermocouple with the environment.

On the basis of the obtained results it can be concluded that the most promising way to increase the efficiency of heat use in the thermal converter is to reduce the heat loss due to convective heat transfer. In so doing, it is necessary to take into account two factors: the first one is the reduction of ambient thermal conductivity by filling the working volume of the thermal converter with gases with low thermal conductivity or evacuation; the second is the change in the shape of the temperature distribution curve in the heater center, provided that all heat is released in its center. In the former case it is necessary to solve mainly technological problems, i.e. develop a vacuum-sealed case and increase the stability of the characteristics of thermocouple and heater materials in vacuum, whereas in the latter case it is necessary to explore the possibility of creating a heater that will provide the maximum temperature in its center.

Conclusion

1. At similar dimensions of the heater and thermocouple, heat loss due to thermal conductivity of the thermocouple and heat exchange with the environment can lead to a decrease of maximum temperature in the heater center by a factor of 1.5, which significantly affects the parameters of the thermal converter and can be largely compensated by evacuation or filling the work space of the thermal converter with the low thermal conductivity inert gas.
2. It is relevant to study the opportunity of using in the design of thermal converter of heaters with a variable section or made of different materials.

References

1. Tashchuk D.D. (2012). Optimization of temperature distribution in thermoelectric measuring transducer. *J.Thermoelectricity*, 4, 95 – 98.
2. Mykytiuk P.D. (2017). Factors of influence on the accuracy of thermal converters. *J.Thermoelectricity*, 5, 76 – 83.
3. Anatychuk L.I., Kuz R.V., Tashchuk D.D. (2015). Differential thermoelectric AC converter in the non-simultaneous comparison mode. *J.Thermoelectricity*, 4, 77 – 82.

Submitted 08.02.2018

Микитюк П.Д. *канд. фіз.-мат. наук*[1,2]
Микитюк О.Ю. *канд. фіз.-мат. наук, доцент*[3]

[1]Інститут термоелектрики, вул. Науки, 1;Чернівці, 58029, Україна;
[2]Чернівецький національний університет імені Юрія Федьковича,
вул. Коцюбинського 2, Чернівці, 58012, Україна;
[3]Вищий державний навчальний заклад України «Буковинський державний
медичний університет», Театральна площа, 2, Чернівці, 58002, Україна

ПРО ВПЛИВ ТЕРМОПАРИ НА РОЗПОДІЛ ТЕМПЕРАТУРИ В НАГРІВНИКУ ВИМІРЮВАЛЬНОГО ТЕРМОПЕРЕТВОРЮВАЧА

Досліджено вплив термопари на розподіл температури в нагрівнику термоперетворювача для випадку подібності геометричних розмірів термопари і нагрівника.
Встановлено, що втрати тепла за рахунок теплопровідності термопари та її теплообміну з оточуючим середовищем зменшують температуру в центрі нагрівника майже в 1,5 рази. Запропоновано варіанти підвищення ефективності використання тепла в термоперетворювачі.
Ключові слова: термоперетворювач, термопара, нагрівник, розподіл температури.

Микитюк П.Д. *канд. физ.-мат. наук*[1,2]
Микитюк О.Ю. *канд. физ.-мат. наук, доцент*[3]

[1]Институт термоэлектричества, ул. Науки, 1;Черновцы, 58029, Украина;
[2]Черновицкий национальный университет имени Юрия Федьковича,
ул. Коцюбинского 2, Черновцы, 58012, Украина;
[3]Высшее государственное учебное заведение Украины «Буковинский государственный медицинский университет», Театральная площадь, 2, Черновцы, 58002, Украина

О ВЛИЯНИИ ТЕРМОПАРЫ НА РАСПРЕДЕЛЕНИЕ ТЕМПЕРАТУРЫ В НАГРЕВАТЕЛЕ ИЗМЕРИТЕЛЬНОГО ТЕРМОПРЕОБРАЗОВАТЕЛЯ

Исследовано влияние термопары на распределение температуры в нагревателе термопреобразователя для случая подобия геометрических размеров термопары и нагревателя.
Установлено, что потери тепла за счет теплопроводности термопары и ее теплообмена с окружающей средой уменьшают температуру в центре нагревателя почти в 1, 5 раза. Предложены варианты повышения эффективности использования тепла в термопреобразователе.
Ключевые слова: термопреобразователь, термопара, нагреватель, распределение температуры.

References

1. Tashchuk D.D. (2012). Optimization of temperature distribution in thermoelectric measuring transducer. *J.Thermoelectricity*, 4, 95 – 98.
2. Mykytiuk P.D. (2017). Factors of influence on the accuracy of thermal converters. *J.Thermoelectricity*, 5, 76 – 83.
3. Anatychuk L.I., Kuz R.V., Tashchuk D.D. (2015). Differential thermoelectric AC converter in the non-simultaneous comparison mode. *J.Thermoelectricity*, 4, 77 – 82.

Submitted 08.02.2018

S.O.Filin

S.O.Filin

West Pomeranian University of Technology, Szczecin
17, al.Piastow, Szczecin, 70-310, Poland,
e-mail: sergiy.filin@zut.edu.pl

THE INFLUENCE OF THERMAL CONTACT BETWEEN COOLING SURFACE AND OBJECT ON THE SPEED OF THERMOELECTRIC BEVERAGE COOLERS

This article describes the design and operational features of modern thermoelectric beverage coolers and heaters, in particular, their dynamic characteristics. The results of comparative tests show the influence of the heat exchange conditions between the can (bottle) and the cooler container on the beverage cooling rate. Filling the gap between the beverage bottle and the cooler container allows significant improvement of the high-speed performance of the cooler. For example, the time of beverage cooling from 25°C to 10°C in the cooler under test has decreased from 67 to 50 minutes. Bibl. 10, Fig. 11, Table 2.

Key words: beverage cooler/heater, cooling rate, heat exchange conditions, experimental tests.

Introduction

Over the past two decades, in the publications on thermoelectric cooling, including proceedings of the International Forums on Thermoelectricity, it has been noted that manufacturers of household thermoelectric products have drastically reduced the requirements to a number of technical characteristics, mainly for the sake of reducing the price and energy consumption of these products [1, 2]. In turn, low price allows considering such products as not subject to repair, and therefore their life cycle is limited to several years. Modern thermoelectric refrigerators (both portable and stationary) are much inferior to their predecessors in the created temperature difference [3]. As a result, the shelf life and assortment of stored products decreases.

Among the proposals appearing on the international market of refrigeration equipment, one can find portable auto refrigerators without thermal insulation. Its role is played by a 20-mm layer of air between the casing and the chamber. And this bears witness to the fact that professionals did not undertake the production of refrigerators, once again discrediting the very idea of thermoelectric cooling.

Unlike refrigerators, thermoelectric coolers and beverage heaters are classified as episodic products. They are characterized by the predominance of dynamic parameters over energy ones. It is the question of the time of beverage cooling from the initial to the final temperature and the average cooling rate. For the consumer it is very important that this time is minimal, especially on a trip or on vacation, i.e. in the absence of other technical means of cooling. A lot of publications, patents and even a monograph [4] are devoted to the analysis of the dynamic characteristics of thermoelectric ice makers[1], whereas beverage coolers obviously remained ignored. A few publications on this subject fall at the turn of the twentieth and twenty-first centuries [5, 6].

Let us remind our readers that in the world there are two competing approaches to cooling of beverages: *the European*, when a beverage is cooled by an external source of cold without

changing the composition of the drink, and *the American*, when a beverage is cooled by slices of water ice dissolved in the drink. This division does not mean that both ways of cooling are not common in the world, but the preferences of the inhabitants of the New and Old World are obviously different [4]. The European approach means both cooling of beverage in its original packaging, to which the main part of the article is devoted, and its cooling in special container or containers, as shown in Fig. 1. On the cooler packing box there is a graph showing the dynamics of beverage temperature decrease from the temperature of 27° C.

Fig.1. A typical commercial (bar) beverage cooler.

Commercial coolers are usually equipped with a compressor refrigeration unit of a rather high capacity, owing to which consumers have no claims to their speed. Below we will consider how the problem of the speed of small thermoelectric beverage coolers is solved, or, on the contrary, not solved, by their manufacturers.

A brief analysis of the market for modern thermoelectric beverage coolers

We shall start the analysis with automobile devices. They are the most numerous and characterized by the simplicity of design. Power supply of the thermoelectric unit is directly from the electrical network of the vehicle 12 – 14 V DC, for example, through the cigarette lighter socket of the car (Fig. 2). A typical modern beverage cooler is designed for cooling and heating beverages in metal cans from 0.25 to 0.5 l with a unified outer diameter of a can 66 mm. A can with the beverage is put into the open top metal container in the form of a glass made of aluminum. Coolers for two cans are less common [6]. The container has an internal diameter 1-2 mm larger than the diameter of the can. In the gap between the can and the container during operation there remains a thin layer of air.

The whole variety of the cooler designs can be reduced to two types: with the lateral and with the bottom location of the unit. In addition to the thermoelectric module, the unit includes a heat sink of the hot[2] side of module and a fan designed for blowing the hot heat sink. The number of controls and automation is also minimized: the mode selection switch with the LED indicator plus (in some models) the temperature relay for protecting the module hot side from overheating. The cold side of the module through the metal heat spreader almost directly contacts the container.

Small household, office and bar ice makers also refer to products of episodic action.

Fig. 2. Typical design of automobile beverage cooler-heater in the cans with a lateral location of the unit.

The household (or table) version of the cooler (Fig. 3) differs from the automobile one by the availability of AC/DC converter. Its presence practically does not affect the dynamic characteristics of the cooler.

Fig. 3. Household thermoelectric beverage coolers-heaters with a bottom location of the unit.

Few manufacturers specify the rate or time of cooling in the specifications for their products, and, as a rule, without specifying the conditions under which this rate is measured. For example, from the information that the cooling rate of a beverage in a 0.33 liter can is 0.3° C/min it is not clear in what temperature range this rate was measured, at what ambient temperature, at what supply voltage, etc. Verification of the characteristics of some coolers, which was carried out at our department as far back as 2002, showed the principal correspondence of the measured and declared characteristics and allowed us to clarify for the consumer to which exactly operating conditions these characteristics correspond to.

Since that time, there have been no revolutionary changes in the energy efficiency of thermoelectric modules, which determined the "freeze" (stabilization) of beverage cooling rate in thermoelectric coolers. But this does not correspond in any way to consumers' expectations. That is why the German company Do-Tech GmbH decided to start a serial production of beer cans with a built-in coil filled with carbon dioxide under pressure. When the can is opened, the integrity of the inner volume of the coil is also impaired. As a result, the gas, leaving a small opening, is throttled, cooling the contents of the can for a few seconds [7].

In a reverse operation of the device, the concepts of "cold" and "hot" side of the module are conventional. To simplify the description, these names are accepted for beverage cooling mode.

Fig. 4. High-speed cooler from German company Do-Tech GmbH [8].

How will the manufacturers of similar thermoelectric products respond? Strangely enough, by slowing down the cooling rate. Some poor designers in pursuit of the cheapening of their products sacrifice their speed and offer very strange innovative solutions. Here are just some of them.

It is difficult to understand the motives of the authors of the cooler shown in Fig.5, who reduced more than twice an already small surface of the contact of the can with the cooler container or rather what was left of it. In addition to increasing the cooling time, the device has a number of operational shortcomings: difficulties with ensuring the thermal contact of the can with the cooler, with mounting the device in the car, with orientation in space, etc.

The authors and manufacturers of cooler-heaters, powered from the computer via the USB port (Fig. 6), went even farther. In these products, the contact surface is limited to a metal stand of diameter 66 – 70 mm. Taking into account that the bottom of the metal can is concave and the cooling capacity of the module is significantly lower, it can be concluded without experimental verification that the cooling rate does not exceed 0.1 ° C / min, which is 5 – 6 times slower than in coolers with a power supply of 12 ... 14 B and isolated container. Reducing the cooling capacity of module is related to the limitation of the power of the USB port: the current strength cannot exceed 0.5 A. The modern serial thermoelectric module is designed for a supply current of 2 to 4 A. A low-current cooling module can be designed and made to be rather powerful (about 50 W of maximum cooling capacity), but this is due to the miniaturization of the module, which in turn leads to a complication of the technology and more than 10-fold increase in the price of the module. Under these conditions, coolers with such modules become uncompetitive.

Fig. 5. Automobile thermoelectric beverage cooler produced by ACT, Krasnoiarsk, Russia.

Fig. 6. Cooler-heater powered from computer through the USB port.

To increase the interest of potential buyers in their products, some manufacturers use techniques that cannot be classified as "fair play". For example, the manufacturer of the Smart Holder Hot automobile cooler (Fig. 3, at the center) declares that this *product "provides cooling of the can or bottle (!) to a temperature of -6°C within 10 minutes and heating to + 60°C within 5 minutes"* [9]. Sellers of this product from the online store www.sititek.ru have to explain to customers that "these temperatures are reached during this time on the wall of the container, and the beverage itself is cooled somewhat slower". This "somewhat slower" means in practice from 40 to 70 minutes. Is it malice or holy simplicity? It is impossible to refrain from commenting on this "masterpiece of technical thought". So:

1) most beverages, including low alcohol drinks, cannot be cooled to a temperature of –6°C, they are frozen;

2) the time for cooling to the desired temperature of a can and a bottle of the same capacity with the same beverage will be different;

3) in order to provide the consumer with complete and truthful information regarding the dynamic characteristics of the device, the manufacturer must specify: the temperature range for cooling and heating the beverage, for example from 25° C to 10° C, ambient temperature, cooling time or average cooling rate in the above range, the mass and type of refrigerated drink and the type of its packaging. Similar data must be specified for the heating mode;

4) if the temperature of the beverage referred to in paragraph 3 is not average in its volume, the exact place of measurement of this temperature should be indicated.

Unfortunately, this is not the only example of an attempt to mislead users of cooler heaters [10].

Few manufacturers of coolers draw the attention of users to the possibility of cooling beverages in plastic and glass bottles. One of them is the company WAECO, known on the market of transport refrigerators (Fig. 7). The reason for this situation is not that the dimensions of the cooler container do not correspond to the outside diameter of the bottle, but that the cooling time of the same mass of the beverage, now in the bottle, is approximately 2 times greater. Therefore, manufacturers are not interested in disclosing such unprofitable information for them.

Fig. 7. Thermoelectric beverage cooler-heater WAECO MyFridge, model MF-1F-12/24.

In electric household heaters for baby food, the internal diameter of the container is on average 5 ... 8 mm larger than the diameter of the bottle. In them, the contents of the bottle is heated in a "water bath", which not only speeds up the process compared to "dry" cooling, but also allows you to keep the beverage longer in a warm state and ensure a more uniform heating of the bottle along its height.

This method with the placement of water in the cooler containers is not used, in spite of the fact that this obvious and not very complicated solution allows improving the dynamic characteristics of the device. However, the use of water in a container requires the development of appropriate innovative technical solutions, including those ensuring the sealing of a water-filled annular gap. The lack of such solutions also explains the lack of information about experimental studies of the effect of the presence of water (or other liquid) in the cooler container during beverage cooling. The data presented in the following sections of the article is intended, at least partially, to fill this gap.

Object of study

Comparative tests of coolers were carried out at the Department of Conditioning and Refrigerating Transport of the West Pomeranian University of Technology in Szczecin in the period of April-May 2018. As a research object, two identical coolers *Car mini-cooler* FM 201.001 manufactured by the Kiev NPF "Module" are used, having a design typical for this class of products. This cooler uses one module of the type MT1.42-1.12-12 with its lateral location relative to the beverage container (Fig. 5). The container in the form of a cylindrical glass with an internal diameter of 67 mm is made of an aluminum alloy, and a removable non-metal bottom. The depth of the glass is 70 mm, which makes it easy to attach and remove a metal can with a 0.33 liter beverage, without resorting to turning the cooler.

In the first series of experiments, 0.33 l metal cans filled with settled water were cooled, and in the second series - plastic bottles with carrot and fruit juice with a capacity of 0.3 liters. At the same time, two coolers with the same drinks were tested, which differed only in the way of thermal contact: in the first case, the so-called "dry" contact (Fig.8, left), in the second – "wet". The container of the second cooler was sealed with silicone and filled with settled water, so that its level in the gap between the can (bottle) and the container was 1 mm below the end of the container.

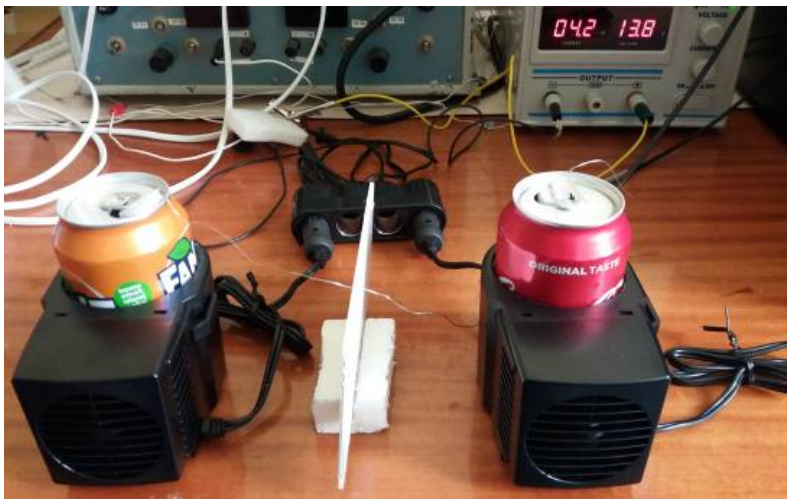

Fig. 8. Fragment of comparative studies of beverage coolers Car mini-cooler FM 201.001.

The two coolers under test differed in the way the thermal contact between the cooling object and the container was organized. In the first cooler (Fig. 8, on the left), a contact between a can of diameter 66 mm

and a container occurred through a thin air gap, and in the second - through a layer filled with liquid. In the case of cooling the can, 15.0 g of water was filled in the container, in the case of the bottle – 62.2 grams[3].

The purpose of the experiments was to determine the influence of the heat exchange conditions between the can (bottle) and the container on the dynamic characteristics of the cooler, namely the speed and the cooling rate in different operating conditions. The further purpose was to verify the technical characteristics of the device supplied by the manufacturer in the operating instructions.

Experimental conditions and description of the test bench

The temperature in the laboratory room was stabilized at 25 + 0.3° C using a *split-type* household air conditioner. All initial temperatures were equal to each other and equal to the temperature in the room.

A simplified schematic of the bench is shown in Fig. 9. The coolers were connected in parallel and powered from the laboratory source D3010 through a car extension with a separator (Fig. 8). Temperature measurements were carried out using thermocouples type J, connected to the 8-channel meter AR206. The mass of beverages, bottles and water was measured on a laboratory scale Radwag WPS 510/C/1 with a division value of 1mg.

The outer diameter of the plastic bottle around the working area was about 56 mm.

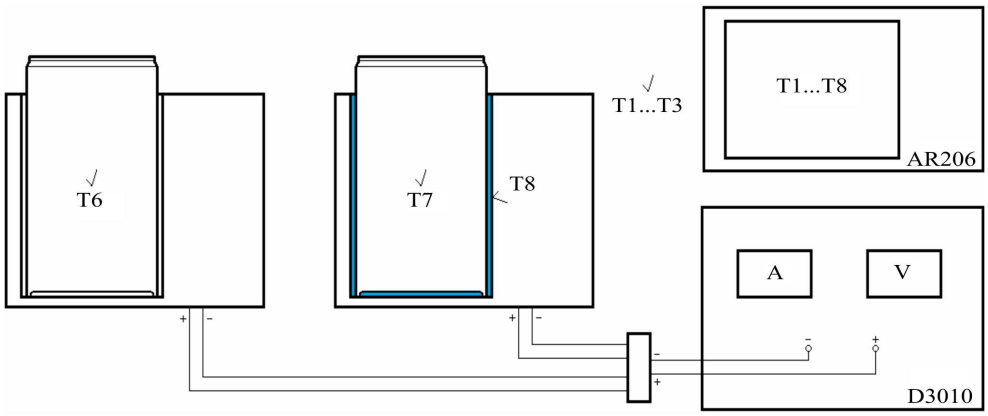

Fig. 9. Simplified schematic of experimental bench; T1-T9 – locations of temperature sensors.

Prior to testing, each cooler was connected to power supply separately, and current flowing through it and power consumption were recorded. The values of the currents measured by the instrument with a 0.01 A division value in the same time intervals from the instant the coolers were switched on differed by no more than 0.02 A. This means that the difference in the internal ohmic resistance of the coolers was minimal and its effect on the result of the comparative tests can be neglected.

During testing, the following parameters were monitored every 5 minutes from the moment the coolers were switched on until the temperature of the beverages[4] was stabilized:

- beverage temperature in the geometric center of the can (bottle);
- air temperature in the room at three points with subsequent averaging of the fixed values. All three temperature sensors were at the level of the upper edge of the cooler container at a distance of 10 ... 30 cm from them (Fig. 9);
- water temperature in the gap between the bottle and the container with periodic monitoring of its variation along the height of the container;
- supply current and voltage of the two coolers.

The coolers were tested at two values of their supply voltage:

12.0 V corresponds to the power supply from the car battery during its parking,

13.8 V corresponds to the power supply from the on-board network (generator), with the car engine running.

Test results and their discussion

Test results in the form of temperature history are represented in Figs.10 and 11, and comparison of actual and manufacturer-declared technical characteristics is given in Table 1.

According to [1], under the stabilization of the beverage temperature we understand that within 30 minutes its temperature does not change by more than 0.1 degrees.

Table 1

Comparison of technical characteristics of the cooler Car mini-cooler FM 201.001 declared by the manufacturer in the Operating instructions and measured as a result of laboratory tests

Characteristics	Declared	Measured	
Supply voltage, V	12	12	13.8
Current, A	2.3	2.35 (start period) 1.8 (average value in the cooling period)	5,1 (start period) 4.2 (average value in the cooling period)
Maximum reduction of beverage temperature with respect to ambient temperature, ^{o}C	15	17	19
Average cooling rate, ^{o}C/min	0.5	0.30 (the first 15 minutes of work) 0.28 (the first 30 minutes of work) 0.22 (the first 60 minutes of work)	0.39 (the first 15 minutes of work) 0.36 (the first 30 minutes of work) 0.26 (the first 60 minutes of work)
Beverage volume, ml	330	330.2	332.0

The data presented in Table 1 refers to cooling of water cans with a volume of 0.33 liters, as shown in Fig. 8. The influence of the type of beverage on the time of its cooling manifests itself through the difference in the mass specific heat ***c***. It is known that water possesses the highest specific heat among all known liquids on the Earth, and therefore the cooling time of a unit of water mass will be greatest. For pure water, c_w = 4.19 kJ / kgK at a temperature of 20°C. Non-alcoholic beverages, such as Cola, Fanta, etc., have ***c*** values close to water that lie within the range 4.13 ... 4.16 kJ / kgK. This means that the estimated reduction in the cooling time of these beverages in comparison with water does not exceed 1% and can be ignored in the engineering calculations and experiments. For natural juices and low-alcohol beverages (Table 2), the value of ***c*** already becomes less than 4.0 kJ / kgK, and, therefore, the cooling time reduction can be 5 – 7 %. But it should be remembered that for juices, the aforementioned reduction will not be proportional to a decrease in specific heat; it will be less, because some juices, such as tomato, peach, plum, are lighter than water.

With an increase in the alcohol content of the drink, c decreases. If the alcohol content is more than 7 %, the influence of specific heat should be taken into account. The method for calculating the cooling time of the beverage in a thermoelectric cooler will be presented in the second part of the article.

[5]Exactly this temperature was taken as the reference temperature, because it is average in a typical process of beverage cooling from 25 ... 27°C to 10 ... 15°C.

Table 2

*Mass specific heat **c** [kJ/kgK] of some beverages at 20°C (the source: information from manufacturers, distributors, information from handbooks and other public data from Internet-pages)*

Water	4.19	Tomato juice	3.98
Beer	3.85…3.94*	Apple juice	3.85
Milk	3.77…3.94**	Orange juice	3.73…3.89***
Vodka (40°)	3.96	Raspberry juice	3.89
Dry wine	3.75	Strawberry juice	3.94
Fortified wine	3.69	Cherry juice	3.85
Alcopop	4.04…4.10*	Grape juice	2.80…3.69***
Cognac spirit	2.42	Pineapple juice	3.77

* - depending on alcohol content
** - depending on the content of fat and dry substances
** * - depending on the content of dry substances

Analysis of the data in Table 1 shows that supply current 2.3 A and the maximum beverage temperature reduction 15°C are achieved by the manufacturer at a supply voltage of 12 V DC. The real characteristics turned out to be better than the declared ones. The situation looks different with the cooling rate. The declared cooling rate of 0.5°C/min was not obtained in any of the experiments. The beverage was cooled most quickly in the time interval between the 5th and 10th minutes after switching on: 0.36° C / min at U = 12V and 0.46°C / min at U = 13.8V. Additional tests carried out at the starting temperature of the beverage and ambient air of 27°C[6] showed no significant differences in the cooling rate as compared to the tests at a temperature of 25 °C.

During the tests, a significant difference in the temperature and dynamic characteristics of the cooler was recorded, depending on the supply voltage. At a voltage of 13.8 V compared to a voltage of 12 V, the depth of cooling increases by 2 degrees, and the average cooling rate by 22 ... 25%.

Much worse results were obtained in the case of cooling juice in a bottle. This applies to both cooling depth, which is only 7 ° C, and cooling rate which is on average 0.1 ° C / min. The main reason for this deterioration in dynamic characteristics is the increased air gap between the container and the bottle. This is further evidence in favor of using a "wet" contact.

[6]On the packing box of the cooler there is a graph showing the dynamics of beverage temperature decrease from the temperature of 27°C.

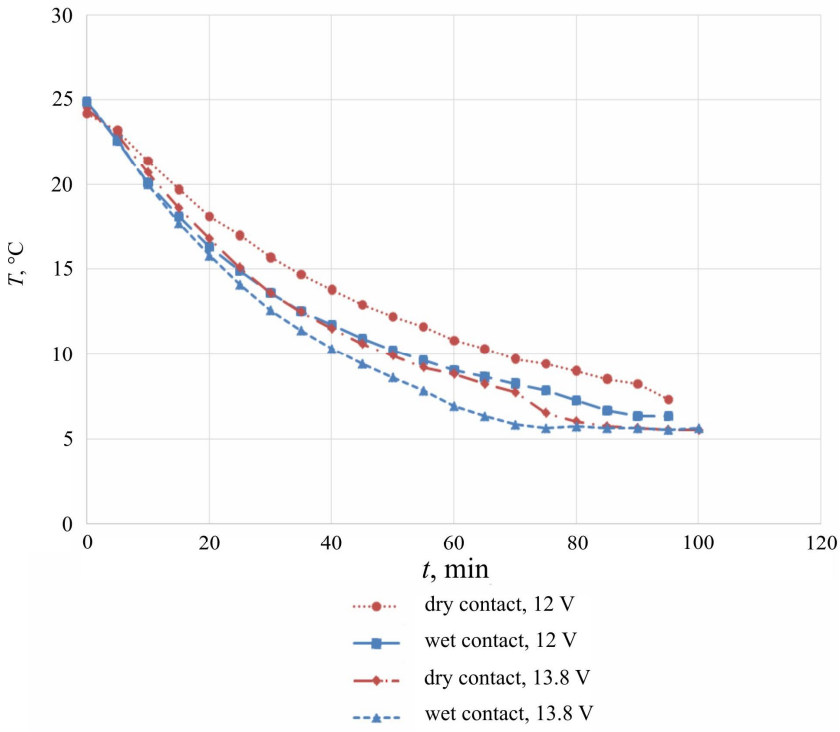

Fig. 10. Comparison of cooling rate of 0.33 l water cans in the presence of water in the gap ("wet" contact) and without water ("dry" contact) in the cooler container Car mini-cooler FM 201.001 for two its supply voltages.

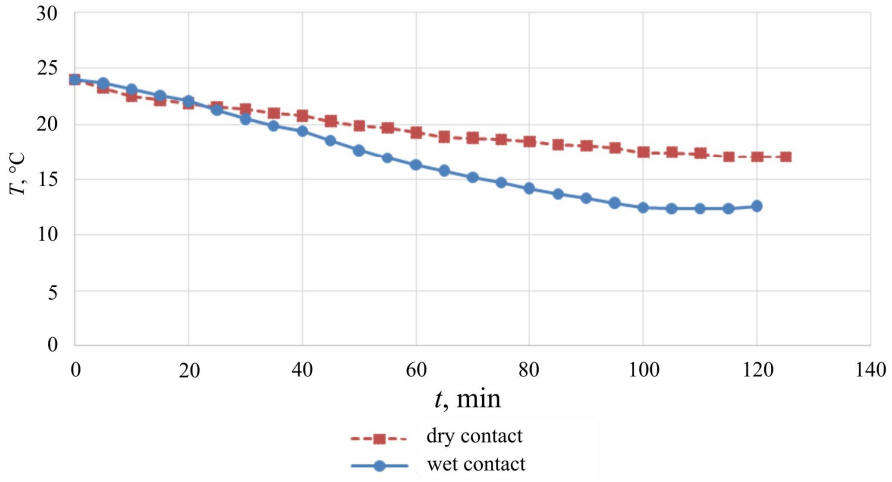

Fig. 11. Comparison of cooling rate of 0.3 l bottles with juice in the presence of water in the gap ("wet" contact) and without water ("dry" contact) in cooler container Car mini-cooler FM 201.001.

Analysis of the plots presented in Figs. 10 and 11 shows a significant improvement in the dynamic characteristics of the cooler, regardless of the type of beverage and its packaging. For example, cooling the beverage 10°C below the initial temperature, which is generally equal to the ambient temperature, with water in the container-can gap occurs for 25 minutes, and without water - for 34 minutes. This is 26.5 % faster . The figures presented concern the cooling of 0.33 l aluminum can at a voltage of 12 V. Similarly, for a supply voltage of 13.8 V, the same figures look like this: 22.5 minutes, 27 minutes, acceleration - 16.7 %.

In the case of cooling a bottle with juice, the advantage of a "wet" contact becomes apparent in 20 minutes after switching on (Fig. 11). This is due to the relatively large mass of water poured into the container. During the first 15 minutes, part of module cooling capacity is spent on cooling this additional mass of water. But within 95 minutes it is possible to lower the temperature of the drink to 12.9° C, which is 5 degrees lower than for the version with a "dry" contact.

Conclusion

1. Manufacturers of modern automobile and household beverage coolers-heaters do not use a simple and effective method of increasing the speed of these devices, namely, the so-called "wet" contact of the can or bottle with the cooler container.
2. Experimental research carried out by the author made it possible to quantify the positive effect of the application of the mentioned solution. The cooling rate of the device chosen for experiments in the presence of water increased by 16 ... 26%.
3. You can expect that in a specially designed cooler with a "wet" contact it will be possible to get even better results, increasing the speed by 30 ... 35%.
4. The works on the creation of such a cooler are carried out at the Department of Conditioning and Refrigeration at the West Pomeranian University of Technology in Szczecin.
5. The results of laboratory tests of the cooler sample will be published later.

References

1. Filin S., Owsicki A. (2010). *Zasady projektowania i eksploatacji chłodziarek termoelektrycznych*. ZAPOL: Szczecin.
2. Filin S., Jasińska B. (2013). Efektywność energetyczna transportowych chłodziarek termoelektrycznych. Energetycznie efektywne rozwiązania urządzeń chłodniczych, klimatyzacyjnych i pomp ciepła. *XLV Dni Chłodnictwa (Poznań. 13-14.11.2013),* p. 63-74.
3. Filin S.O. (2017). Comparative analysis of energy characteristics of contemporary thermoelectric refrigerators. *J.Thermoelectricity*, 6, 83-91.
4. Sergiy Filin. (2006). *Technika i technologia produkcji lodu spożywczego*. Masta: Gdańsk.
5. Anatychuk L., Filin S., Danko E. (1998). Cool before drinking. *Office*, 5, 39-40.
6. Sergiy Filin. (2002). Współczesne transportowe chłodziarki do napojów. *Technika Chłodnicza i Klimatyzacyjna* 2, 60-62 .
7. Self-cooled can for beer. Retrieved from: http://forum.beermir.com/viewtopic.php?t=1808&postdays=0&postorder=asc&start=25
8. Retrieved from: http://mirbeer.blogspot.com/2014/02/blog-post_24.html
9. Retrieved from: http://personal-security.ru/lichnaja-bezopasnost/avto-i-velo-aksessuary-dlja-bezopasnostiikomforta? product_id=7392
10. Automobile coolers for beverages: no ice! Retrieved from: https://www.zr.ru/content/articles/679099- avtomobilnye-oxladiteli-napitkov-ne-ajs/ 04.08.2014

Submitted 28.02.2018

Філін С.О. *доктор техн. наук*

Західнопоморський технологічний університет у Щецині
алея Піастів 17, Щецин, 70-310, Польща;
e-mail: Sergiy.Filin@zut.edu.pl

ВПЛИВ ТЕПЛОВОГО КОНТАКТУ ПОВЕРХНІ ОХОЛОДЖЕННЯ З ОБ'ЄКТОМ НА ШВИДКОДІЮ ТЕРМОЕЛЕКТРИЧНИХ ОХОЛОДЖУВАЧІВ НАПОЇВ

У статті розглядаються конструктивні та експлуатаційні характеристики сучасних термоелектричних охолоджувачів і підігрівників напоїв, зокрема динамічні характеристики. Наведено результати порівняльних випробувань, що показують вплив умов теплообміну між банкою (пляшкою) і контейнером охолоджувача на швидкість охолодження напою. Заповнення щілини між пляшкою з напоєм і ємністю охолоджувача дозволяє суттєво підвищити швидкодію охолоджувача. Наприклад, час охолодження напою від 25 °C до 10 °C у випробуваному охолоджувачі знизився з 67 до 50 хвилин. Бібл. 10, Рис. 11, Табл. 2.
Ключові слова: охолоджувач/підігрівник напоїв, темп охолодження, умови теплообміну, експериментальні дослідження.

Філін С.О. *доктор техн. наук*

Западнопоморский технологический университет в Щецине
аллея Пиастов 17, Щецин, 70-310, Польша
e-mail: Sergiy.Filin@zut.edu.pl

ВЛИЯНИЕ ТЕПЛОВОГО КОНТАКТА ПОВЕРХНОСТИ ОХЛАЖДЕНИЯ С ОБЪЕКТОМ НА БЫСТРОДЕЙСТВИЕ ТЕРМОЭЛЕКТРИЧЕСКИХ ОХЛАДИТЕЛЕЙ НАПИТКОВ

В статье рассматриваются конструктивные и эксплуатационные характеристики современных термоэлектрических охладителей и подогревателей напитков, в частности динамические характеристики. Приведены результаты сравнительных испытаний, показывающие влияние условий теплообмена между банкой (бутылкой) и контейнером охладителя на скорость охлаждения напитка. Заполнение щели между бутылкой с напитком и ёмкостью охладителя позволяет существенно повысить быстродействие охладителя. Например, время охлаждения напитка от 25°C до 10°C в испытуемом охладителе снизилось с 67 до 50 минут. Библ. 10, Рис. 11, Табл. 2.
Ключевые слова: охладитель/подогреватель напитков, темп охлаждения, условия теплообмена, экспериментальные исследования.

References

1. Filin S., Owsicki A. (2010). *Zasady projektowania i eksploatacji chłodziarek termoelektrycznych*. ZAPOL: Szczecin.
2. Filin S., Jasińska B. (2013). Efektywność energetyczna transportowych chłodziarek termoelektrycznych. Energetycznie efektywne rozwiązania urządzeń chłodniczych, klimatyzacyjnych i pomp ciepła. *XLV Dni Chłodnictwa (Poznań. 13-14.11.2013),* p. 63-74.
3. Filin S.O. (2017). Comparative analysis of energy characteristics of contemporary thermoelectric refrigerators. *J.Thermoelectricity*, 6, 83-91.
4. Sergiy Filin. (2006). *Technika i technologia produkcji lodu spożywczego*. Masta: Gdańsk.
5. Anatychuk L., Filin S., Danko E. (1998). Cool before drinking. *Office*, 5, 39-40.
6. Sergiy Filin. (2002). Współczesne transportowe chłodziarki do napojów. *Technika Chłodnicza i Klimatyzacyjna* 2, 60-62 .
7. Self-cooled can for beer. Retrieved from: http://forum.beermir.com/viewtopic.php?t=1808&postdays=0&postorder=asc&start=25
8. Retrieved from: http://mirbeer.blogspot.com/2014/02/blog-post_24.html
9. Retrieved from: http://personal-security.ru/lichnaja-bezopasnost/avto-i-velo-aksessuary-dlja-bezopasnostiikomforta? product_id=7392
10. Automobile coolers for beverages: no ice! Retrieved from: https://www.zr.ru/content/articles/679099- avtomobilnye-oxladiteli-napitkov-ne-ajs/ 04.08.2014

Submitted 28.02.2018

V.P.Zaykov[1], *Candidate of Tech. science*,
V.I.Mescheryakov[2], *Doctor of Tech. science*,
Gnatovskaya A.A.[2]
Yu. I. Zhuravlov[3], *Candidate of Tech. science*

[1]SHTORM Research Institute, 27, Tereshkova str., Odesa, Ukraine
[2]Odesa State Ecological University, 15, Lvivskastr,, Ukraine
[3]NationalUniversity "Odesa Maritime Academy", 8, Didrikhson str., Ukraine

COMPARATIVE ANALYSIS OF THE DYNAMICS OF OPERATION OF A SINGLE-STAGE THERMOELECTRIC COOLING DEVICE WITH DIFFERENT GEOMETRY OF THERMOELEMENT LEGS

A comparative analysis was carried out of the dynamicsof operation of a single-stage thermoelectric cooling device with a variation in the geometry of thermoelement legs taking into account the influence of structural and technological elements for different characteristic current operating modes, temperature drops and thermal load. It is shown that as the aspect ratio of thermoelement leg increases, the time to reach the steady-state operating mode and the magnitude of the operating current decrease, the voltage drop with constant energy consumption for various operating modes increases. As the temperature drop grows, the time to reach the steady-state operating mode for different operating modes increases. Bibl. 12, Fig. 13, Table 2.

Key words: thermoelectric cooler, geometry of thermoelementlegs, reliability indicators, time to reach the mode, temperature drop.

Introduction

Thermoelectric coolers are among the fastest devices providing thermal modes for radio electronic equipment, which is primarily due to the principle of generation of heat and cold [1], small dimensions and mass [2].The most important indicator of thermoelectric coolers is operational reliability, which is determined by the failure rate and the probability of failure-free operation [3], and outperforms the compression coolers due to the absence of mobile components [4].At the same time, progressively more stringent requirements for the performance of heat-loaded elements lead to the need to find ways to improve reliability indicators under the influence of negative climatic [5] and mechanical [6] factors, heat load [7].The increase in speed requirements is associated with an increase in temperature gradients [8], reliability indicators, and has not received adequate attention when designing thermoelectric coolers.To analyze one aspect of this problem related to the influence of the geometry of thermoelement legs on the dynamics and reliability indicators of single-stage thermoelectric coolers is an urgent task.The practical significance of this approach is due to the fact that there is no need to change module manufacturing technology, which also affects reliability indicators [9].

The purpose of the work is to analyze the dynamic characteristics and reliability indicators of a single-stage thermoelectric cooler in the range of unified geometry of thermoelement legs in various current operating modes from the minimum failure rate to the maximum cooling capacity.

Model of relation between the time to reach the steady-state mode by thermoelectric cooler and structural parameters and energy indicators

In [10, 11], the influence of current operating modes on the basic parameters, reliability indicators and the dynamics of operation of thermoelectric cooling device is considered with regard to structural and technological elements in the range of temperature drops from $\Delta T = 5K$ to $\Delta T = 60K$ and thermal load from $Q_0 = 0{,}5Bm$ to $Q_0 = 20Bm$ at a given geometry of thermoelement legs $l/s = 10$. At the same time, it is of interest to assess the influence on the dynamics and reliability indicators of the unified range of the geometry of thermoelement legs from $l/s = 4{,}5$ to $l/s = 40$ (the ratio of thermoelementheight l to its cross-sectional area s).In so doing, it is necessary to take into account the influence of structural and technological elements for different temperature drops and thermal load for different current operating modes.

For this purpose, we use the previously obtained relations [12]. Expressions for determining the time to reach the steady-state operating mode τ , depending on the current mode of operation, can be written in the form:

$$\tau = \frac{\sum\limits_i M_i C_i}{K_k\left(1 + 2B_K \cdot \dfrac{\Delta T_{\max}}{T_0}\right)} \cdot \ln \frac{\gamma \cdot B_H\left(2 - B_H\right)}{2B_K - B_K^2 - \theta},$$

where $\gamma = \dfrac{I^2{}_{\max_H} \cdot R_H}{I^2_{\max_K} \cdot R_K}$

$\sum\limits_i M_i C_i$ – the sum of the products of the heat capacity by the mass of the components of structural and technological elements for a given geometry of thermoelementlegs, $\dfrac{J}{K}$;

$I_{\max H}$, R_H – maximumoperatingcurrent (A) andelectricalresistance (Ohm) ofthermoelementleg, respectively, at the beginning of cooling process $\tau_H = 0$;

$I_{\max K}$, R_K – maximum operating current (A) and electrical resistance (Ohm) of thermoelement leg, respectively, at the end of cooling process τ_K ;

$B_H = \dfrac{I}{I_{\max_H}}$ –relativeoperating current at $\tau_H = 0$;

$B_K = \dfrac{I}{I_{\max_K}}$ –relative operating current at τ_K ;

$I_{\max_H} = \dfrac{\bar{e}_H T}{R_H}$ – maximum operating current at $\tau_H = 0$;

$I_{\max_K} = \dfrac{\bar{e}_K T_0}{R_K}$ – maximumoperatingcurrentat τ_K .

If the currents are equal at the beginning and at the end of cooling process

$$I = B_H I_{\max_H} = B_K I_{\max_K}$$

$\bar{e}_H$, $\bar{e}_K$ – averaged thermoelectric coefficient of thermoelement leg at the beginning and at the end of cooling process;

T_0 – temperature of heat-absorbing junction at the end of cooling process (K) at τ_K;

T – temperature of heat-absorbing junction at the beginning of cooling process (K) at $\tau_H = 0$;

$\theta = \dfrac{\Delta T}{\Delta T_{\max}}$ – relative temperature drop;

$\Delta T = T - T_0$ – operating temperature drop of TEC (K);

$\Delta T_{\max} = 0{,}5\bar{z} \cdot T_0^2$ –maximum temperature drop (K);

$\bar{z}$ – averaged value of thermoelectric material efficiency in a module ($1/K$);

$K_K = \dfrac{\bar{\chi}_K}{l/S}$ – heattransfer coefficient (W/K)

$\bar{\chi}_K$ – averaged value of thermal conductivity coefficient $\left(\dfrac{W}{sm \cdot K}\right)$;

I – the value of operating current (A).

The number of thermoelements n can be determined from the ratio:

$$n = \frac{Q_0}{I^2_{\max_K} \cdot R_K \left(2B_K - B_K^2 - \theta\right)}$$

where Q_0 – the value of thermal load (W)

The power consumption W_K of TEC can be calculated by the formula:

$$W_K = 2n \cdot I^2_{\max_K} \cdot R_K \cdot B_K \left(B_K + \frac{\Delta T_{\max}}{T_0}\theta\right)$$

voltage drop $U_K = \dfrac{W_K}{I}$, and coefficient of performance $E = \dfrac{Q_0}{W_K}$.

Failure rate λ/λ_0 according to [12] can be determined by the formula:

$$\lambda/\lambda_0 = n \cdot B_K^2 \left(\theta + C_K\right) \cdot \frac{\left(B_K + \dfrac{\Delta T_{\max}}{T_0}\theta\right)^2}{\left(1 + \dfrac{\Delta T_{\max}}{T_0}\theta\right)^2} \cdot K_{T_i}$$

where $C_K = \dfrac{Q_0}{I^2_{\max_K} \cdot R_K \cdot n}$ – relativethermalload; K_{T_i} – significantcoefficient of temperature decrease.

Calculated results ofthe basic parameters of reliability indicators and the time to reach the steady-state operating mode fordifferent l/S and current operating modes at temperature

drop $\Delta T = 40K$ and thermal load $Q_0 = 1{,}0Bm$ at $T = 300K$; $m_0 c_0 \to 0$ (absence of cooling object); $\lambda_0 = 3 \cdot 10^{-8}$ 1/hand $t = 10^4$ hare given in Table 1.

Analysis of calculated results given in Table 1 has shown that with an increase of ratio l/s for different operating modes:

– the value $\sum_i m_i c_i$ of structural and technological elements decreases(Fig. 1);

– thetimetoreachthe steady-state operating mode τ (Fig. 2) decreases on the average by 30 – 33%:

from $\tau = 7{,}8$ *сек* at $l/s = 4{,}5$ to $\tau = 5{,}2$*сек* at $l/s = 40$ for the mode $Q_{0\max}$;

from $\tau = 9{,}2$ *сек* at $l/s = 4{,}5$ to $\tau = 6{,}3$*сек* at $l/s = 40$ for the mode $\left(Q_0/I\right)_{\max}$;

Table 1.

Calculated resultsofthe basicparameters of the time to reach the steady-state mode and reliability indicators

l/s	n, pcs	I, A	W, W	U, V	E	τ, sec	B_H	B_K	$\sum_i m_i c_i$	λ/λ_0	$\lambda \cdot 10^{-8}$, 1/h	P
Mode $Q_{0\max}$ – $\Delta T = 40K$; $Q_0 = 1{,}0\,W$; $\theta = 0{,}5$												
4.5	3.6	11.1		0.36		7.8			451.7	3.15	9.45	0.99906
10	7.8	5.0	4.0	0.91	0.25	6.50	0.93	1.0	175.0	8.0	24.0	0.99760
20	15.8	2.50		1.62		6.0			85.8	12.3	36.9	0.9963
40	32.0	1.25		3.50		5.20			36.1	24.4	73.2	0.9927
Mode $\left(Q_0/I\right)_{\max}$												
4.5	4.6	8.0		0.38		9.2			451.7	0.88	2.65	0.99974
10	9.4	3.55	2.80	0.83	0.36	7.85	0.656	0.707	175.0	2.46	7.4	0.99926
20	20.6	1.78		1.70		7.4			85.8	4.0	12.0	0.99880
40	41.6	0.88		3.40		6.30			36.1	7.9	23.7	0.9976
Mode $\left(Q_0/I^2\right)_{\max}$ $\left(B = \theta\right)$												
l/s	n, pcs	I, A	W, W	U, V	E	τ, sec	B_H	B_K	$\sum_i m_i c_i$	λ/λ_0	$\lambda \cdot 10^{-8}$, 1/h	P
4.5	8.4	5.6		0.52		12.9			451.7	0.38	1.13	0.999887
10	15.8	2.51	2.70	1.04	0.37	11.0	0.465	0.50	175.0	1.0	3.0	0.99970
20	36.6	1.26		2.30		10.6			85.8	1.66	5.0	0.99950
40	74.8	0.63		4.7		8.9			36.1	2.82	8.46	0.99915
Mode $\lambda_{\min}$ $\left(B = \eta\theta\right)$												
4.5	13.2	4.80		0.74		16.0			451.7	0.30	0.90	0.999909
10	24.0	2.10	3.20	1.40	0.31	14.0	0.395	0.425	175.0	0.71	2.14	0.99979
20	58.6	1.07		3.24		13.3			85.8	1.35	4.0	0.99960

40	119	0.53		6.60		11.2			36.1	2.70	8.10	0.99920

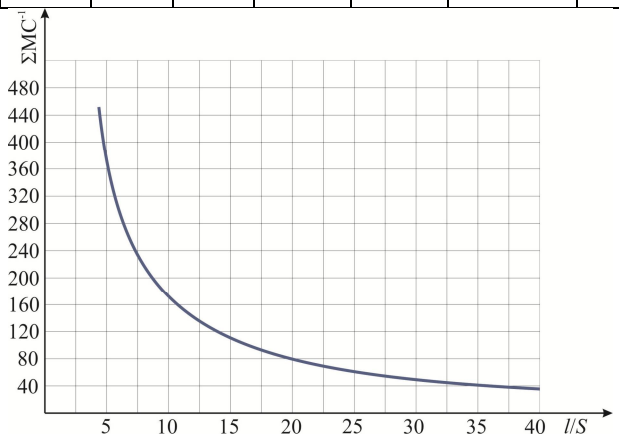

Fig.1 – Dependence of $\sum_i M_i C_i$ *value of a single-stage TEC on the geometry of thermoelement legs* l/s *at* $T = 300\ K$

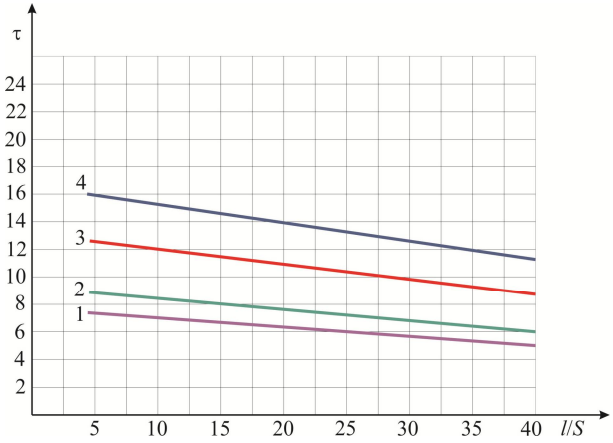

Fig. *2 – Dependenceofthetimetoreachthesteady-stateoperating mode* τ *of a single-stage TEC on the ratio* l/s *for different operating modesat* $T = 300\ K$; $\Delta T = 40K$; $Q_0 = 1,0 Bm$ *.1 – mode* $Q_{0_{max}}$ *; 2 – mode* $\left(Q_0/I\right)_{max}$ *; 3 – mode* $\left(Q_0/I^2\right)_{max}$ *; 4 – mode* λ_{min}

from $\tau = 12,9 сек$ at $l/s = 4,5$ to $\tau = 8,9 сек$ at $l/s = 40$ for the mode $\left(Q_0/I^2\right)_{max}$;

from $\tau = 16,0 сек$ at $l/s = 4,5$ to $\tau = 11,2 сек$ at $l/s = 40$ for the mode λ_{min}.

Minimum time to reach the steady-state operating mode τ_{min} is provided in the mode $Q_{0_{max}}$ at $l/s = 40$:

– thevalueofoperatingcurrent I (Fig. 3) for different operating modes decreases(on the average by 89%);

from $I = 11,1 A$ at $l/s = 4,5$ to $I = 1,25 A$ at $l/s = 40$ for the mode $Q_{0_{max}}$;

from $I = 8,0 A$ at $l/s = 4,5$ to $I = 0,88 A$ at $l/s = 40$ for the mode $\left(Q_0/I\right)_{max}$;

from $I = 5{,}6A$ at $l/s = 4{,}5$ to $I = 0{,}63A$ at $l/s = 40$ for the mode $\left(Q_0/I^2\right)_{\max}$;

from $I = 4{,}8A$ at $l/s = 4{,}5$ to $I = 0{,}53A$ at $l/s = 40$ for the mode $\lambda_{\min}$.

Minimum value of operating current $I_{\min}$ is provided in the mode $\lambda_{\min}$ at $l/s = 40$:

– thenumberofthermoelements(Fig. 4) for different operating modes increases(on the average by a factor of 9):

$n = 3,6\ pcs$ at $l/s = 4{,}5$ to $n = 32\ pcs$ at $l/s = 40$ for the mode $Q_{0_{\max}}$;

$n = 4,6\ pcs$ at $l/s = 4{,}5$ to $n = 41,6\ pcs$ at $l/s = 40$ for the mode $\left(Q_0/I\right)_{\max}$;

$n = 8,4\ pcs$ at $l/s = 4{,}5$ to $n = 74,8\ pcs$ at $l/s = 40$ for the mode $\left(Q_0/I^2\right)_{\max}$;

$n = 13,2\ pcs$ at $l/s = 4{,}5$ to $n = 119\ pcs$ at $l/s = 40$ for the mode $\lambda_{\min}$.

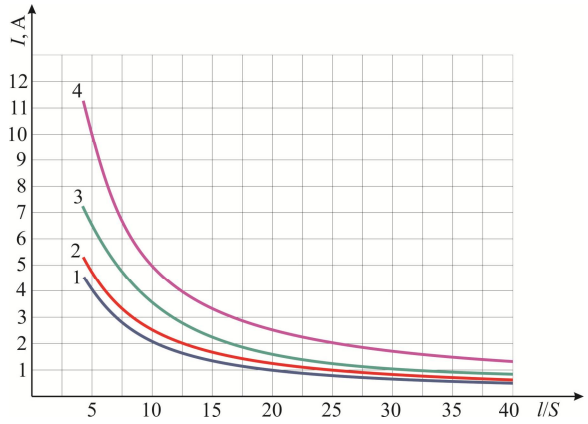

Fig. 3 – Dependenceof operating current I *on the ratio* l/s *for different operating modes* $T = 300K$; $\Delta T = 40K$; $Q_0 = 1{,}0\ W$ *1 – mode* $Q_{0_{\max}}$; *2 – mode* $\left(Q_0/I\right)_{\max}$; *3 – mode* $\left(Q_0/I^2\right)_{\max}$; *4 – mode* $\lambda_{\min}$

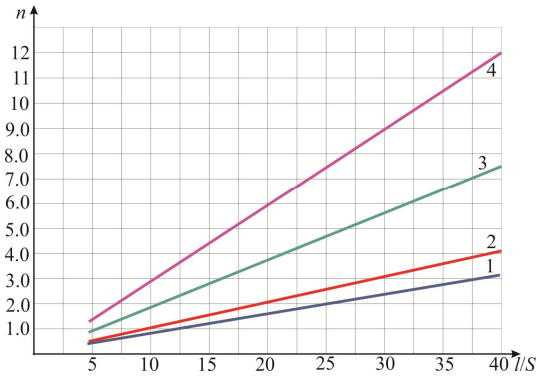

Fig. 4 – Dependence of the number of thermoelements n *at* $T = 300K$; $\Delta T = 40K$; $Q_0 = 1{,}0\ W$ *on the ratio* l/s *for operating modes:*

1 – $Q_{0_{\max}}$; *2 –* $\left(Q_0/I\right)_{\max}$; *3 –* $\left(Q_0/I^2\right)_{\max}$; *4 –* $\lambda_{\min}$

Minimum number of thermoelements $n_{\min}$ is provided in the mode $Q_{0_{\max}}$:

– coefficient of performance E remains constant for different operating modes and does not depend on the geometry of thermoelement legs:

$E = 0{,}25$ at $l/s = 4{,}5; 10; 20; 40$; in the mode $Q_{0_{max}}$;

$E = 0{,}36$ at $l/s = 4{,}5; 10; 20; 40$; in the mode $\left(Q_0/I\right)_{max}$;

$E = 0{,}37$ at $l/s = 4{,}5; 10; 20; 40$; in the mode $\left(Q_0/I^2\right)_{max}$;

$E = 0{,}31$ at $l/s = 4{,}5; 10; 20; 40$; in the mode λ_{min} .

Maximum value of coefficient of performance $E = 0{,}37$ is provided in the mode $\left(Q_0/I^2\right)_{max}$:

– relativeoperatingcurrent B_K and B_H remainsconstantand does not depend on the geometry of thermoelement legs;

– thevalueof voltage drop U (Fig. 5) increases on the average by a factor of $9{,}0 \div 9{,}7$

$U = 0{,}36\,V$ at $l/s = 4{,}5$ and $U = 3{,}5\,V$ at $l/s = 40$ for the mode $Q_{0_{max}}$;

$U = 0{,}38\,V$ at $l/s = 4{,}5$ and $U = 3{,}4\,V$ at $l/s = 40$ for the mode $\left(Q_0/I\right)_{max}$;

$U = 0{,}52\,V$ at $l/s = 4{,}5$ and $U = 4{,}7\,V$ at $l/s = 40$ for the mode $\left(Q_0/I^2\right)_{max}$;

$U = 0{,}74\,V$ at $l/s = 4{,}5$ and $U = 6{,}6\,V$ at $l/s = 40$ for the mode λ_{min} .

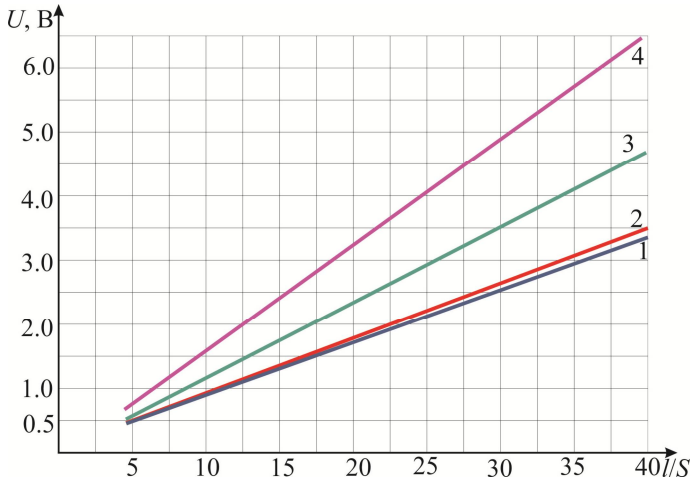

Fig. 5 – Dependence of voltage drop U *of a single-stage TEC on the ratio* l/s *for different operating modes*

$T = 300K$; $\Delta T = 40K$; $Q_0 = 1{,}0\,W$.

1 – mode $Q_{0_{max}}$; *2 – mode* $\left(Q_0/I\right)_{max}$; *3 – mode* $\left(Q_0/I^2\right)_{max}$; *4 – mode* λ_{min}

Maximum voltage drop U_{max} is provided in the mode λ_{min} :

– failurerate λ/λ_0 (Fig. 6) increases on the average from 7,4 to 9,0 times:

$\lambda/\lambda_0 = 3{,}15$ at $l/s = 4{,}5$ and $\lambda/\lambda_0 = 24{,}4$ at $l/s = 40$ for the mode $Q_{0_{max}}$;

$\lambda/\lambda_0 = 0{,}88$ at $l/s = 4{,}5$ and $\lambda/\lambda_0 = 7{,}9$ at $l/s = 40$ for the mode $\left(Q_0/I\right)_{max}$;

$\lambda/\lambda_0 = 0{,}38$ at $l/s = 4{,}5$ and $\lambda/\lambda_0 = 2{,}82$ at $l/s = 40$ for the mode $\left(Q_0/I^2\right)_{max}$;

$\lambda/\lambda_0 = 0{,}30$ at $l/s = 4{,}5$ and $\lambda/\lambda_0 = 2{,}70$ at $l/s = 40$ for the mode λ_{min}.

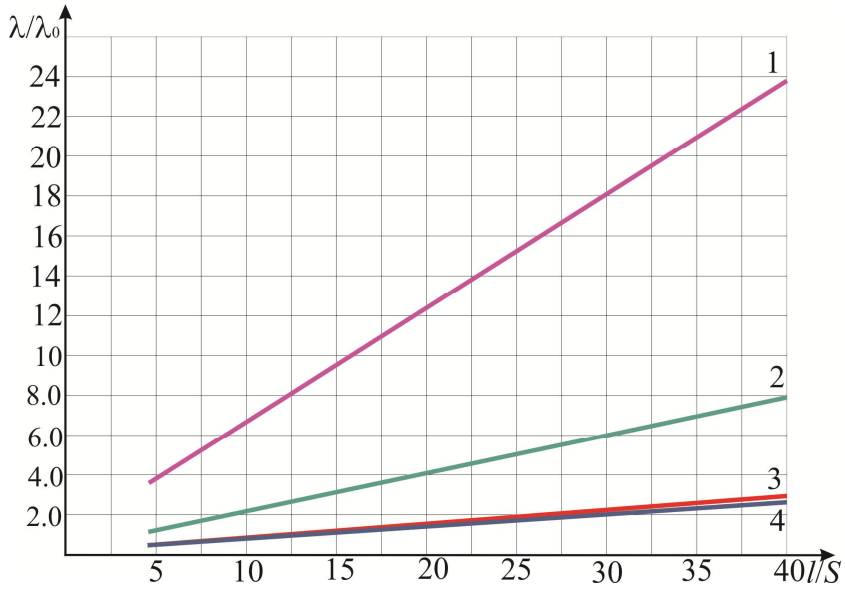

Fig. 6 – Dependenceoffailurerate λ/λ_0 of a single-stage TEC on the ratio l/s for different operating modes

$T = 300K$; $\Delta T = 40K$; $Q_0 = 1{,}0\ W$

Minimum failure rate λ/λ_0 is provided in the mode λ_{min}:

– the probability of failure-free operation P is reduced (Fig. 7).

Maximumprobabilityoffailure-freeoperation P is provided in the mode λ_{min}:

– the relative value of the time to reach the steady-state operating mode $\frac{\Delta\tau}{\tau} = \frac{\tau_{4,5} - \tau_i}{\tau_{4,5}}$% of a single-stage TEC depending on the geometry of thermoelement legs l/s for different operating modes increases(Fig. 8).

As the relative operating current B_K increases,the time to reach the steady-state operating mode τ for different geometry of thermoelement legs l/s (Fig. 9) decreasesat $T = 300K$, $\Delta T = 40K$, $Q_0 = 1{,}0\ W$. At a given B_K (current operating mode) the time to reach the steady-state operating mode τ decreases from $l/s = 4{,}5$ to $l/s = 40$.

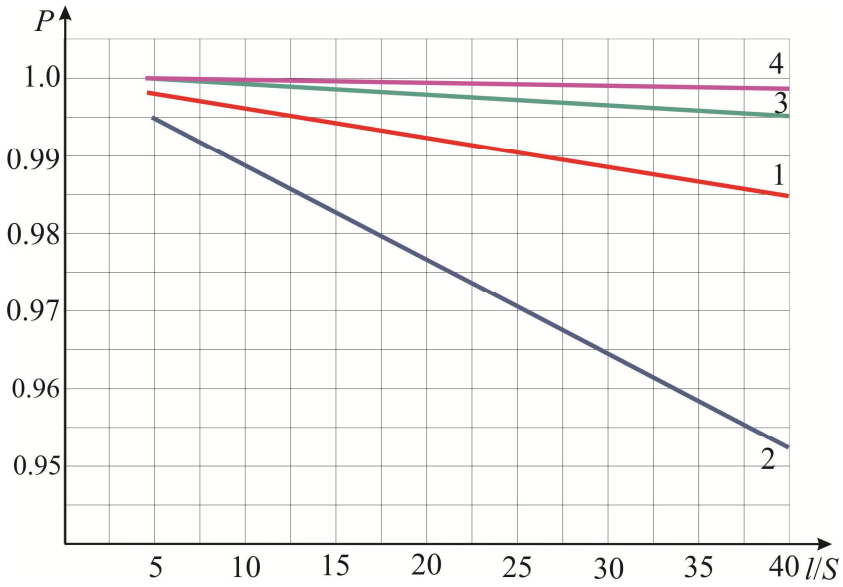

Fig. 7 – Dependenceofa probability of failure-free operation P *of a single-stage TEC on the ratio* l/s *for different operating modes* $\mathrm{T}=300\mathrm{K}$; $\Delta\mathrm{T}=40\mathrm{K}$; $Q_0=1{,}0\ W$; $t=10^4\ h$

1 – mode $\mathrm{Q}_{0_{\max}}$; *2 – mode* $\left(\mathrm{Q}_0/\mathrm{I}\right)_{\max}$; *3 – mode* $\left(Q_0/I^2\right)_{\max}$; *4 – mode* $\lambda_{\min}$

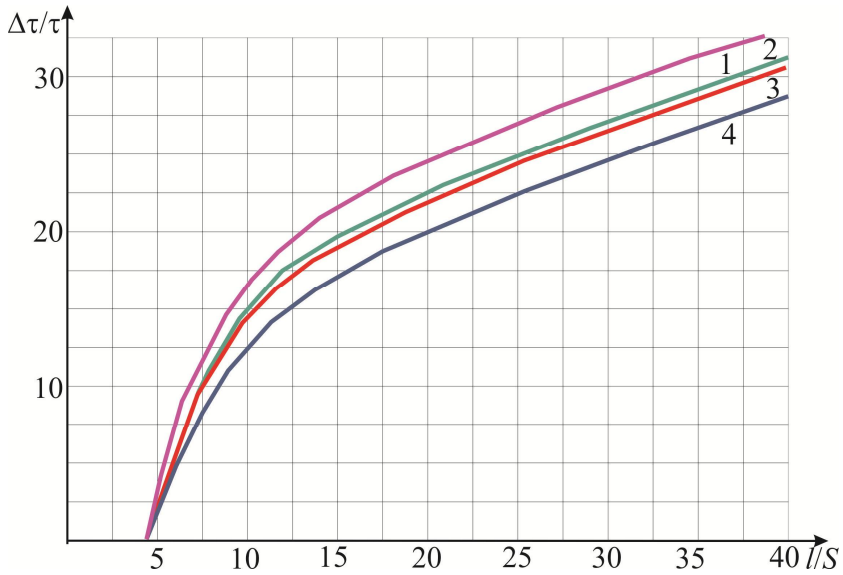

Fig. 8 – Dependence of a relative value of the time to reach the steady-state operating mode $\frac{\Delta\tau}{\tau}=\frac{\tau_{4,5}-\tau_i}{\tau_{4,5}}\%$ *of a single-stage TEC on the geometry of thermoelement legs* l/s

for different operating modes $\mathrm{T}=300\mathrm{K}$; $Q_0=1{,}0Bm$; *(i = 4,5; 10; 20; 40);* $\Delta\mathrm{T}=40\mathrm{K}$

1 – mode $\mathrm{Q}_{0_{\max}}$; *2 – mode* $\left(\mathrm{Q}_0/\mathrm{I}\right)_{\max}$; *3 – mode* $\left(\mathrm{Q}_0/\mathrm{I}^2\right)_{\max}$; *4 – mode* $\lambda_{\min}$

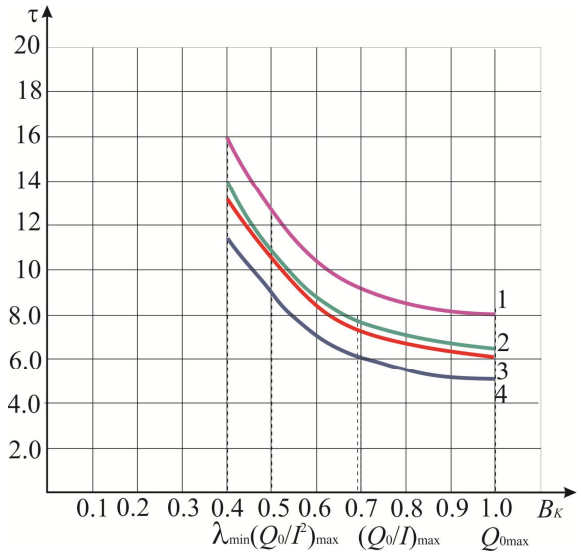

Fig. 9 – Dependenceofthe timetoreachthesteady-stateoperatingmode τ *ofa single-stage TEC on the relative operating current* B_K *for different geometry of thermoelement legs* l/s *at* $T = 300K$; $\Delta T = 40K$; $Q_0 = 1,0Bm$

.Operatingmodes: λ_{min}; $\left(Q_0/I^2\right)_{max}$; $\left(Q_0/I\right)_{max}$; $Q_{0_{max}}$

1 – $l/s = 4,5cm^{-1}$; *2 –* $l/s = 10cm^{-1}$; *3 –* $l/s = 20cm^{-1}$; *4 –* $l/s = 40cm^{-1}$

Calculated results of the dynamics of operation for different temperature drops ΔT and different operating modes are given in Table 2.

Table 2a.

Calculated results of the dynamics of operation of TEC at different temperatures forcurrent modes $Q_{0_{max}}$ *and* $\left(Q_0/I\right)_{max}$

$T = 300K$, $Q_0 = 1,0\,W$										
l/s	mode $Q_{0_{max}}$					mode $\left(Q_0/I\right)_{max}$				
	I, A	B_H	B_K	τ, sec	$\frac{\lambda}{\lambda_0}$	I A	B_H	B_K	τ, sec	$\frac{\lambda}{\lambda_0}$
$\Delta T = 10K$, $T_0 = 290K$, $\Delta T_{max} = 100,5K$, $\theta = 0,10$										
4,5	11,9	0,988	1,0	1,36	1,58	3.80	0,31	0,316	2,9	0,02
10	5,32	0,985	1,0	1,0	3,6	1,68	0,31	0,316	2,3	0,046
20	2,67	0,99	1,0	0,96	6,9	0,85	0,31	0,316	2,2	0,088
40	1,33	0,985	1,0	0,85	13,6	0,42	0,31	0,316	1,86	0,17
$\Delta T = 20K$, $T_0 = 280K$, $\Delta T_{max} = 93,7K$, $\theta = 0,213$										
4,5	11,6	0,97	1,0	3,0	1,86	5,45	0,447	0,46	4,7	0,105
10	5,24	0,970	1,0	2,3	4,4	2,42	0,445	0,46	3,8	0,26
20	2,62	0,97	1,0	2,2	7,8	1,21	0,45	0,46	3,65	0,47
40	1,31	0,97	1,0	1,91	15,6	0,60	0,45	0,46	3,10	0,94
$\Delta T = 30K$, $T_0 = 270K$, $\Delta T_{max} = 86,5K$, $\theta = 0,346$										
4,5	11,5	0,96	1,0	4,9	2,33	6,90	0,565	0,588	6,7	0,4

Continued of table 2a

10	5,19	0,96	1,0	4,0	5,7	3,05	0,565	0,588	5,5	0,87
20	2,59	0,959	1,0	3,8	9,7	1,52	0,56	0,59	5,3	1,52
40	1,30	0,96	1,0	3,3	19,3	0,76	0,56	0,588	4,5	3,0
$\Delta T = 40K$, $T_0 = 260K$, $\Delta T_{max} = 79{,}8K$, $\theta = 0{,}50$										
4,5	11,1	0,93	1,0	7,8	3,15	8,0	0,656	0,707	9,2	2,888
10	5,02	0,93	1,0	6,4	8,0	3,55	0,656	0,707	7,7	2,46
20	2,51	0,93	1,0	6,0	12,3	1,78	0,66	0,707	7,4	4,0
40	1,25	0,93	1,0	5,2	24,4	0,88	0,66	0,707	6,3	7,9
$\Delta T = 50K$, $T_0 = 250K$, $\Delta T_{max} = 73{,}4K$, $\theta = 0{,}68$										
4,5	10,9	0,91	1,0	12,2	5,16	9,1	0,75	0,825	13,1	2,5
10	4,90	0,91	1,0	10	13,6	4,0	0,75	0,825	11,0	7,2
20	2,45	0,91	1,0	9,5	19,5	2,0	0,75	0,825	10,6	10,9
40	1,22	0,91	1,0	8,3	38,6	1,0	0,75	0,825	9,2	22,2
$\Delta T = 60K$, $T_0 = 240K$, $\Delta T_{max} = 66{,}8K$, $\theta = 0{,}90$										
4,5	10,5	0,88	1,0	22,8	19,3	10,2	0,83	0,95	22,5	15,1
10	4,74	0,88	1,0	19,0	47,8	4,5	0,83	0,95	19,1	40,4
20	2,38	0,88	1,0	18,3	69,4	2,3	0,836	0,95	18,6	67,0
40	1,18	0,88	1,0	15,3	139	1,12	0,836	0,95	15,7	135

Table 2b

Calculated results of the dynamics of operation of TEC at different temperatures

for current modes $\left(Q_0 / I^2\right)_{\max}$ *and* $\lambda_{\min}$

$T = 300K$, $Q_0 = 1{,}0\,W$										
l/s	mode $\left(Q_0 / I^2\right)_{\max}$					mode $\lambda_{\min}$				
	I	B_H	B_K	τ, сек	$\frac{\lambda}{\lambda_0}$	I	B_H	B_K	τ, сек	$\frac{\lambda}{\lambda_0}$
$\Delta T = 10K$, $T_0 = 290K$, $\Delta T_{\max} = 100{,}5K$, $\theta = 0{,}10$										
4,5	1,20	0,098	0,10	9,9	0,00051	0,85	0,070	0,071	16,9	0,0008
10	0,53	0,098	0,10	8,2	0,0012	0,38	0,070	0,071	14,5	0,0009
20	0,27	0,098	0,10	8,0	0,0023	0,19	0,071	0,072	13,7	0,0013
40	0,133	0,98	0,10	6,8	0,0045	0,096	0,071	0,072	11,5	0,0025
$\Delta T = 20K$, $T_0 = 280K$, $\Delta T_{\max} = 93{,}7K$, $\theta = 0{,}213$										
4,5	2,5	0,206	0,213	10,6	0,010	1,9	0,155	0,16	16,5	0,0016
10	1,12	0,207	0,213	8,8	0,025	0,84	0,155	0,16	13,8	0,015
20	0,56	0,207	0,213	8,6	0,047	0,42	0,155	0,16	13,5	0,029
40	0,28	0207	0,213	7,3	0,094	0,21	0,155	0,16	11,4	0,048
$\Delta T = 30K$, $T_0 = 270K$, $\Delta T_{max} = 86{,}5K$, $\theta = 0{,}346$										
4,5	4,0	0,33	0,35	11,5	0,078	3,2	0,266	0,28	15,5	0,054
10	1,80	0,33	0,35	9,45	0,19	1,44	0,27	0,28	13,3	0,13
20	0,90	0,33	0,35	9,40	0,35	0,72	0,266	0,277	13,1	0,24
40	0,45	0,33	0,35	7,90	0,70	0,36	0267	0,277	11,0	0,49

Continued of table 2a

$\Delta T = 40K$, $T_0 = 260K$, $\Delta T_{max} = 79{,}8K$, $\theta = 0{,}50$										
4,5	5,6	0,464	0,50	12,9	0,38	4,8	0,39	0,425	16,0	0,3
10	2,51	0,465	0,50	11,0	0,98	2,1	0,39	0,425	14,0	0,4
20	1,26	0,465	0,50	10,6	1,66	1,07	0,395	0,425	13,3	1,35
40	0,63	0,463	0,50	8,9	2,82	0,53	0,394	0,405	11,2	2,7
$\Delta T = 50K$, $T_0 = 250K$, $\Delta T_{max} = 73{,}4K$, $\theta = 0{,}68$										
4,5	7,5	0,62	0,68	15,6	1,71	6,80	0,355	0,612	17,9	1,58
10	3,33	0,62	0,68	13,4	4,4	3,0	0,555	0,612	15,2	3,7
20	1,67	0,62	0,68	12,9	7,6	1,5	0,555	0,612	14,9	7,0
40	0,83	0,62	0,68	10,9	15,2	0,75	0,553	0,612	12,6	14,0
$\Delta T = 60K$, $T_0 = 240K$, $\Delta T_{max} = 66{,}8K$, $\theta = 0{,}90$										
4,5	9,6	0,79	0,90	23,4	15,9	9,30	0,766	0,87	24,2	16,6
10	4,3	0,79	0,90	20,4	35,0	4,1	0,76	0,87	21,0	34,6
20	2,14	0,79	0,90	19,4	70,0	2,07	0,77	0,87	20,2	75,6
40	1,07	0,79	0,90	16,4	140,0	1,0	0,77	0,87	17,0	162

Note that with increase in temperature drop ΔT for different geometry of thermoelement legs l/s and operating modes:

– thetime to reach the steady-state mode τ for the mode $Q_{0_{max}}$ increases (Fig. 10).

Thus, ata giventemperaturedrop ΔT, forinstance, $\Delta T = 40K$, the timetoreachthe steady-state mode τ decreases from $\tau = 7{,}8$ sec for $l/s = 4{,}5$ to $\tau = 5{,}2$ secfor $l/s = 40$, i.e. by 33%:

– the time to reach the steady-state operating mode τ for the mode $\left(Q_0/I\right)_{max}$ increases (Fig.11).

Thus, ata giventemperaturedrop ΔT, forinstance, $\Delta T = 40K$, the timeto reach the steady-state operating mode τ decreases from $\tau = 9{,}2$ secfor $l/s = 4{,}5$ to $\tau = 6{,}3$ secfor $l/s = 40$, i.e. by 31.5%:

– thetimetoreachthe steady-state operating mode τ for the mode $\left(Q_0/I^2\right)_{max}$ increases (Fig.12).

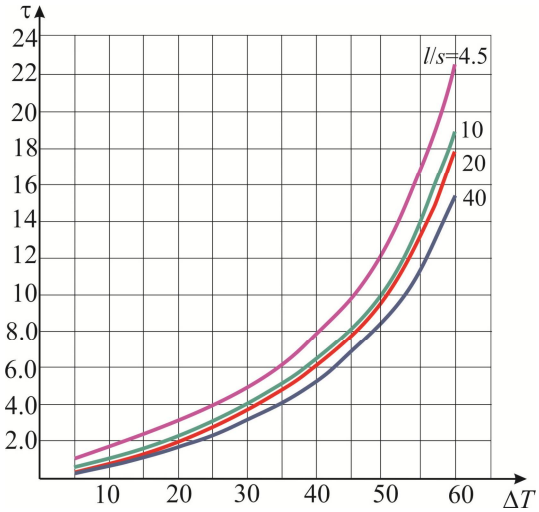

Fig. 10 – Dependence of the time to reach the steady-state operating mode τ *of a single-stage TEC on temperature drop* ΔT *for different geometry of thermoelement legs* l/s *in the mode* $Q_{0_{max}}$ *at* $T = 300K$

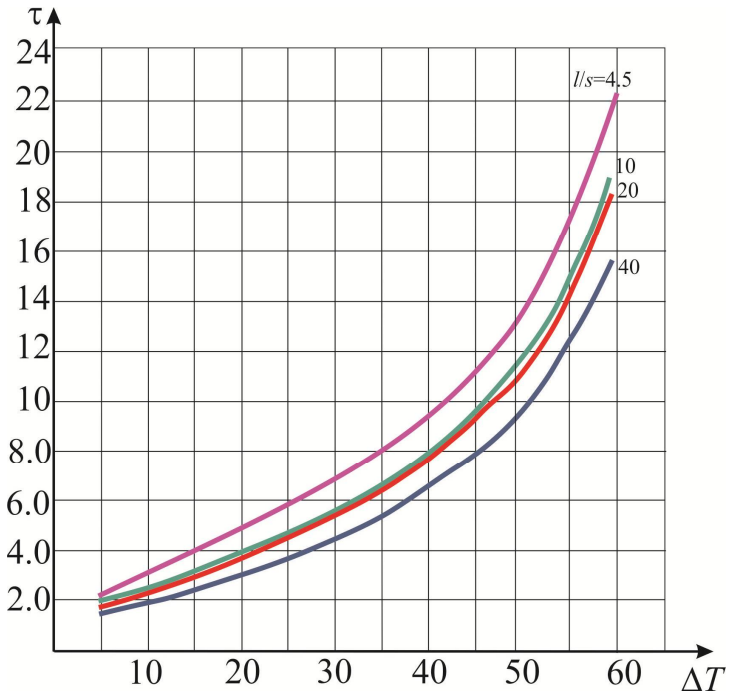

Fig. 11 – Dependence of the time to reach the steady-state operating mode τ *of a single-stage TEC on temperature drop* ΔT *for different geometry of thermoelement legs* l/s *in the mode* $\left(Q_0/I\right)_{max}$ *at* $T = 300K$; $Q_0 = 1,0\ W$

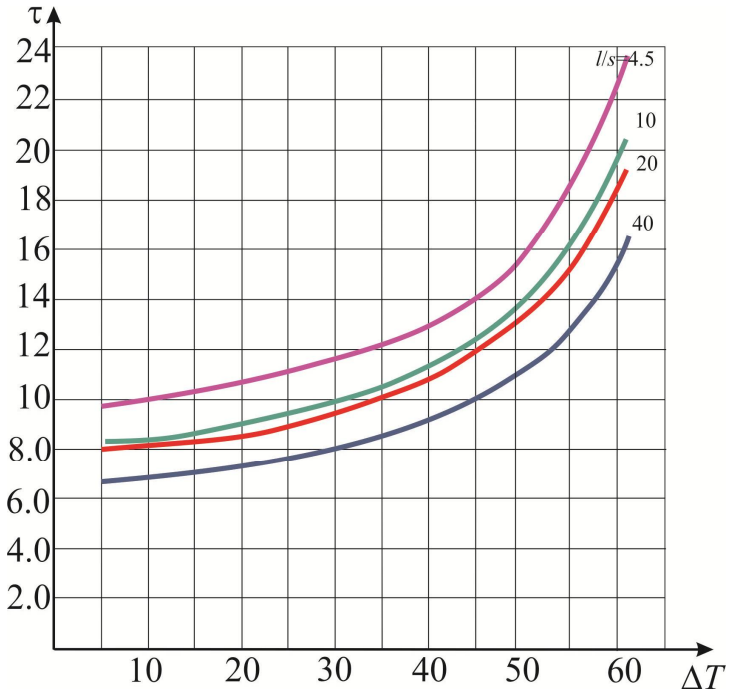

Fig. 12 – Dependenceofthe timetoreachthesteady-stateoperatingmode τ *ofa single-stage TEC on temperature drop* ΔT *for different geometry of thermoelement legs* l/s *in the mode* $\left(Q_0/I^2\right)_{max}$ *at* $T = 300K$; $Q_0 = 1,0Bm$

Thus, ata giventemperaturedrop ΔT, forinstance, $\Delta T = 40K$, timetoreachthe steady-state operating mode τ decreases from $\tau = 12,9$ secfor $l/s = 4,5$ to $\tau = 8,9$ secfor $l/s = 40$, i.e. by 31.0%.

– functional dependence $\tau = f(\Delta T)$ has a flat minimum at $\Delta T = 30K$ (Fig. 13) for the mode λ_{min}.

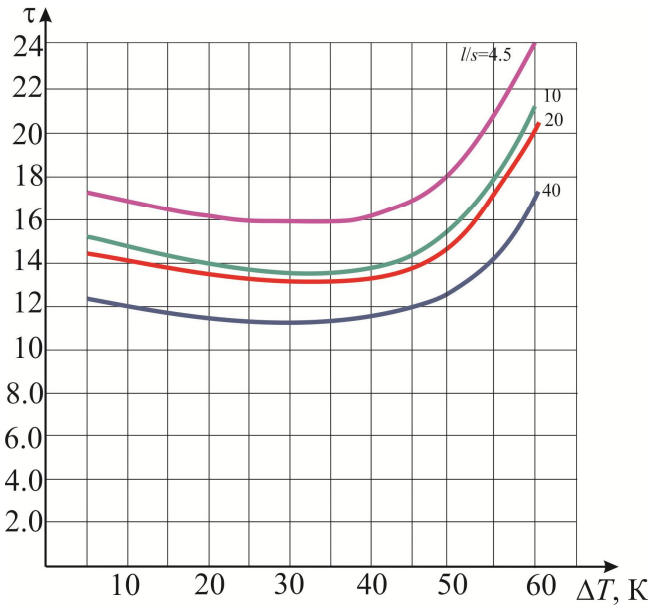

Fig. 13 – Dependenceofthe timetoreachthesteady-stateoperatingmode τ *ofasingle-stage TEC on temperature drop* ΔT *for different geometry of thermoelement legs* l/s *in the mode* λ_{min} *at* $T = 300K$; $Q_0 = 1,0\ W$

Thus, ata giventemperaturedrop ΔT, forinstance, $\Delta T = 40K$, the timeto reach the steady-state operating mode τ decreases from $\tau = 16$ secfor $l/s = 4,5$ to $\tau = 11,2$ secfor $l/s = 40$, i.e. by 30%.

Discussion of the results of analysis of the dynamics of operation of a single-stage thermoelectric cooling device with different geometry of thermoelement legs

The timetoreachthesteady-state operating mode τ of a single-stage thermoelectric cooling device at a given temperature drop ΔT and thermal load Q_0 depends on the geometry of thermoelement legs (ratio l/s) for different operating modes.

With increase in the ratio l/s from $l/s = 4,5$ to $l/s = 40$ for different operating modes:

– thetime to reach the steady-state operating mode τ decreases on the average by 30 – 33%;

– minimumtimetoreachthesteady-state operating mode τ_{min} is provided in the mode $Q_{0_{max}}$;

– the value of operating current I decreases up to 9 times;

– the number of thermoelements n increasesup to 9 times;

– minimum number of thermoelements n_{min} is provided in the mode $Q_{0_{max}}$;

– coefficient of performance E remains constant and does not depend on the geometry of thermoelement legs;

– thegreatestcoefficient of performance E is provided in the mode $\left(Q_0/I^2\right)_{max}$;

– voltage drop U increases up to 9 times;

– maximum voltage drop U_{max} is provided in the mode λ_{min};

– failure rate λ/λ_0 increases ;

– minimum failure rate λ/λ_0 is provided in the mode λ_{min};

– theprobabilityoffailure-free operation P decreases;

– maximum probability of failure-free operation P_{max} is provided in the mode λ_{min};

– withincreaseintemperaturedrop ΔT, thetime to reach the steady-state operating mode τ increases for different operating modes.

A comparative analysis of the basic parameters, reliability indicators and dynamic characteristics makes it possible to choose trade-off solutions for the construction of a TEC taking into account the validity of each of the limiting requirements.

Conclusion

1. By changing the geometry of thermoelement legs in the unification range for a wide use in the design of thermoelectric cooling devices, it is possible to reduce the dynamic characteristics to 30% without changing their manufacturing technique.
2. The interrelation between the dynamic characteristics of thermoelectric coolers and reliability indicatorsis shown which allows byvarying the geometry of thermoelements and current operating modes to choose coolers that provide a reasonable compromise in the design of thermoelectric systems for providing thermal modes for heat-loaded radioelectronic equipment.

References

1. AnatychukL.I. (1979). *Termoelementyitermoelektricheskiieustroistva. Spravochnik [Thermoelementsandthermoelectricdevices. Handbook]*. Kyiv: NaukovaDumka [in Russian].
2. ZebarjadiM., Esfarjani K., Dresselhaus M.S., Ren Z.F., Chen G. (2012). Perspectivesonthermoelectrics: fromfundamentalstodeviceapplications.*Energy & Environmental Science*, 5, 5147–5162.
3. Hyoung–Seuk Choi. (2011). Prediction of reliability on thermoelectric module through accelerated life test and Physics –of –failure.*Electronic Materials Letters*, 7,271.
4. TsarevA.V., ChugunkovV.V. (2008). Issledovaniiekharakteristiktermoelektricheskikhustroistvdlia system termostatirovaniiastartovykhkompleksov [Research on characteristics of thermoelectric devices for thermostatting systems of start complexes]. *Aktualnyieproblemyrossiiskoikosmonautiki. Materialy XXXII akademicheskikhchteniipokosmonautike [Current Problems of Russian Cosmonautics: Proc. of XXXII Academic Readings on Cosmonautics]. (pp.320-321)*.M: Commissionofthe RussianAcademyof Sciences [in Russian].
5. Yang Ping (2010). Approach on thermoelectricity reliability of board –level backplane based on the orthogonal experiment design. *International Journal of Materials and Structural Integrity*,4(2–4), 170–185.
6. Wereszczak A. A., Wang H. (2011). Thermoelectric mechanical reliability. *Vehicle Technologies Annual Merit Reviewand Peer Evaluation Meeting*(USA, Arlington, 11 May 2011) (P. 18).
7. Rowe, D. M.(2012). Thermoelectrics and its Energy Harvesting. Materials, Preparation, and Characterization in Thermoelectrics. (Boca Raton: CRC Press, 2012) (544 p).
8. Zaikov V., Meshcheriakov V., Zhuravlev Yu. (2017). Analysis of the model of interdependence of thermoelement branch geometry and reliability indicators of the single–stage cooler.*Eastern – European Journal of Enterprise Technologies*, 1/1 (85), 26–33.
9. Zaikov, V., MeshcheriakovV., ZhuravlevYu. (2017). Modelofinterrelationbetweenindicatorsofasingle-stagecoolerand the geometry of thermoelement legs. *J.Thermoelectricity*, 6, 59 –76.
10. Zaikov, V., MeshcheriakovV., ZhuravlevYu. (2017). Analysis of the possibility to control the inertia of the thermoelectric cooler.*Eastern–European Journal of Enterprise Technologies*, 6/8 (90), 17–24.

11. Zaikov,V., Meshcheriakov V., Zhuravlev (2018). Analysis of relationship between of a thermoelectric cooler and its design and mode of operation. *Eastern –European Journal of Enterprise Technologies*, 1/8 (91), 12–24.
12. ZaikovV.P., KinshovaL.A., MoiseevV.F. (2009). *Prognozirovaniiepokazateleinadezhnostitermoelektricheskikhokhlazhdaiiushchikhustroistv. Kniga 1. Odnokaskadnyieustroistva. [Predictionofreliabilityindicatorsofthermoelectriccoolingdevices. Book 1. Single-stagedevices]*.Odessa: Politekhperiodika [in Russian].

Submitted 12.03.2018

Зайков В.П. *канд. техн. наук.*[1],
Мещеряков В.І. *доктор техн. наук.*[2],
Гнатовська А.А.[2], **Журавльов Ю.І.** *канд. техн. наук*[3]

[1]Науково-дослідний інститут ШТОРМ,
вул. Терешкової, 27, Одеса, Україна;
e-mail: grand@i.ua;
[2]Одеський державний екологічний університет,
вул. Львівська, 15, Україна; *e-mail: grand@ua.fm;*
[3]Національний університет «Одеська морська академія»,
вул. Дідріхсона, 8, Україна; *e-mail: zhuravlov.y@ya.ru.*

ПОРІВНЯЛЬНИЙ АНАЛІЗ ДИНАМІКИ ФУНКЦІОНУВАННЯ ОДНОКАСКАДНОГО ТЕРМОЕЛЕКТРИЧНОГО ОХОЛОДЖУВАЛЬНОГО ПРИСТРОЮ З РІЗНОЮ ГЕОМЕТРІЄЮ ГІЛОК ТЕРМОЕЛЕМЕНТІВ

Проведено порівняльний аналіз динаміки функціонування однокаскадного термоелектричного охолоджувального пристрою при варіації геометрії гілок термоелементів з урахуванням впливу конструктивних і технологічних елементів для різних характерних струмових режимів роботи, перепадів температури й теплового навантаження. Показане, що з ростом відношення висоти до площі перерізу гілки термоелемента зменшується час виходу на стаціонарний режим роботи та величина робочого струму, збільшується падіння напруги за сталого енергоспоживання для різних режимів роботи. Зі зростанням перепаду температури збільшується час виходу на стаціонарний режим роботи для різних режимів роботи. Бібл. 10, Рис. 11, Табл. 2.
Ключові слова: термоелектричний охолоджувач, геометрія гілок термоелементів, показники надійності, час виходу на режим, перепад температур.

Зайков В.П. *канд. техн. наук.*[1],
Мещеряков В.И. *доктор техн. наук.*[2],
Гнатовська А.А.[2], **Журавлев Ю.И.**[3] *канд. техн. наук.*

[1]Научно-исследовательский институт ШТОРМ,
ул. Терешковой, 27, Одесса, Украина; *e-mail: grand@i.ua;*
[2]Одесский государственный экологический университет,
ул. Львовская, 15, Одесса, Украина; *e-mail: grand@ua.fm;*

[3]Национальный университет «Одесская морская академия»,
ул. Дидрихсона, 8, Одесса, Украина; *e-mail: zhuravlov.y@ya.ru.*

СРАВНИТЕЛЬНЫЙ АНАЛИЗ ДИНАМИКИ ФУНКЦИОНИРОВАНИЯ ОДНОКАСКАДНОГО ТЕРМОЭЛЕКТРИЧЕСКОГО ОХЛАЖДАЮЩЕГО УСТРОЙСТВА С РАЗЛИЧНОЙ ГЕОМЕТРИЕЙ ВЕТВЕЙ ТЕРМОЭЛЕМЕНТОВ

Проведен сравнительный анализ динамики функционирования однокаскадного термоэлектрического охлаждающего устройства при вариации геометрии ветвей термоэлементов с учетом влияния конструктивных и технологических элементов для различных характерных токовых режимов работы, перепадов температуры и тепловой нагрузки. Показано, что с ростом отношения высоты к площади сечения ветви термоэлемента уменьшается время выхода на стационарный режим работы, величины рабочего тока, увеличивается падение напряженияпри постоянном энергопотреблениидля различных режимов работы. С ростом перепада температуры увеличивается время выхода на стационарный режим работыдля различных режимов работы. Библ.10, Рис.11, Табл.2

Ключевые слова: термоэлектрический охладитель, геометрия ветвей термоэлементов, показатели надежности, время выхода на режим, перепад температур.

References

1. AnatychukL.I. (1979). *Termoelementyitermoelektricheskiieustroistva. Spravochnik [Thermoelementsandthermoelectricdevices. Handbook]*. Kyiv: NaukovaDumka [in Russian].
2. ZebarjadiM., Esfarjani K., Dresselhaus M.S., Ren Z.F., Chen G. (2012). Perspectivesonthermoelectrics: fromfundamentalstodeviceapplications.*Energy & Environmental Science*, 5, 5147–5162.
3. Hyoung–Seuk Choi. (2011). Prediction of reliability on thermoelectric module through accelerated life test and Physics –of –failure.*Electronic Materials Letters*, 7,271.
4. TsarevA.V., ChugunkovV.V. (2008). Issledovaniiekharakteristiktermoelektricheskikhustroistvdlia system termostatirovaniiastartovykhkompleksov [Research on characteristics of thermoelectric devices for thermostatting systems of start complexes]. *Aktualnyieproblemyrossiiskoikosmonautiki. Materialy XXXII akademicheskikhchteniipokosmonautike [Current Problems of Russian Cosmonautics: Proc. of XXXII Academic Readings on Cosmonautics]. (pp.320-321)*.M: Commissionofthe RussianAcademyof Sciences [in Russian].
5. Yang Ping (2010). Approach on thermoelectricity reliability of board –level backplane based on the orthogonal experiment design. *International Journal of Materials and Structural Integrity*,4(2–4), 170–185.
6. Wereszczak A. A., Wang H. (2011). Thermoelectric mechanical reliability. *Vehicle Technologies Annual Merit Reviewand Peer Evaluation Meeting*(USA, Arlington, 11 May 2011) (P. 18).
7. Rowe, D. M.(2012). Thermoelectrics and its Energy Harvesting. Materials, Preparation, and Characterization in Thermoelectrics. (Boca Raton: CRC Press, 2012) (544 p).
8. Zaikov V., Meshcheriakov V., Zhuravlev Yu. (2017). Analysis of the model of interdependence of thermoelement branch geometry and reliability indicators of the single–stage cooler.*Eastern – European Journal of Enterprise Technologies*, 1/1 (85), 26–33.
9. Zaikov, V., MeshcheriakovV., ZhuravlevYu. (2017). Modelofinterrelationbetweenindicatorsofasingle-stagecoolerand the geometry of thermoelement legs. *J.Thermoelectricity*, 6, 59 –76.

10. Zaikov, V., MeshcheriakovV., ZhuravlevYu. (2017). Analysis of the possibility to control the inertia of the thermoelectric cooler.*Eastern–European Journal of Enterprise Technologies*, 6/8 (90), 17–24.
11. Zaikov,V., Meshcheriakov V., Zhuravlev (2018). Analysis of relationship between of a thermoelectric cooler and its design and mode of operation. *Eastern –European Journal of Enterprise Technologies*, 1/8 (91), 12–24.
12. Zaikov V.P., Kinshova L.A., Moiseev V.F. (2009). *Prognozirovaniie pokazatelei nadezhnosti termoelektricheskikh okhlazhdaiiushchikh ustroistv. Kniga 1. Odnokaskadnyie ustroistva. [Prediction of reliability indicators of thermoelectric coolingdevices. Book 1. Single-stagedevices]*.Odessa: Politekhperiodika [in Russian].

Submitted 12.03.2018

NEWS
OF INTERNATIONAL THERMOELECTRIC ACADEMY

STEPAN VASYLYOVYCH MELNYCHUK

(Dedicated to the 70-th anniversary)

On January 14, 2018 the scientific community celebrated the 70th anniversary of Stepan Vasylyovych Melnychuk, Doctor of Science in Physics and Mathematics, professor, academician of International Thermoelectric Academy, Laureate of State Prize of Ukraine in Science and Technology, rector of Yuri Fedkovych Chernivtsi National University.

Stepan Vasylyovych Melnychuk was born in the village of Toporivtsi, Novoselytsia district, Chernivtsi region.

He graduated with distinction from Physics Faculty and the postgraduate course of Theoretical Physics Department of Chernivtsi National University.

Stepan Melnychuk started his career in 1973 in the capacity of an engineer, and then a junior research fellow of Chernivtsi Division of Institute of Semiconductors NAS Ukraine. Two years later he maintained his PhD Thesis ("Research on Impurity States in Excitonic Insulator").

Since 1976 he worked as a senior lecturer, and then associate professor of Theoretical Physics Department; having maintained DSc Thesis ("Localized States in Electron and Vibration Spectra of $A^{II}B^{VI}$ Semiconductors Doped with 3*d*-Elements") – as a professor of this department.

In 2001 S.V. Melnychuk was appointed a pro-rector of research, and in 2004 – the first pro-rector of Chernivtsi National University. In March 2005 року Stepan Vasylyovych was elected rector of Yuri Fedkovych Chernivtsi National University.

Of high priority in the multifarious activity of the university leader is his fruitful research, pedagogical and public work. He is head of Computer Systems and Networks Department of Computer Sciences Faculty, delivers lecture courses to students, supervises the work of postgraduates. Under his guidance, 11 PhD Theses and 1 Doctoral Thesis have been maintained.

Professor S.V. Melnychuk is the author and co-author of over 160 scientific works, notably a monograph, a textbook and several manuals for students and two secondary school books.

The scope of professor's research interests covers the problems of mathematical simulation of physical characteristics of semiconductor materials and structures used for elements and devices of computer electronic, including infrared technique, which is reflected in the monograph (in co-authorship) "Cadmium Telluride: Impurity-Defect States and Detector Properties" (2000).

S.V. Melnychuk is Excellent Worker of National Education, Honoured Worker of Science and Technology of Ukraine.

Professor S.V. Melnychuk was honored with a distinguished title of Laureate of State Prize of Ukraine in Science and Technology (2007).

By Decree of the President of Ukraine for considerable personal contribution to development of national education, many years of fruitful scientific and pedagogical activity Stepan Vasylyovych Melnychuk was awarded with Third Class Order of Merit (2008).

International Thermoelectric Academy, Institute of Thermoelectricity of the National Academy of Sciences and Ministry of Education and Science, Youth and Sports of Ukraine, "Journal of Thermoelectricity" founders and its editorial board cordially congratulate the esteemed Stepan Vasylyovych on his glorious 70th jubilee, wishing him sound health and creative inspiration for may years to come!

ARTICLE SUBMISSION GUIDELINES

For publication in a specialized journal, scientific works are accepted that have never been printed before. The article should be written on an actual topic, contain the results of an in-depth scientific study, the novelty and justification of scientific conclusions for the purpose of the article (the task in view).

The materials published in the journal are subject to internal and external review which is carried out by members of the editorial board and international editorial board of the journal or experts of the relevant field. Reviewing is done on the basis of confidentiality. In the event of a negative review or substantial remarks, the article may be rejected or returned to the author(s) for revision. In the case when the author(s) disagrees with the opinion of the reviewer, an additional independent review may be done by the editorial board. After the author makes changes in accordance with the comments of the reviewer, the article is signed to print.

The editorial board has the right to refuse to publish manuscripts containing previously published data, as well as materials that do not fit the profile of the journal or materials of research pursued in violation of ethical norms (for instance, conflicts between authors or between authors and organization, plagiarism, etc.). The editorial board of the journal reserves the right to edit and reduce the manuscripts without violating the author's content. Rejected manuscripts are not returned to the authors.

Submission of manuscript to the journal

The manuscript is submitted to the editorial office of the journal in paper form in duplicate and in electronic form on an electronic medium (disc, memory stick). The electronic version of the article shall fully correspond to the paper version. The manuscript must be signed by all co-authors or a responsible representative.

In some cases it is allowed to send an article by e-mail instead of an electronic medium (disc, memory stick).

English-speaking authors submit their manuscripts in English. Russian-speaking and Ukrainian-speaking authors submit their manuscripts in English and in Russian or Ukrainian, respectively. Page format is A4. The number of pages shall not exceed 15 (together with References and extended abstracts). By agreement with the editorial board, the number of pages can be increased.

To the manuscript is added:

1. Official recommendation letter, signed by the head of the institution where the work was carried out.

2. License agreement on the transfer of copyright (the form of the agreement can be obtained from the editorial office of the journal or downloaded from the journal website – Dohovir.pdf). The license agreement comes into force after the acceptance of the article for publication. Signing of the license agreement by the author(s) means that they are acquainted and agree with the terms of the agreement.

3. Information about each of the authors – full name, position, place of work, academic title, academic degree, contact information (phone number, e-mail address), ORCID code (if available). Information about the authors is submitted as follows:

authors from Ukraine - in three languages, namely Ukrainian, Russian and English;

authors from the CIS countries - in two languages, namely Russian and English;

authors from foreign countries – in English.

4. Medium with the text of the article, figures, tables, information about the authors in electronic

form.

5. Colored photo of the author(s). Black-and-white photos are not accepted by the editorial staff. With the number of authors more than two, their photos are not shown.

Requirements for article design

The article should be structured according to the following sections:

- *Introduction*. Contains the problem statement, relevance of the chosen topic, analysis of recent research and publications, purpose and objectives.
- *Presentation of the main research material* and the results obtained.
- *Conclusions* summing up the work and the prospects for further research in this direction.
- *References*.

The first page of the article contains information:

1) in the upper left corner – UDC identifier (for authors from Ukraine and the CIS countries);

2) surname(s) and initials, academic degree and scientific title of the author(s);

3) the name of the institution where the author(s) work, the postal address, telephone number, e-mail address of the author(s);

4) article title;

5) abstract to the article – not more than 1 800 characters. The abstract should reflect the consistent logic of describing the results and describe the main objectives of the study, summarize the most significant results;

6) key words – not more than 8 words.

The text of the article is printed in Times New Roman, font size 11 pt, line spacing 1.2 on A4 size paper, justified alignment. There should be no hyphenation in the article.

Page setup: "mirror margins" – top margin – 2.5 cm, bottom margin – 2.0 cm, inside – 2.0 cm, outside – 3.0 cm, from the edge to page header and page footer – 1.27 cm.

Graphic materials, pictures shall be submitted in color or, as an exception, black and white, in .opj or .cdr formats, .jpg or .tif formats being also permissible. According to author's choice, the tables and partially the text can be also in color.

Figures are printed on separate pages. The text in the figures must be in the font size 10 pt. On the charts, the units of measure are separated by commas. Figures are numbered in the order of their arrangement in the text, parts of the figures are numbered with letters – a, b, .. On the back of the figure, the title of the article, the author (authors) and the figure number are written in pencil. Scanned images and graphs are not allowed to be inserted.

Tables are provided on separate pages and must be executed using the MSWord table editor. Using pseudo-graph characters to design tables is inadmissible.

Formulae shall be typed in Equation or MatType formula editors. Articles with formulae written by hand are not accepted for printing. It is necessary to give definitions of quantities that are first used in the text, and then use the appropriate term.

Captions to figures and tables are printed in the manuscript after the references.

Reference list shall appear at the end of the article. References are numbered consecutively in the order in which they are quoted in the text of the article. References to unpublished and unfinished works are inadmissible.

Attention! In connection with the inclusion of the journal in the international bibliographic abstract database, the reference list should consist of two blocks: CITED LITERATURE and REFERENCES (this requirement also applies to English articles):

CITED LITERATURE – sources in the original language, executed in accordance with the Ukrainian standard of bibliographic description DSTU 8302:2015. With the aid of VAK.in.ua

(http://vak.in.ua) you can automatically, quickly and easily execute your "Cited literature" list in conformity with the requirements of State Certification Commission of Ukraine and prepare references to scientific sources in Ukraine in understandable and unified manner. This portal facilitates the processing of scientific sources when writing your publications, dissertations and other scientific papers.

REFERENCES – the same cited literature list transliterated in Roman alphabet (recommendations according to international bibliographic standard APA-2010, guidelines for drawing up a transliterated reference list "References" are on the site http//www.dse.org.ua, section for authors).

To speed up the publication of the article, please adhere to the following rules:

- in the upper left corner of the first page of the article – the UDC identifier;
- family name and initials of the author(s);
- academic degree, scientific title;

begin a new line, Times New Roman font, size 12 pt, line spacing 1.2, center alignment;

- name of organization, address (street, city, zip code, country), e-mail of the author(s);

begin a new line 1 cm below the name and initials of the author(s), Times New Roman font, size 11 pt, line spacing 1.2, center alignment;

- the title of the article is arranged 1 cm below the name of organization, in capital letters, semi-bold, font Times New Roman, size 12 pt, line spacing 1.2, center alignment. The title of the article shall be concrete and possibly concise;
- the abstract is arranged 1 cm below the title of the article, font Times New Roman, size 10 pt, in italics, line spacing 1.2, justified alignment in Ukrainian or Russian (for Ukrainian-speaking and Russian-speaking authors, respectively);
- key words are arranged below the abstract, font Times New Roman, size 10 pt, line spacing 1.2, justified alignment. The language of the key words corresponds to that of the abstract. Heading "Key words" - font Times New Roman, size 10 pt, semi-bold;
- the main text of the article is arranged 1 cm below the abstract, indent 1 cm, font Times New Roman, size 11 pt, line space spacing 1.2, justified alignment;
- formulae are typed in formula editor, fonts Symbol, Times New Roman. Font size is "normal" – 12 pt, "large index" – 7 pt, "small index" – 5 pt, "large symbol" – 18 pt, "small symbol" – 12 pt. The formula is arranged in the text, center aligned and shall not occupy more than 5/6 of the line width, formulae are numbered in parentheses on the right;
- dimensions of all quantities used in the article are represented in the International System of Units (SI) with the explication of the symbols employed;
- figures are arranged in the text. The figures and pictures shall be clear and contrast; the plot axes – parallel to sheet edges, thus eliminating possible displacement of angles in scaling; figures are submitted in color, black-and-white figures are not accepted by the editorial staff of the journal;
- tables are arranged in the text. The width of the table shall be 1 cm less than the line width. Above the table its ordinary number is indicated, right alignment. Continuous table numbering throughout the text. The title of the table is arranged below its number, center alignment;
- references should appear at the end of the article. References within the text should be

enclosed in square brackets behind the text. References should be numbered in order of first appearance in the text. Examples of various reference types are given below.

Examples of LITERATURE CITED

Journal articles

Anatychuk L.I., Mykhailovsky V.Ya., Maksymuk M.V., Andrusiak I.S. Experimental research on thermoelectric automobile starting pre-heater operated with diesel fuel. *J.Thermoelectricity*. 2016. №4. P.84–94.

Books

Anatychuk L.I. *Thermoelements and thermoelectric devices. Handbook.* Kyiv, Naukova dumka, 1979. 768 p.

Patents

Patent of Ukraine № 85293. Anatychuk L.I., Luste O.J., Nitsovych O.V. Thermoelement.

Conference proceedings

Lysko V.V. *State of the art and expected progress in metrology of thermoelectric materials.* Proceedings of the XVII International Forum on Thermoelectricity (May 14-18, 2017, Belfast). Chernivtsi, 2017. 64 p.

Authors' abstracts

Kobylianskyi R.R. *Thermoelectric devices for treatment of skin diseases*: extended abstract of candidate's thesis. Chernivtsi, 2011. 20 p.

Examples of REFERENCES

Journal articles

Gorskiy P.V. (2015). Ob usloviakh vysokoi dobrotnosti i metodikakh poiska perspektivnykh sverhreshetochnykh termoelektricheskikh materialov [On the conditions of high figure of merit and methods of search for promising superlattice thermoelectric materials]. *Termoelektrichestvo - J.Thermoelectricity,* 3, 5 – 14 [in Russian].

Books

Anatychuk L.I. (2003). *Thermoelectricity. Vol.2. Thermoelectric power converters*. Kyiv, Chernivtsi: Institute of Thermoelectricity.

Patents

Patent of Ukraine № 85293. Anatychuk L. I., Luste O.Ya., Nitsovych O.V. Thermoelements [In Ukrainian].

Conference proceedings

Rifert V.G. Intensification of heat exchange at condensation and evaporation of liquid in 5 flowing-down films. In: *Proc. of the 9th International Conference Heat Transfer.* May 20-25, 1990, Israel.

Authors'abstracts

Mashukov A.O. *Efficiency hospital state of rehabilitation of patients with color carcer.* PhD (Med.) Odesa, 2011 [In Ukrainian].

ISSN 1607-8829. Journal of Thermoelectricity. 2018. № 1. 1-104